

DYNAMIC SIMULATION AND OPTIMIZATION OF AMPICILLIN CRYSTALLIZATION

Antonios Dafnomilis

School of Chemical Engineering, National Technical University of Athens, Athens 15780, Greece

Research Project conducted under the Erasmus+ student exchange program.

University of Edinburgh Supervisor: Dr. Dimitrios Gerogiorgis

National Technical University of Athens Supervisor: Prof. Andreas Boudouvis

NATIONAL TECHNICAL UNIVERSITY OF ATHENS

School of Chemical Engineering

June 2019

Acknowledgments

I would like to express my gratitude to my supervisor, Dr. Dimitrios Gerogiorgis, for giving me the opportunity to conduct my research project in the University of Edinburgh. I thank him for his enthusiasm, dedication and support throughout my project and for his faith in my abilities. Finally, I thank him for standing by me after an accident of mine forced me to undergo surgery mere months before the start of the project.

Thank you to Prof. Andreas Boudouvis my NTUA supervisor for his guidance, advice and support throughout my studies. His advice into administrative and personal matters was invaluable during my project.

Thank you to Mr. Samir Diab for his kind words, advice and guidance during the project. I would especially like to thank him for his patience in his efforts to improve my professional writing as well as my presentational skills.

Thank you to Mr. Alistair Rodman for his valuable support in conducting dynamic optimization studies, his insightful words of advice and his efforts into improving the quality of my work.

Without you all, I would not have enjoyed the experience of this project nearly as much.

Finally, I would like to acknowledge the financial support received from the Erasmus+ Teaching Exchange Travel Scholarship.

ΠΕΡΙΛΗΨΗ ΔΙΠΛΩΜΑΤΙΚΗ ΕΡΓΑΣΙΑΣ ΜΕ ΘΕΜΑ

ΔΥΝΑΜΙΚΗ ΠΡΟΣΟΜΟΙΩΣΗ ΚΑΙ ΒΕΛΤΙΣΤΟΠΟΙΗΣΗ ΤΗΣ ΚΡΥΣΤΑΛΛΩΣΗΣ ΤΟΥ ΑΝΤΙΒΙΟΤΙΚΟΥ ΑΜΠΙΚΙΛΛΙΝΗ

Αντώνιος Δαφνομήλης 05114038 10ο Εξάμηνο

Σχολή Χημικών Μηχανικών, Εθνικό Μετσόβιο Πολυτεχνείο, Αθήνα 15780, Ελλάδα

Η διπλωματική εργασία διεξάχθηκε μέσω του προγράμματος Erasmus+
σε συνεργασία με το Πανεπιστήμιο του Εδιμβούργου (University of Edinburgh).

Υπεύθυνος καθηγητής στο Πανεπιστήμιο του Εδιμβούργου: Δρ. Δημήτριος Γερογιώργης.

Υπεύθυνος διπλωματικής εργασίας στο ΕΜΠ: Καθηγητής Ανδρέας Μπουντουβής.

Εισαγωγή

Η διεργασία της κρυστάλλωσης αποτελεί αναπόσπαστο τμήμα της βιομηχανίας φαρμάκων. Η κρυστάλλωση χρησιμοποιείται τόσο για τον διαχωρισμό ενδιάμεσων προϊόντων όσο και για την παραγωγή των τελικών δραστικών φαρμακευτικών ουσιών. Οι διεθνείς προδιαγραφές που αφορούν την ποιότητα των φαρμακευτικών ουσιών γίνονται κάθε χρόνο όλο και πιο αυστηρές με αποτέλεσμα πλέον ο ακριβής έλεγχος της κρυστάλλωσης να αποτελεί ζήτημα υψίστης σημασίας έτσι ώστε να εξασφαλίζεται ότι το τελικό προϊόν είναι εντός προδιαγραφών.[5]

Η αμπικιλλίνη είναι μια ευρέος φάσματος ημισυνθετική πενικιλλίνη που ασκεί βακτηριοκτόνο δράση εναντίον πολλών θετικών και αρνητικών κατά Gram μικροοργανισμών. Ο Διεθνής Οργανισμός Υγείας περιλαμβάνει την αμπικιλλίνη ανάμεσα στα κρίσιμα και απαραίτητα αντιβιοτικά για την διασφάλιση της παγκόσμιας υγείας.

Η συγκεκριμένη διπλωματική μελετά την κρυστάλλωση της αμπικιλλίνης σε κρυσταλλωτήρα διαλείποντος έργου. Όπου το pH χρησιμοποιείται έτσι ώστε να επιφέρει υπερκορεσμό στο εσωτερικό του κρυσταλλωτήρα με συνέπεια να προκύπτει πρωτογενής και δευτερογενής πυρήνωση καθώς και ανάπτυξη κρυστάλλων. Ένα πρόσφατα δημοσιευμένο άρθρο παρουσιάζει ένα νέο κινητικό μοντέλο για την κρυστάλλωση της αμπικιλλίνης, το οποίο έχει παραμετροποιηθεί από πειράματα τα οποία έγιναν σε διαφορετικές συνθήκες προσφέροντας στο μοντέλο μια γενικευμένη αποτύπωση του φαινομένου.[1] Το μοντέλο είναι κατάλληλο για την διεξαγωγή δυναμικής βελτιστοποίησης της διαλείποντος έργου κρυστάλλωσης της αμπικιλλίνης.

Βασιζόμενοι στο δημοσιευμένο μοντέλο θα πραγματοποιηθεί δυναμική προσομοίωση και βελτιστοποίηση για διαφορετικές αντικειμενικές συναρτήσεις με σκοπό να βρεθούν οι βέλτιστες συνθήκες λειτουργίας του συστήματος. Έχει δειχθεί στη βιβλιογραφία ότι τέτοιες μελέτες είναι σε θέση να ανακαλύπτουν τα θετικά αλλά και τα αρνητικά διάφορων σεναρίων σχεδιασμού καθώς και τις βέλτιστες συνθήκες λειτουργίας της διεργασίας.[22]

Θεωρία

Το κινητικό μοντέλο που περιγράφει την διεργασία κρυστάλλωσης της αμπικιλλίνης λαμβάνει υπόψιν την πρωτογενή και δευτερογενή πυρήνωση καθώς και την χρήση αρχικών κρυστάλλων (seeding). Οι ρυθμοί πυρήνωσης και ανάπτυξης των κρυστάλλων περιγράφονται από τις παρακάτω εξισώσεις:

$$G(t) = k_G\,(SS(t) - 1)^g \tag{1}$$

$$B_1(t) = k_{B1} \exp\left(\frac{-B_0}{\ln(SS(t)^2)}\right) \tag{2}$$

$$B_2(t) = k_{B2}\, M(t)^b (SS(t) - 1)^s \tag{3}$$

$$J(t) = B_1(t) + B_2(t) \tag{4}$$

Όπου G είναι ο ρυθμός ανάπτυξης των κρυστάλλων, B_1 και B_2 είναι οι ρυθμοί πρωτογενούς και δευτερογενούς πυρήνωσης μέσα στον κρυσταλλωτήρα με υπερκορεσμό SS αντίστοιχα. J ο συνολικός ρυθμός πυρήνωσης στο σύστημα ενώ M είναι η μάζα των κρυστάλλων μέσα στον κρυσταλλωτήρα, η οποία υπολογίζεται από την εξίσωση:

$$M(t) = ([Amp]_0 - [Amp]_t) \cdot m \tag{5}$$

Όπου, $[Amp_0]$ είναι η αρχική συγκέντρωση αμπικιλλίνης και $[Amp_t]$ η συγκέντρωση της αμπικιλλίνης στο διάλυμα $\forall t$. Τέλος m, η μάζα του αρχικού μητρικού διαλύματος. Οι κινητικές εκφράσεις έχουν υπολογιστεί σε σχέση με τον υπερκορεσμό που υπάρχει στο διάλυμα ο οποίος υπολογίζεται από:

$$SS(t) = \frac{[Amp](t)}{[Amp^*](t)} \tag{6}$$

Όπου, $[Amp]$ είναι η συγκέντρωση της αμπικιλλίνης στο διάλυμα και $[Amp^*]$ η διαλυτότητα της αμπικιλλίνης. Οι παράμετροι k_G, g, B_0, k_{B1}, k_{B2}, b και s του κινητικού μοντέλου έχουν προκύψει από την προσαρμογή πειραματικών μετρήσεων και δίνονται στην βιβλιογραφία.

Από την εξίσωση (6) είναι φανερό ότι για τον υπολογισμό του υπερκορεσμού κάθε χρονική στιγμή t είναι απαραίτητος ο υπολογισμός της διαλυτότητας. Χρησιμοποιήθηκε ένα νέο θερμοδυναμικό μοντέλο το οποίο έχει δημιουργηθεί συγκεκριμένα για αμινοξέα και β- λακταμικά αντιβιοτικά όπως η αμπικιλλίνη.[40] Το μοντέλο συνδέει την διαλυτότητα σε κάθε τιμή του pH με αυτήν στο ισοηλεκτρικό σημείο pI. Χρησιμοποιεί τις σταθερές διάστασης καθώς και "extended Pitzer parameters" έτσι ώστε να προβλεφθεί με ακρίβεια η μη-ιδανική φύση του διαλύματος:

$$\log\frac{S(pH)}{S(pI)} = pI - pH + \log\left[\frac{1+10^{pH-p_{K_{A1}}}}{1+10^{pI-p_{K_{A1}}}}\right] + \log\left[\frac{1+10^{pH-p_{K_{A2}}}}{1+10^{pI-p_{K_{A2}}}}\right] + \frac{2}{\ln 10}\lambda[S(pI) - S(pH)] \tag{33}$$

Όπου $S(pH)$ και $S(pI)$ η διαλυτότητα της αμπικιλλίνης για κάθε pH και για το ισοηλεκτρικό σημείο αντίστοιχα. Ενώ $p_{K_{A1}}$ και $p_{K_{A2}}$ οι σταθερές διάστασης της αμπικιλλίνης. Τέλος λ είναι ο συντελεστής των διαμοριακών αλληλεπιδράσεων.

Ένα σύστημα κρυστάλλωσης περιγράφεται από το ισοζύγιο του πληθυσμού των κρυστάλλων (population balance equation). Αν παραληφθεί η συσσωμάτωση και η θραύση των κρυστάλλων το ισοζύγιο για έναν ημι-διαλείποντος έργου κρυσταλλωτήρα μπορεί να εκφραστεί ως:

$$\frac{\partial n(t,L)}{\partial t} = - \frac{\partial\big(G(t)n(t,L)\big)}{\partial L} \tag{39}$$

Όπου, $n(t, L)$ είναι η πυκνότητα του πληθυσμού των κρυστάλλων, G είναι ο ρυθμός ανάπτυξης των κρυστάλλων και L το συνολικό μήκος των κρυστάλλων βασιζόμενο στον συνολικό ωφέλιμο όγκο του κρυσταλλωτήρα.

Παράλληλα εκφράζεται και το ισοζύγιο μάζας της αμπικιλλίνης:

$$\frac{\mathrm{d}[Amp]}{\mathrm{d}t} = - \frac{\mathrm{d}m_{\mathrm{T}}}{\mathrm{d}t} \tag{42}$$

Όπου m_{T} είναι η πυκνότητα των κρυστάλλων.

Το ισοζύγιο του πληθυσμού είναι μια μη γραμμική μερική διαφορική εξίσωση πρώτης τάξης. Η λύση της παραμένει δύσκολη παρά την ισχύ των σημερινών υπολογιστών, για αυτό το λόγο χρησιμοποιήθηκε η μέθοδος των ‘στιγμών’ (Method of moments). Συμφώνα με την μέθοδο εφαρμόζεται ένας μαθηματικός μετασχηματισμός στην εξίσωση (39) από την οποία προκύπτουν συνήθεις διαφορικές εξισώσεις, οι οποίες αναπαριστούν στιγμές ‘moments’ του πληθυσμού. Η λύση του προβλήματος λοιπόν ανάγεται στην λύση ενός συστήματος από συνήθεις διαφορικές εξισώσεις.

$$\frac{\mathrm{d}m_0}{\mathrm{d}t} = J \tag{44}$$

$$\frac{\mathrm{d}m_1}{\mathrm{d}t} = G\, m_0 \tag{45}$$

$$\frac{\mathrm{d}m_2}{\mathrm{d}t} = 2\, G\, m_1 \tag{46}$$

$$\frac{\mathrm{d}m_3}{\mathrm{d}t} = 3\, G\, m_2 \tag{47}$$

Όπου m_0, m_1, m_2, m_3 είναι η μηδενική, πρώτη, δεύτερη και τρίτη στιγμή του ισοζυγίου του πληθυσμού αντίστοιχα.

Σύμφωνα με την μέθοδο μπορούν να εκφραστούν άπειρες στιγμές του ισοζυγίου του πληθυσμού. Παρόλα αυτά συνηθίζεται να χρησιμοποιούνται οι εξισώσεις μόνο μέχρι την τρίτη στιγμή όπου και υπάρχει άμεση συσχέτιση των ‘στιγμών’ με την φυσική του προβλήματος. Συγκεκριμένα η μηδενική στιγμή αναφέρεται στον αριθμό των κρυστάλλων ανά μονάδα όγκου, η πρώτη στιγμή στο συνολικό μήκος των κρυστάλλων ανά μονάδα όγκου, η δεύτερη στιγμή στην συνολική επιφάνεια των κρυστάλλων ανά μονάδα όγκου και τέλος η τρίτη στιγμή στον συνολικό όγκο των κρυστάλλων ανά μονάδα όγκου.

Η γνώση της φυσικής σημασίας είναι απαραίτητη στο σύστημα, καθώς οι αρχικές τιμές των ‘στιγμών’ είναι απαραίτητες κατά την ταυτόχρονη λύση των διαφορικών εξισώσεων. Έτσι σε περίπτωση που στο σύστημα δεν υπάρχουν αρχικοί κρύσταλλοι (seeding) οι αρχικές τιμές των στιγμών είναι μηδενικές, διαφορετικά υπολογίζονται και λαμβάνονται υπόψιν σύμφωνα με την βιβλιογραφία.[45,46]

Παράλληλα το ισοζύγιο μάζας της αμπικιλλίνης μπορεί να εκφραστεί συναρτήσει των στιγμών:

$$\frac{\mathrm{d}[Amp]}{\mathrm{d}t} = -\rho_c k_V \frac{\mathrm{d}m_3}{\mathrm{d}t} = -3\rho_c k_V G m_2 \qquad (48)$$

Όπου ρ_c είναι η πυκνότητα των κρυστάλλων και k_v ο συντελεστής σχήματος όγκου των κρυστάλλων.

Η ταυτόχρονη λύση των εξισώσεων (44)-(48) περιγράφει το σύστημα. Αξίζει να σημειωθεί ότι ο μετασχηματισμός του ισοζυγίου του πληθυσμού καθιστά αδύνατο τον απευθείας υπολογισμό της κατανομής μεγέθους των κρυστάλλων (CSD), η οποία αποτελεί βασικό μέγεθος στην αξιολόγηση της τελικής ποιότητας του προϊόντος. Ωστόσο οι στιγμές του πληθυσμού διατηρούν φυσική σημασία και επιτρέπουν τον υπολογισμό παραμέτρων όπως το μέσο μέγεθος των κρυστάλλων (MCS), τη διασπορά (STD) και τον συντελεστή διακύμανσης (CV). Αυτά τα μεγέθη παράλληλα με την απόδοση της διεργασίας σε στερεό προϊόν μπορούν να χρησιμοποιηθούν για την αξιολόγηση της διεργασίας.

Αποτελέσματα

Αρχικά πραγματοποιήθηκαν μια σειρά από δυναμικές προσομοιώσεις έτσι ώστε να διαπιστωθεί ότι το δημοσιευμένο μοντέλο είχε αναπαραχθεί σωστά. Το άρθρο που παρουσιάζει το μοντέλο χρησιμοποιεί έξι διαφορετικά πειράματα (A-F) για την παραμετροποίηση των διαφορετικών παραμέτρων του μοντέλου. Χρησιμοποιώντας την ode113 εξίσωση του MATLAB κάθε πείραμα προσομοιώθηκε και τα αποτελέσματα συγκρίθηκαν με αυτά που παρουσιάζονται στο άρθρο. Συγκεκριμένα σε κάθε περίπτωση υπολογίστηκαν η συγκέντρωση της αμπικιλλίνης $\forall t\ [Amp](t)$ καθώς και το τελικό MCS. Έπειτα από ενδελεχή μελέτη των δεδομένων και των αποτελεσμάτων διαπιστώθηκε ότι το μοντέλο αναπαρήχθη επιτυχώς.

Στην συνέχεια ακολούθησε η δυναμική βελτιστοποίηση της διεργασίας. Βέλτιστα προφίλ pH αποκτήθηκαν χρησιμοποιώντας το υπολογιστικό πακέτο DynOpt για το MATLAB. Το πακέτο εφαρμόζει μια ταυτόχρονη μέθοδο βελτιστοποίησης την ‘orthogonal collocation on finite elements’. Η μέθοδος εκτελεί διακριτοποίηση του χρόνου σε διαστήματα N, ορίζοντας σημεία (collocation points) σε κάθε διάστημα και στην συνέχεια προσεγγίζει την λύση των διαφορικών εξισώσεων με πολυώνυμα Lagrange. Με αυτόν τον τρόπο οι διαφορικές εξισώσεις μετατρέπονται σε αλγεβρικές εξισώσεις οι οποίες συμμετέχουν σε ένα σύστημα μη-γραμμικού προγραμματισμού (NLP). Οι μετασχηματισμένες εξισώσεις, παράλληλα με τις εξισώσεις συνέχειας και τους απαραίτητους περιορισμούς σχηματίζουν ένα πρόβλημα μη γραμμικού προγραμματισμού το οποίο λύνεται με έναν NLP αλγόριθμο βελτιστοποίησης. Για τη λύση του προβλήματος NLP χρησιμοποιήθηκε η συνάρτηση fmincon του MATLAB. Η λύση ενός τέτοιου του προβλήματος αριστοποίησης καταλήγει στην εύρεση ενός βέλτιστου προφίλ pH(t) το οποίο επιτυγχάνει την ελαχιστοποίηση της αντικειμενικής συνάρτησης ενώ ικανοποιεί τους περιορισμούς.

Για το πρόβλημα της αριστοποίησης επιλέχθηκε η ακόλουθη αντικειμενική συνάρτηση:

$$\min_{pH(t),t_f} f(x, t_f) = W_\sigma \, \sigma^2 \; - \; W_{\mathrm{MCS}} \, MCS \tag{61}$$

Σκοπός της συνάρτησης είναι η ταυτόχρονη αύξηση του μέσου μεγέθους των κρυστάλλων (MCS) και η μείωση της διακύμανσης σ^2 στο μέγεθος των κρυστάλλων. Με αυτόν τον τρόπο επιτυγχάνεται ταυτόχρονη αύξηση του μέσου μεγέθους των κρυστάλλων καθώς και η μείωση της διασποράς καταλήγοντας σε τελικό προϊόν με βελτιωμένα ποιοτικά χαρακτηριστικά. W_σ και W_{MCS} αποτελούν συντελεστές βαρύτητας στην αντικειμενική συνάρτηση. Παράλληλα εφαρμόστηκαν τέσσερις διαφορετικοί περιορισμοί στο σύστημα:

$$pH(t_0) > 7 \text{ περιορισμός στο } t_0 \tag{62}$$

$$[Amp](t_f) < target_{[Amp]} \text{ περιορισμός στο } t_f \tag{63}$$

$$SS(t) > 1 \text{ περιορισμός } \forall t \tag{64}$$

$$5.5 > pH(t) > 7.84$$

Οι περιορισμοί είναι απαραίτητοι έτσι ώστε η λύση του συστήματος να είναι δόκιμη. Αρχικά ορίζεται ότι η αρχική τιμή του pH θα πρέπει να είναι μεγαλύτερη του 7, αυτός ο περιορισμός εξασφαλίζει το φυσικό νόημα της λύσης. Η αμπικιλλίνη παράγεται εργοστασιακά σε ελαφρώς βασικό pH 7.0-7.5. Στην περίπτωση που το αρχικό pH είναι μικρότερο του 7 το σύστημα ξεκινά από την αρχή με υψηλό υπερκορεσμό και η αμπικιλλίνη ξεκινά να κρυσταλλώνει χωρίς την ανάγκη μείωσης του pH. Ο δεύτερος περιορισμός εξασφαλίζει ότι στο τέλος του χρόνου της διεργασίας η ζητούμενη ποσότητα προϊόντος $target_{[Amp]}$ θα έχει κρυσταλλωθεί, αποτελεί πρακτικά έναν περιορισμό για την απόδοση της διεργασίας. Ο τρίτος περιορισμός εξασφαλίζει την ακρίβεια του μοντέλου. Για να υπάρξει το φαινόμενο της κρυστάλλωσης είναι απαραίτητο να υπάρχει υπερκορεσμός στο σύστημα καθ'όλη τη διάρκεια της διεργασίας, διαφορετικά θα παρατηρηθεί το αντίθετο φαινόμενο. Ωστόσο αν κατά την διάρκεια της διεργασίας δεν υπάρχει υπερκορεσμός, το μοντέλο παράγει μιγαδικούς αριθμούς με αποτέλεσμα να χάνεται το φυσικό νόημα της λύσης. Τέλος ορίζεται ότι το pH θα κυμαίνεται μέσα στα όρια όπου το θερμοδυναμικό μοντέλο διατηρεί την ακρίβεια του.

Χρησιμοποιώντας το πακέτο DynOpt λήφθηκαν διαφορετικά βέλτιστα προφίλ pH(t) για διαφορετικές τιμές των συντελεστών βαρύτητας, $target_{[Amp]}$ και N. Αναλύοντας τα αποτελέσματα, μπορούν να προκύψουν συμπεράσματα για την σχέση μεταξύ της απόδοσης της διεργασίας σε τελικό προϊόν και των παραμέτρων ποιότητας όπως το MCS, το CV και το STD.

Αρχικά επιλέχθηκε να γίνει δυναμική βελτιστοποίηση για το πείραμα D ένα από τα έξι πειράματα που αναφέρονται στη βιβλιογραφία.[1]
Έτσι εξασφαλίζεται ότι οι αρχικές παράμετροι του προβλήματος που βελτιστοποιείται περιγράφουν ένα ρεαλιστικό πρόβλημα. Το πείραμα D επιλέχθηκε καθώς αποτελεί ένα σύστημα το οποίο παρουσιάζει το μικρότερο αρχικό seeding. Για τα πειράματα χρησιμοποιήθηκαν τρεις διαφορετικοί βαθμοί διακριτοποίγσης N=[10 20 30] και τέσσερις διαφορετικοί συνδυασμοί συντελεστών βαρύτητας για την αντικειμενική συνάρτηση:

Table 8: Διαφορετικοί συνδυασμοί των συντελεστών βαρύτητας.

W_σ	W_{MCS}
1.0	0.0
1.0	0.5
1.0	1.0
1.0	1.5

Ανάλογα με τον αριθμό των σημείων (collocation points) που χρησιμοποιούνται για την αναπαράσταση του pH και των διαφορικών εξισώσεων διαφοροποιείται και η ακρίβεια της λύσης. Για το pH χρησιμοποιήθηκε ένα σημείο καθιστώντας το προφίλ (Piece Wise Constant, PWC) εννοώντας ότι σε κάθε διακριτοποίημενο διάστημα η τιμή του pH παραμένει σταθερή, οπότε το $pH(t)$ μεταβάλλεται πρακτικά με 'σκαλοπάτια'. Αντίθετα χρησιμοποιήθηκαν τρία σημεία για τις διαφορικές εξισώσεις όποτε σε κάθε διακριτοποιήμενο διάστημα υπολογίζονταν ένα πολυώνυμο τετάρτου βαθμού για κάθε λύση της διαφορικής εξίσωσης.

Κατά την διάρκεια της βελτιστοποίησης παρατηρήθηκε ότι η κλίμακα των μεταβλητών παρουσίαζε προβλήματα. Το πρόβλημα εντοπίστηκε στο γεγονός ότι η μηδενική στιγμή που αντιστοιχεί στο πλήθος των κρυστάλλων έχει μέγεθος της τάξης του 10^9 ενώ για παράδειγμα η τρίτη στιγμή έχει κλίμακα στης τάξης του 10^{-3}. Αυτή η ανομοιομορφία στα μεγέθη των παραμέτρων δημιουργούν προβλήματα στην επίλυση του προβλήματος. Συνήθως σε προβλήματα αριστοποίησης συστημάτων διαφορικών εξισώσεων η ανομοιομορφία στην κλίμακα των πρώτων μερικών παραγώγων είναι η αιτία προβλημάτων στην επίλυση του συστήματος. Ιδανικά θα έπρεπε λοιπόν να προσαρμοστούν τα μεγέθη όλων των μερικών παραγώγων του συστήματος. Μία τέτοια διαδικασία είναι αρκετά περίπλοκη, για αυτό το λόγο αρχικά έγινε προσαρμογή των τιμών των ίδιων των διαφορικών εξισώσεων και παρατηρήθηκε ότι τα προβλήματα στην επίλυση επιλύθηκαν σε ένα ικανό σημείο, οπότε μπορούσαν πλέον να ληφθούν αποτελέσματα. Εφαρμόστηκε λοιπόν μια απλή διαδικασία προσαρμογής (scaling) στις τιμές των διαφορικών εξισώσεων.

Για την περεταίρω ακρίβεια και ταυτόχρονη επιτάχυνση της επίλυσης του προβλήματος το πακέτο DynOpt προσφέρει τη δυνατότητα να δοθούν οι αναλυτικές πρώτες μερικές παράγωγοι τόσο των διαφορικών εξισώσεων, όσο και της αντικειμενικής συνάρτησης και των περιορισμών. Ωστόσο η εξίσωση (33) δεν είναι δυνατόν να εκφραστεί ως συνάρτηση της διαλυτότητας λόγω της μορφής της. Κατά την διάρκεια των δυναμικών προσομοιώσεων η εξίσωση λυνόταν αριθμητικά. Σε αυτήν την περίπτωση όμως είναι απαραίτητη η αναλυτική έκφραση της. Για αυτό το λόγο η εξίσωση (33) προσεγγίστηκε από την εξίσωση:

$$\left[Amp^*\right](pH) = a_s\, e^{b_s\, pH} + c_s\, e^{d_s\, pH} \tag{37}$$

όπου $[Amp^*]$ η διαλυτότητα της αμπικιλλίνης, a_s, b_s, c_s και d_s οι παράμετροι της εξίσωσης προσέγγισης υπολογισμένες από το πακέτο 'curve fitting toolbox' του MATLAB.

Από τα αποτελέσματα της βελτιστοποίησης είναι φανερό ότι στην αρχή της διεργασίας μια αρχική πτώση του pH είναι απαραίτητη έτσι ώστε να προκύψει αρχικά πρωτογενής και δευτερογενής πυρήνωση, μετέπειτα το pH αυξάνεται έτσι ώστε να λαμβάνει χώρα κυρίως η ανάπτυξη των

κρυστάλλων. Η εκτεταμένη ανάπτυξη των κρυστάλλων οδηγεί σε κρυστάλλους με μεγαλύτερο MCS και μικρότερη διασπορά σ^2. Μετά την αρχική πτώση του pH παρατηρείται μια ενδιάμεση φάση όπου το pH παραμένει σχεδόν σταθερό ενώ παρατηρείται μια σταδιακή μείωση σε σχέση με το χρόνο. Το μέγεθος της μείωσης είναι αναλογικό με την αυστηρότητα του περιορισμού στην απόδοση της διεργασίας. Εάν απαιτείται μεγαλύτερη απόδοση η πτώση του pH είναι εντονότερη. Αυτή η σταδιακή μείωση επιτρέπει στην ελεγχόμενη αύξηση του υπερκορεσμού που συνεπάγεται περεταίρω αύξηση της κρυσταλλικής ανάπτυξης. Στο τέλος της ενδιάμεσης φάσης παρατηρείται μια τελική πτώση του pH η οποία εξασφαλίζει ότι περισσότερο προϊόν θα κρυσταλλωθεί με σκοπό να ικανοποιηθεί ο περιορισμός της απόδοσης ενώ μεγιστοποιούνται τα ποιοτικά χαρακτηριστικά του τελικού προϊόντος.

Από την παρατήρηση των λύσεων για διαφορετικούς βαθμούς διακριτοποίησης N, διαφορετικούς συντελεστές βαρύτητας στην αντικειμενική συνάρτηση και διαφορετικούς περιορισμούς στην απόδοση της διεργασίας προκύπτουν τα παρακάτω συμπεράσματα.

<u>Επίδραση του περιορισμού στην απόδοση.</u>

Σχεδόν σε κάθε περίπτωση η τελική συγκέντρωση αμπικιλλίνης [*Amp*](*tf*) ταυτίστηκε με την τιμή του $target_{[Amp]}$ σημαίνοντας ότι υπάρχει μια σαφής ανταποδοτική σχέση μεταξύ της απόδοσης και των ποιοτικών χαρακτηριστικών. Παρατηρείται λοιπόν ότι για να βελτιωθούν τα ποιοτικά χαρακτηριστικά είναι απαραίτητο να 'θυσιαστεί' μέρος της απόδοσης της διεργασίας.

Όταν απαιτείται μεγαλύτερη απόδοση η τελική πτώση του pH παρατηρείται ότι συμβαίνει νωρίτερα και για πολύ αυστηρές απαιτήσεις ο υπερκορεσμός παρουσιάζει μια μεγάλη αύξηση στην αρχή και μετά μειώνεται εκθετικά σημαίνοντας ότι για να αυξηθεί η απόδοση σε προϊόν απαιτούνται απότομα προφίλ pH με συνεχώς μειούμενο υπερκορεσμό. Τέτοια απότομα προφίλ οδηγούν σε προϊόν με σαφώς κατώτερα ποιοτικά χαρακτηριστικά.

<u>Επίδραση της διακριτοποίησης του χρόνου N.</u>

Για να εξακριβωθεί η επίδραση της διακριτοποίησης N, λήφθηκαν λύσεις για N=[10 20 30] όπου το N αναπαριστά τον αριθμό των ισαπέχοντων χρονικών διαστημάτων όπου σε καθένα από αυτά το pH παραμένει σταθερό. Παρατηρήθηκε ακόμη και με N=10 ότι η μορφή της λύσης δεν παρουσίαζε μεγάλες διαφορές. Ωστόσο μια αύξηση στην διακριτοποίηση επιτρέπει στο σύστημα να μεταβάλει το pH πιο ιδιαίτερα σε ένα μικρότερο χρονικό διάστημα. Αυτή η δυνατότητα είναι επιθυμητή καθώς ο κώδικας μπορεί να επιλέγει μικρές μεταβολές στο pH έτσι ώστε να μειωθεί η πυρήνωση και να προτιμηθεί η ανάπτυξη των κρυστάλλων. Στην ουσία η φύση της λύσης παραμένει η ίδια αλλά παρατηρείται περεταίρω 'ομαλότητα' στην λύση. Ωστόσο από την παρατήρηση των λύσεων δεν είναι σαφές ότι η αύξηση του N οδηγεί συνεχώς σε λύσεις με καλύτερα ποιοτικά χαρακτηριστικά.

<u>Επίδραση των συντελεστών βαρύτητας της αντικειμενικής συνάρτησης.</u>

Η επίδραση των διάφορων συντελεστών βαρύτητας συνάδει με τις αρχικές προβλέψεις. Έτσι όταν W_σ= 1 και W_{MCS}= 0 ο μόνος σκοπός της αριστοποίησης είναι η μείωση της διακύμανσης και έτσι παρατηρείται ότι οι λύσεις παρουσιάζουν μειωμένα CV και STD αλλά και μειωμένο MCS. Αντίθετα όταν W_σ= 1 και W_{MCS}= 1.5 παρατηρείται αύξηση στο MCS ενώ τα CV και STD παραμένουν σε χαμηλά επίπεδα. Γενικότερα η επίδραση ενός υψηλού W_{MCS} στα CV και MCS είναι μικρότερη από την

επίδραση του W_{MCS}=0 στο MCS. Συμπεραίνεται λοιπόν ότι και οι δύο συντελεστές βαρύτητας πρέπει να χρησιμοποιούνται έτσι ώστε να υπάρχει βελτίωση σε όλα τα ποιοτικά χαρακτηριστικά. Παρατηρώντας τις διαφορετικές λύσεις για W_{MCS}=0 και W_{MCS}=1.5 παρατηρούνται τα εξής. Διατηρώντας υψηλές και σταθερές τιμές pH στην ενδιάμεση φάση αυξάνει το MCS, διαφορετικά η σταδιακή βηματική μείωση του pH κατά την διάρκεια της ενδιάμεσης φάσης επιτυγχάνει μείωση των CV και STD αλλά ταυτόχρονη μείωση του MCS.

Μέτωπα Pareto

Ένα μέτωπο Pareto είναι ένα πλήθος από μη-εξαρτώμενες λύσεις, οι οποίες επιλέγονται σαν βέλτιστες, εάν κανένα ζητούμενο δεν μπορεί να βελτιωθεί περαιτέρω χωρίς να θυσιάζεται τουλάχιστον ένα ζητούμενο. Ένα μέτωπο Pareto είναι σε θέση να υπογραμμίσει τις βέλτιστες λύσεις ανάμεσα στις βελτιστοποιημένες λύσεις και μάλιστα να αναδείξει σαφώς την ανταποδοτική σχέση μεταξύ των διάφορων χαρακτηριστικών. Στα πλαίσια αυτής της εργασίας κατασκευάστηκε το τρισδιάστατο μέτωπο Pareto με άξονες ([Amp](tf), CV και MCS) , στην συνέχεια κατασκευάστηκαν οι προβολές του 3D Pareto στις δύο διαστάσεις.

Από την παρατήρηση των αποτελεσμάτων προέκυψε το συμπέρασμα ότι υπάρχει μια σαφής ανταποδοτική σχέση τόσο μεταξύ των [Amp](tf) και CV όσο και μεταξύ των [Amp](tf) και MCS. Παρατηρήθηκε ότι είναι δυνατόν να βελτιωθεί το CV από 0.9 σε 0.8 χωρίς υπερβολική μείωση σε τελικό προϊόν. Αντίθετα όταν το CV είναι μικρότερο του 0.8, η ποσότητα του μη-ανακτώμενου προϊόντος είναι δυσανάλογα υψηλή για να δικαιολογήσει την βελτίωση στο CV. Παρόμοια αποτελέσματα ίσχυαν και για το MCS. Παρατηρήθηκε ότι όλα τα βέλτιστα προφίλ pH ακολουθούν την μορφή που περιεγράφηκε παραπάνω. Διακρίθηκε σαφώς η ύπαρξη της αρχικής πτώσης του pH, ακολουθημένη από την ενδιάμεση φάση και από την τελική πτώση του pH. Όσο αυξάνεται η απόδοση, τόσο συρρικνώνεται η διάρκεια της ενδιάμεσης φάσης. Επιπλέον παρατηρήθηκε ότι λύσεις που έχουν προκύψει με σκοπό την έμφαση στην μείωση της διακύμανσης εμφανίζουν εντονότερη σταδιακή μείωση του pH κατά την διάρκεια της ενδιάμεσης φάσης. Αντίθετα όταν κύριος στόχος είναι η αύξηση του MCS η τιμή του pH παραμένει περισσότερο σταθερή. Συμπεράθηκε λοιπόν ότι η διάρκεια και η τιμή του pH της ενδιάμεσης φάσης είναι οι κύριοι παράμετροι που επηρεάζουν άμεσα τα ποιοτικά χαρακτηριστικά του τελικού προϊόντος.

Παράλληλα παρατηρήθηκε στο μέτωπο Pareto δεν υπάρχουν λύσεις από τον συνδυασμό W_{MCS}=0 και W_{MCS}=1.5. Προκύπτει λοιπόν το συμπέρασμα ότι η αντικειμενική συνάρτηση πρέπει να εμπεριέχει και τους δύο όρους (διακύμανση και μέσο μέγεθος) έτσι ώστε τη τελική λύση να είναι βέλτιστη.

Η χρησιμότητα των μετώπων Pareto έγκειται στο γεγονός ότι μπορούν να υπογραμμίσουν τις βέλτιστες συνθήκες λειτουργίας ανάλογα με το ζητούμενο. Έτσι αν κύριος σκοπός είναι η μεγιστοποίηση της απόδοσης τότε επιλέγεται pH(t)=5.5 (το μικρότερο επιτρεπτό pH) όπου επιτυγχάνεται η μεγαλύτερη απόδοση αλλά η ταχύτατη πυρήνωση που προκύπτει οδηγεί σε τελικό προϊόν με υποβαθμισμένα ποιοτικά χαρακτηριστικά. Αντίθετα ανάλογα με τα επιθυμητά ποιοτικά χαρακτηριστικά μπορεί να επιλεχθεί ένα προφίλ pH το οποίο να βελτιστοποιεί την απόδοση.

Επίδραση της αρχικής ποσότητας κρυστάλλων (initial crystallizer seeding).

Για την εύρεση της επίδρασης της αρχικής ποσότητας των κρυστάλλων στο βέλτιστο προφίλ pH εφαρμόστηκε ακριβώς η ίδια διαδικασία αριστοποίησης για τα πειράματα E και F που αναφέρονται στην βιβλιογραφία.[1] Τα πειράματα D, E, F διέθεταν wt= 1.8%, 3% και 15% αρχικών κρυστάλλων αντίστοιχα. Επίσης οι τελικοί χρόνοι της διεργασίας ήταν t_f = 250, 350 και 1500 min αντίστοιχα. Οι συνθήκες του πειράματος E πέρα από τον τελικό χρόνο και την ποσότητα αρχικών κρυστάλλων ήταν παρόμοιες με αυτές του πειράματος D. Αντίθετα το πείραμα F είχε αρχικά μεγαλύτερη $[Amp](t_0)$ οπότε το σύστημα ήταν από την αρχή αρκετά υπερκορεσμένο. Από την μελέτη βελτιστοποίησης λήφθηκαν βέλτιστα προφίλ pH για τα πειράματα E και F και σχηματίστηκαν τα αντίστοιχα μέτωπα Pareto. Για το πείραμα E παρατηρήθηκαν αντίστοιχα αποτελέσματα με αυτά για το πείραμα D. Παρατηρήθηκε ίδια μορφή στα προφίλ pH και τα μέτωπα Pareto είχαν παρόμοιο σχήμα και συμπεριφορά. Επιβεβαιώθηκε λοιπόν η ύπαρξη ανταποδοτικής σχέσης τόσο μεταξύ των [Amp](tf) και CV όσο και μεταξύ των ([Amp](tf) και MCS. Αντίθετα για το πείραμα F παρά την ύπαρξη παραπάνω από 130 λύσεων, μόνο έξι αποτέλεσαν το μέτωπο Pareto το οποίο είχε πάρα πολύ μικρή έκταση. Συμπεράθηκε ότι πρακτικά δεν παρατηρείται ανταποδοτική σχέση μεταξύ των χαρακτηριστικών ποιότητας και της απόδοσης της διεργασίας. Με άλλα λόγια η μείωση της απόδοσης δεν βελτιώνει αποτελεσματικά τα χαρακτηριστικά ποιότητας. Σε αυτήν την περίπτωση το βέλτιστο pH είναι το pH(t)= 5.5 το οποίο επιτυγχάνει την μέγιστη απόδοση.

Συνήθως ένα προφίλ που επιβάλει πολύ υψηλό κορεσμό καταλήγει σε ταχεία πυρήνωση και υποβαθμισμένα ποιοτικά χαρακτηριστικά. Σε αυτή όμως την περίπτωση ο υψηλός αριθμός κρυστάλλων στην αρχή εξασφαλίζει ότι το φαινόμενο της ανάπτυξης των κρυστάλλων θα επικρατήσει, αναιρώντας την ανάγκη για περίπλοκα προφίλ pH. Ωστόσο ένα τέτοιο σύστημα δεν είναι ευέλικτο καθώς διαθέτει μόνο ένα βέλτιστο σημείο λειτουργίας και δεν επιτρέπει την αριστοποίηση με βάση τους περιορισμούς στα ποιοτικά χαρακτηριστικά του τελικού προϊόντος.

Συμπεράσματα

Κατά την διάρκεια αυτής της διπλωματικής εργασία μελετήθηκε η διαλείποντος έργου κρυστάλλωση του αντιβιοτικού αμπικιλλίνη. Διενεργήθηκε δυναμική προσομοίωση για διάφορες συνθήκες λειτουργίας και επιβεβαιώθηκε η σωστή αναπαραγωγή του κινητικού μοντέλου. Έπειτα διενεργήθηκε μια μελέτη δυναμικής βελτιστοποίησης για τρία διαφορετικά σενάρια όπου το καθένα είχε διαφορετικό αριθμό αρχικών κρυστάλλων (seeding). Μελετήθηκαν διαφορετικοί συνδυασμοί αντικειμενικών συναρτήσεων και περιορισμών και βρέθηκαν βέλτιστα προφίλ pH, τα οποία μεγιστοποιούσαν διάφορα ποιοτικά χαρακτηριστικά ενώ ικανοποιούσαν τους περιορισμούς. Τέλος σχηματίστηκαν τα μέτωπα Pareto όπου επισημάνθηκαν τα βέλτιστα σημεία λειτουργίας και αναλύθηκε η ανταποδοτική σχέση μεταξύ της απόδοσης και των ποιοτικών χαρακτηριστικών. Όλα τα αποτελέσματα παρουσιάστηκαν σε γραφική μορφή ή σε πίνακες και συζητήθηκαν. Τέλος προτάθηκαν προτάσεις για μελλοντική ερευνητική δουλεία πάνω στο θέμα, όπως το να συμπεριληφθεί ο τελικός χρόνος t_f στην αντικειμενική συνάρτηση.

Abstract

Ampicillin a broad spectrum semi-synthetic penicillin derived β-lactam antibiotic is according to the World Health organization critically important and a high priority antimicrobial, essential for the world healthcare system. Crystallization is a crucial unit operation in the production of ampicillin, which influences essential product attributes like the bioavailability, safety and stability of the antibiotic. In this work, dynamic simulation and subsequent dynamic profile optimization for the batch crystallization of ampicillin was implemented. Recently a new model for the crystallization kinetics of ampicillin was published.[1] This model was utilized in order to perform dynamic simulation under a variety of conditions for design space investigation. Afterwards, optimization studies were conducted using the orthogonal collocation on finite elements method and the fmincon algorithm was employed to solve the Non-Linear Programming problem. A weighted multi-objective function was utilized in order to enhance crucial quality attributes of the final crystalline product while satisfying yield constraints. Results for three different values of time domain discretization and four different combinations of objective function weights were obtained and discussed. Finally, Pareto fronts exhibiting the tradeoff relationship between different objectives and constraints are detailed.

Table of Contents

List of Figures

List of Tables

1. Introduction

1.1. Global antibiotics consumption

Global antibiotic consumption increased by 65% between 2000 and 2015, while consumption rate increased by 39 %.[2] In Fig. 1 it is apparent that the reason for this trend lies primarily with the increase of antibiotic usage from low and medium income countries. While the use of antibiotics in high income countries has either stayed constant or slightly increased.

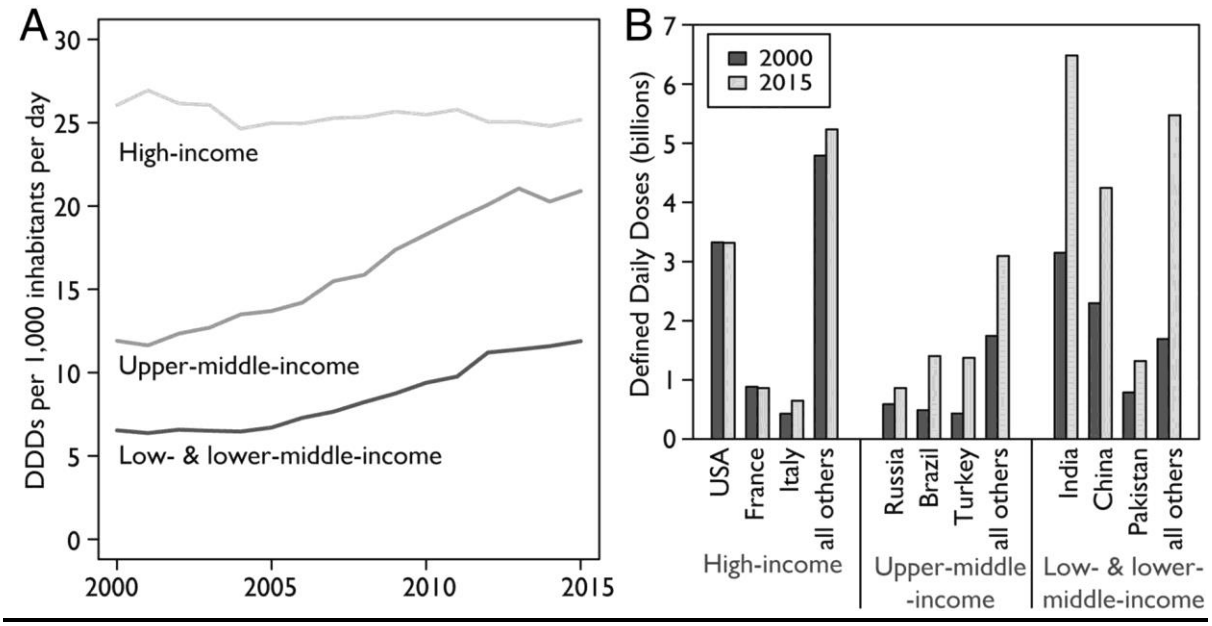

Figure 1: Global antibiotic consumption by country income classification: 2000–2015.[2]

Fig. 2 provides data on the consumption of the four most consumed classes of antibiotics between 2000 and 2015. Broad-spectrum penicillins are the most commonly consumed class of antibiotics (39% of the world consumption in 2015) and their use has increased by 36% between 2000 and 2015 globally. The greatest increase was on low income countries (56%), although high income countries also saw an increase (15%).[2] It is apparent that the production of those antibiotics remains of the utmost importance. In the same time period cephalosporin, quinolones and macrolides all increased overall, even though the consumption rate decreased in high income countries by 18, 1 and 25% respectively. The overall increase in consumption is due to low income countries, in which the antibiotic consumption rate increased by 399, 125, and 119% for cephalosporins, quinolones, and macrolides, respectively.

In Fig. 3 several projections are presented concerning the global antibiotic consumption until 2030. If global consumption rates remain constant accounting only for the increasing population ('Baseline' curve, in Fig. 3) then an increase of 15% between 2015 and 2030 will be observed. If all countries increase their consumption rates at their compounded annual growth rates ('Cont. Growth' curve in Fig. 3), it is estimated that the increase in global consumption will be 202%. While if, all countries converge on the global median antibiotic consumption rate in 2015 by 2020 ('Conv. Median' in Fig. 3), it is estimated that the global antibiotic consumption would increase by 32%. While the consumption of antibiotics increases every year, the Food and Drug Administration (FDA) and other regulatory agencies constantly set new regulations to ensure the safety and stability of pharmaceutical products. The

required increase in production capacity and the pressure to adhere to the international regulations provides strong incentives for pharmaceutical companies to alter their established production strategies. Advances in process design and control offer production strategies with great economic benefits making them attractive for implementation.

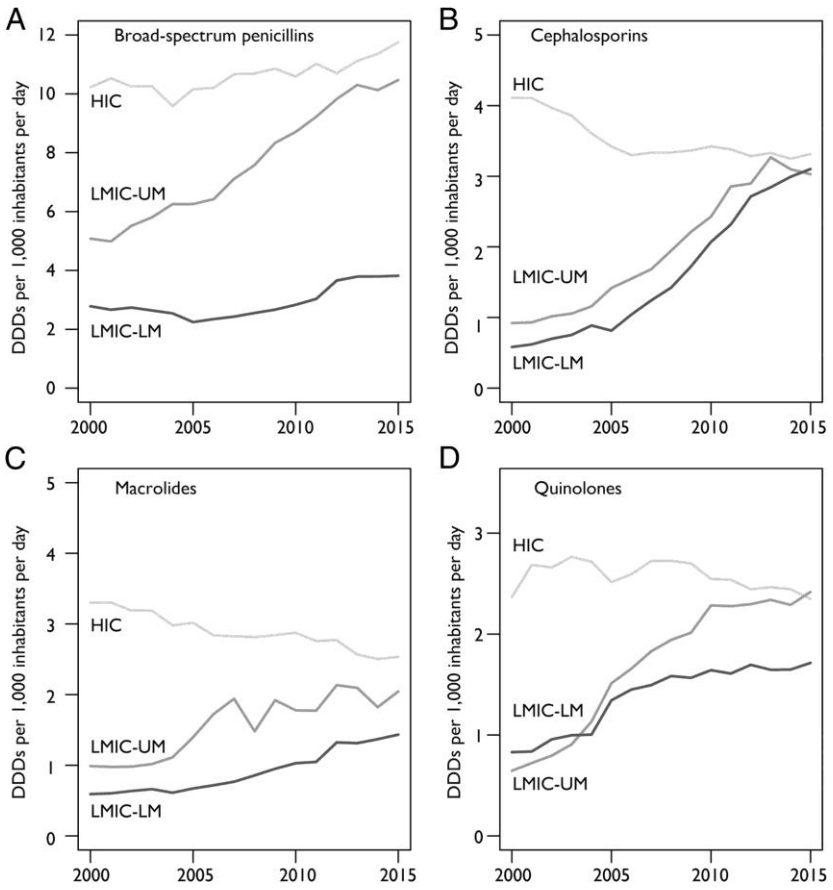

Figure 2: Antibiotic consumption rate for the four most-consumed therapeutic classes of antibiotics by country income classification: 2000–2015.[2]

1.2. Crystallization

Crystallization is a separation and purification technique employed to produce a variety of solid products. It is an essential process in the pharmaceutical industry being commonly used for the separation of intermediates or as the final process in the production of an active pharmaceutical ingredient (API). During the crystallization process a condition is created where the equilibrium solubility value of the solute is below that of the concentration of the solute in the solution, thus creating supersaturation inducing crystal nucleation and growth and resulting in crystallization.

Crystallization can be accomplished by reducing temperature as in cooling crystallization, by removing solvent as in evaporative crystallization, or by altering the composition of the solution through the addition of acid, base, miscible antisolvents, or salts as in a precipitating crystallization.[4] Apart from the pharmaceutical industry crystallization is widely used in other industries such as the chemical and food industries. Crystallization in the pharmaceutical industry directly parallels crystallization in other

industries with the defining feature being the chemical complexity of the substances that are crystallized. The complexity and chemical diversity impact the thermodynamics such as solubility behavior as well as the kinetics of crystallization which in turn influence the crystal structure. The final size, shape and form of the crystals influences not only downstream operations but also the physical and chemical properties of the solid product.[5] These properties often represent important quality attributes in the pharmaceutical manufacturing process with one of the most important being the bioavailability of the crystalline product.

Due to the application of pharmaceutical crystalline products in biological systems, strict control is required on their purity, crystal form, morphology and particle size distribution. These parameters are essential to the safety, stability and bioavailability of the final crystalline product. A recent FDA warning issued to a pharmaceutical company details an alarming instance were traces of β-lactam antibiotics were found in other antibiotics.[6] This warning highlights that dedicated units or plants are needed for the production of specific antibiotic classes in order to avoid cross-contamination between different products. The establishment of new dedicated plants focusing on specific antibiotics production allows for the implementation of specific design decisions. Process simulation and optimization are integral steps in the design process, providing feedback on the most appropriate design decisions.

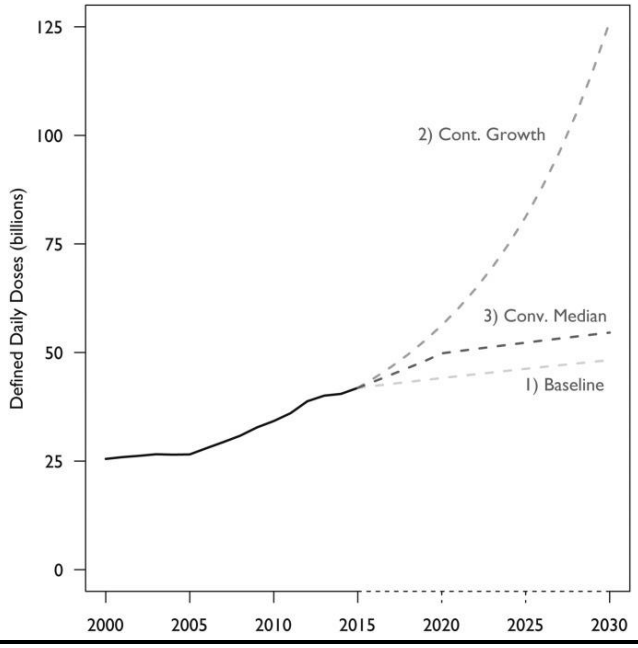

Figure 3: Projections for the global antibiotics consumption from 2015-2030.[2]

Several advances in API crystallization process design and control have occurred over the last couple of decades. The development of real-time monitoring and emerging commercial software for the crystallization process, such as gCRYSTAL®,[7] DynoChem®,[8] and COMSOL Multiphysics® software[9] have greatly improved the process design progress. Process-modelling software permits more effective design and operation of crystallizers, and facilitates the optimization of seeding, operation profiling, and scaling up.[10] Differences in lab-scale and industrial scale crystallization pose scale-up challenges in areas such as hydrodynamics, heat, mass transfer performance, and so forth. Scaling up can lead to changes in nucleation, growth, breakage and agglomeration and will affect crystal qualities.[11] New types

of crystallization processes have also been proposed, including membrane crystallization[12] and supercritical fluid crystallization.[13] Wherein membrane crystallization a membrane is utilized acting as a selective gate for solvent evaporation, modulating the final degree and the rate for the generation of the supersaturation.[14] In supercritical fluid crystallization supercritical fluids are used as solvents or antisolvents. In both solvent and antisolvent cases, an expansion of a solution is used to create supersaturation, which in turn is the driving force for nucleation and growth of the solute. The selection of a specific type of crystallization process mostly depends on the features of the model API.

Attempts have been made to better understand process mechanisms, constraints and the effect of disturbances, process uncertainties, and model/process mismatches in order design robust crystallization processes able to adhere to regulations while maximizing profitability. By combining crystallization process modelling and control with optimization algorithms, model-based control strategies can be developed to provide tight quality control in the presence of uncertainties and disturbances, while requiring fewer experiments.[11,15–18] Model-based optimization is subject to the constraints of the system, for crystallization these constraints may be control variable limits like temperature or pH at which API degradation occurs if the constraints are not satisfied. For crystallization typical objective functions for model-based optimization include maximizing the product yield and mean crystal size, or minimizing batch/residence time and narrowing the width of the crystal size distribution (CSD). Other possibilities include minimizing cost or maximizing total profit.[19–22]

1.3. Ampicillin use and discovery

Penicillin and β-lactam antibiotics, in general, were the first antibiotics to be discovered. The discovery of antibiotics marks one of the most important achievements in human history. The use of antibiotics has resulted in immeasurable benefits to medicine, phycology and biology.[23] Ampicillin is a broad-spectrum, semi-synthetic, β-lactam antibiotic with bactericidal activity. Ampicillin is commonly used to treat various bacterial infections such as urinary and respiratory tract infections, it is one of the ten most consumed antibiotics worldwide. Doyle et al. first synthesised ampicillin in 1962, the synthesis involved the reaction of ice-cold solutions of D(−)-α-benzyloxycarbonylamino-α-phenylacetic acid and 6-aminopenicillanic acid, producing the intermediate 6-[D(−)-α-(benzyloxycarbonylamino)-α-phenylacetamido]penicillanic acid, which was separated and hydrogenated over a palladium catalyst in order to produce ampicillin.[24] After extensive research ampicillin was shown to be very acid-stable, well absorbed and effective at low minimal inhibitory concentration against a wide variety of Gram-negative as well as Gram-positive organisms. Ampicillin binds to and inactivates penicillin-binding proteins (PBP) located in the inner membrane of the bacterial cell wall interfering with the cross-linkage of peptidoglycan chains necessary for bacterial cell wall strength and rigidity. This results in the weakening of the bacterial cell wall and causes cell lysis. Ampicillin is stable against hydrolysis by a variety of β-lactamases, therefore, can be used in a wide range of gram-positive and -negative infections. In a recent report the World Health Organization (WHO) characterized penicillins as critically important and high priority antimicrobials essential for the world healthcare system.[25] Due to its significant societal importance it is crucial that ampicillin is manufactured efficiently and at high capacity in order to satisfy the increasing global demand.

1.4. Ampicillin industrial production methods

1.4.1. Chemical route for ampicillin synthesis

Ampicillin before the 1990s was traditionally produced via a chemical route.[26] The main reaction was condensing 6-aminopenicillanic acid (6-APA) with a protected α-phenylglycine (PG). In order to protect the α-phenylglycine a large amount of protection-deprotection reactions were performed. As a result, highly reactive derivatives of PG were used such as phenylglycine chloride hydrochloride which is highly unstable. Moreover, very low temperatures (-30 °C), anhydrous conditions and the use of toxic compounds like pyridine, dimethylaniline and dichloromethane were required. As a result the whole process generated considerable amounts of waste that required complicated disposal procedures.[27,28] All of the above describe a process with high economic and environmental consequences. For that reason, alternative methods of β-lactam production were investigated leading to the discovery of the enzymatic synthesis route.

1.4.2. Enzymatic based ampicillin synthesis

Enzyme based synthesis routes are acknowledged as an environmental-friendly approach, avoiding organochloride solvents and operating at room temperatures.[29] Kinetically controlled synthesis using immobilised penicillin G acylase (PGA) in aqueous environment, with the simultaneous crystallization of the product, is an approach that has been rigorously researched in recent years.[1,3,15,30]

PGA, the biocatalyst for the reaction, is a high monetary value compound. In order to avoid the enzyme losses downstream and/or the need for frequent enzyme separation and recycling processes, immobilizing the enzyme prior to industrial use is preferred to maintain the profitability of the process. The enzyme is covalently immobilized with insoluble matrix beads or particles being the conventional solution.[29,31] PGA is one of the few biocatalysts to be used immobilized in large scale industrial processes.[32]

The overall enzymatic reaction scheme for ampicillin is presented in Fig. 4 and it consists of three distinct reactions. The main reaction producing ampicillin is the condensation of 6-APA with D-phenylglycine methyl ester (PGME) which serves as the acyl-donor. The reaction produces ampicillin and methanol (MeOH) as a by-product. Apart from ampicillin many other antibiotics such as amoxicillin, cephalexin and other cephalosporins can be synthesised using different acyl-donors with PG.[29]

Apart from catalysing the main reaction PGA also catalyses the two hydrolysis reactions. The primary hydrolysis reaction is the hydrolysis of PGME into PG and MeOH, while the secondary hydrolysis reaction is the hydrolysis of ampicillin into PG and 6-APA. This reaction scheme is a classic example of a kinetically controlled synthesis in which ampicillin is the intermediate product in a set of series-parallel reactions.[29] While PGA is essential for the reaction, it acts as either a transferase, transferring the acyl-group thus catalysing the synthesis reaction or a hydrolase catalysing the undesirable hydrolysis reactions. Therefore, the economic feasibility of the synthesis route depends to a large extent on the reactor operational conditions optimization. The main goal of such an optimization is to maximize the selectivity of ampicillin while decreasing the primary and secondary hydrolysis rates.

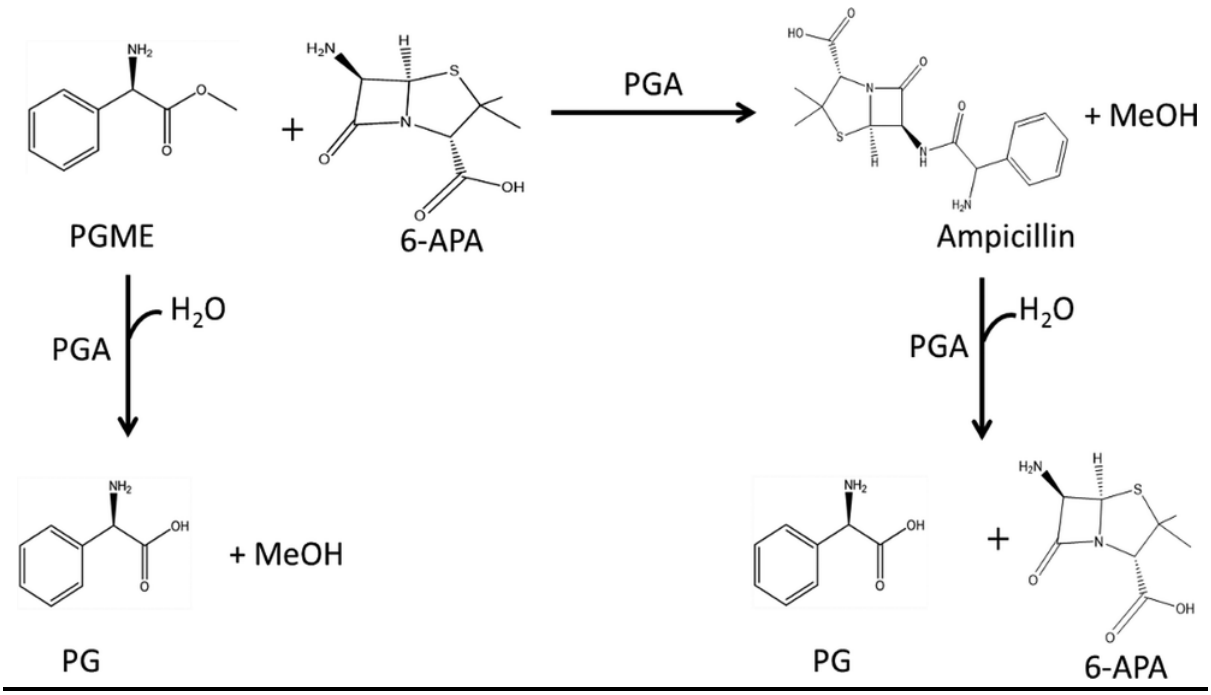

Figure 4: Enzymatic synthesis of ampicillin.[3]

1.5. Ampicillin batch crystallization

Crystallization is a particularly suitable technique when the recovery and separation of pharmaceutical products with relatively low solubility in water, such as ampicillin, is concerned. Because ampicillin is a large molecule, low diffusivity and high steric hindrance is observed resulting in the crystallization rate being relatively low. For this reason optimizing the crystallization process is of high importance.[33] Variations in the crystalline structure can cause significant changes in the physical and chemical properties between the different polymorphs, such as hardness, solubility, density, melting range, stability, among others. It is of grave importance that the API is crystallized in the preferred polymorphic form. The presence of an undesirable polymorph can reduce the bioavailability of the drug, reducing its effects. In the literature several case studies have been reported where variations in the polymorphic form of an API resulted in reduced bioavailability and stability of the final product causing product clinical failures and product recalls.[34] The literature reports that ampicillin can exist in two anhydrous polymorphic forms (I and II) and two hydrated forms (monohydrated and trihydrated).[35]A study between the deferent polymorphs found that the monohydrate form appears to be amorphous, though it has the appearance of crystals. The zwitterionic form of ampicillin is present in significant concentrations at physiological pH increasing as the pH is decreased. In the Trihydrate and anhydrous form I, ampicillin zwitterions are stabilized by a complex network of H-bonds involving the amine group. The presence of zwitterions in the solid state can be related to their stabilization by crystal packing. The anhydrous form II also suggests that zwitterions are present though a looser crystal size is observed, with a possible distortion of the H-bond system. For form II the exact structure is not yet known.[35]

The preferred polymeric form is ordinarily the most stable form in order to prevent polymorphic alterations during manufacturing, delivery, or storage. In general, the selected polymorph should be thermodynamically stable during the drug development process and remain stable during the manufacturing process too.[36] Ampicillin trihydrate is the most stable form in pure water at room temperature among the polymorphs and it is the polymorphic form present in commercial products.

One of the most important parameters influencing ampicillin production and crystallization is pH. Ampicillin has limited chemical stability at and below pH 5, under such conditions, degradation products are formed and the main degradation product identified is ampicillin penilloic acid.[15] PGA exhibits the highest activity for pH values above 8 but in spite of this, the optimum pH for the synthesis of antibiotics departing from ester acyl derivatives is between 6.0 and 6.5. That is because at lower pH values the main reaction is favored and the production of ampicillin is higher than the byproducts, this increase in ampicillin production compensates the decrease in productivity due to lower enzyme activity.[29,30] This result also favors ampicillin crystallization because the solubility of ampicillin and β-lactams in general increases with pH, so a reactor pH in the range of 6.0 and 6.5 makes the subsequent crystallization process more straightforward because the solution will already be supersaturated and a smaller pH gradient will be required to induce crystallization. Furthermore reactive crystallization reactor configurations have been illustrated recently in the literature allowing for simultaneous ampicillin synthesis and crystallization.[30,37]

Due to the high dependency of ampicillin solubility on pH, it is possible to crystallize ampicillin in a batch crystallizer altering the pH in a specific pH range. It has been shown that the pH should be lower than 8 allowing ampicillin to crystallize in its trihydrate form.[38] Overall strongly basic conditions are unfavourable because large amounts of product will remain in the solution.[30] This behavior is due to the low solubility of the zwitterionic form in water.[28] At values of pH near the isoelectric point the solubility is lower with the overall solubility curve having a distinctive U shape. Extremely high supersaturations are generally undesirable in crystallization processes because they induce uncontrolled nucleation leading to small crystals and incorporation of impurities, moreover it usually results in broad CSDs which is highly unfavourable. Seed crystals promote secondary nucleation which should occur at significantly lower supersaturations than primary nucleation. Finally, in cases where several solutes are present the use of seed crystals enable to selectively crystallize the desirable product, therefore negating the need for subsequent product recovery and purification.[3]

1.6. This work

In this work a recently published model on ampicillin crystallization kinetics is utilized.[1] Based on the model, dynamic simulation of ampicillin batch crystallization under a variety of conditions for design space investigation is performed. The crystallization of ampicillin is simulated for different linearly decreasing pH profiles varying the pH change rate and the initial and final pH values. For each scenario, the mother solute concentration as a function of time and the final mean crystal size are computed. From every scenario the optimal profile, that was able to replicate more accurately the published results, was identified. Afterwards, dynamic pH profile optimization studies are performed. The objective is to minimize the objective function consisting of weighted CSD quality attributes subject to various constraints, such as the final mother liquor solute concentration. The optimization studies are performed using the orthogonal collocation on finite elements method.[39] The fmincon MATLAB algorithm is

employed to solve the Non-Linear Programming (NLP) problem. Results from each optimization strategy are obtained and discussed. Finally, Pareto fronts exhibiting the tradeoff relationship between different objectives and constraints are detailed.

2. Methods

2.1. Batch crystallization model for ampicillin

The crystallization kinetics of ampicillin have been researched in the literature.[1,15,33] A recent article presents a kinetic model which has been validated for multiple experiments and starting conditions. The model takes into account primary, secondary nucleation and the use of seed crystals. The model utilizes the method of moments consisting of 5 ordinary differential equations (ODEs) using seven estimated parameters. The model is able to predict the supersaturation curve as well as the final mean crystal size of the crystals. In this work that particular article was used because it allows for the examination of different crystallization design options and different optimization objective functions.[1]

The batch crystallization assumes a clear and homogenous feed mother liquor stream. It is assumed that crystal breakage and agglomeration do not take place. Moreover, crystal growth is assumed size-independent, this assumption coincides is McCabes's ΔL law, where all crystals that are geometrically similar and of the same material in the same solution grow at the same rate and the growth is measured on the basis of increase in length ΔL. In essence it is assumed that crystal growth is independent of the size of the crystals at any time point.

The batch crystallization model describes crystallization kinetics, API solubility, crystal population balances and process mass balances. The model takes into account potential seeding of the crystallizer providing results for both seeded and unseeded scenarios. The simultaneous solution of these equations describes the batch crystallization. During the dynamic simulations the model is solved in MATLAB using ode113. While for the dynamic optimization the DynOpt dynamic optimization code is utilized using MATLAB's fmincon solver as the NLP solver.[39]

2.2. Crystallization kinetics

Crystal growth and nucleation kinetics are described by the following equations:

$$G(t) = k_G (SS(t) - 1)^g \quad (1)$$

$$B_1(t) = k_{B1} \exp\left(\frac{-B_0}{\ln(SS(t)^2)}\right) \quad (2)$$

$$B_2(t) = k_{B2} M(t)^b (SS(t) - 1)^s \quad (3)$$

$$J(t) = B_1(t) + B_2(t) \quad (4)$$

wherein G is the crystal growth rate, B_1 and B_2 are the primary and secondary nucleation rates in the crystallizer at supersaturation SS respectively. J is the overall nucleation rate of ampicillin crystals in the system. M corresponds to the mass of crystals inside the crystallizer calculated from:

$$M(t) = ([Amp]_0 - [Amp]_t) \cdot m \quad (5)$$

wherein [Amp_0] is the initial ampicillin concentration and [Amp_t] is the concentration of ampicillin in the solute at a specific time *t*. Finally, *m* is the mass of the mother liquor solution. The crystallization kinetics are calculated with regards to the system supersaturation *SS* calculated from the equation:

$$SS\,(t) = \frac{[Amp](t)}{[Amp^*](t)} \tag{6}$$

wherein [*Amp*] is the concentration of ampicillin in the solute and [Amp^*] is the solubility of ampicillin. Growth kinetic parameters are k_G, the growth rate constant and *g*, the growth rate exponent. Nucleation kinetic parameters are B_0, the primary nucleation constant, k_{B1}, the primary nucleation rate constant, k_{B2}, the secondary nucleation rate constant, *b*, the secondary nucleation mass of crystals exponent and *s*, the secondary nucleation saturation exponent. Crystallization kinetic parameters are summarized in Table 1.

Table 1: Crystallization kinetics model parameters.[1]

Symbol	Value	Units
k_G	$8.95 \cdot 10^6$	m min^{-1}
g	1.87	–
B_0	1.27	–
k_{B1}	$5 \cdot 10^{10}$	# crystals $(g/kg)^{-1}$ min^{-1}
k_{B2}	$2.2 \cdot 10^9$	# crystals $(g/kg)^{-1}$ min^{-1}
b	0.6	–
s	1.37	–

2.3. Ampicillin solubility

2.3.1. Solid-Liquid equilibrium

Ampicillin features in its molecular form one amine and one carboxylic acid that participate in protonation equilibria. For that reason, ampicillin can exist in the solution in four different forms: non-ionized [*Amp*], anion [Amp^-], cation [Amp^+] and zwitterion [$Amp^\pm$]. A model describing the solubility of ampicillin is required in order to accurately model the crystallization. The solubility of ampicillin is calculated based on a resently published article proposing a new model for amino acid and β-lactam solubility.[40] The model associates the solubility at any *pH* with that at the isoelectric point, *pI*. It uses the dissociation constants as well as extended Pitzer parameters to model the solubility thus taking into account the non-ideal nature of the solution.

From the basics of thermodynamics, the condition for solid-liquid equilibrium for any system, in which the solid phase is unique and contains only molecules of solute, is:

$$\mu_i^S = \mu_i^L \tag{7}$$

wherein μ_i^S and μ_i^L are the chemical potentials of solute *i* in the solid and liquid phase respectively. Neglecting the effect pressure has on chemical potential and assuming isothermal conditions, the chemical potential of the solid phase remains constant. Thus, the chemical potential of the liquid phase

must also remain constant meaning that the *pH* value does not affect the solute chemical potential in the liquid phase.

Using the molality scale to calculate μ_i^L:

$$\mu_i^L = \mu_i^* + RT \ln \frac{\gamma_i m_i}{m^*} \tag{8}$$

wherein μ_i^* is the standard state chemical potential of solute *i* in a hypothetical ideal solution with unit concentration (m^* = 1.0 mol kg^{-1}), γ_i is the activity coefficient of solute *i* and m_i is the molality of *i* in the liquid phase.

The fact that the solid phase is electrically neutral leads to the conclusion that only the electrically neutral forms of ampicillin participate in the equilibrium, so it can be argued that the activity of electrically neutral molecules of ampicillin is constant with any variation of *pH*.[40] The experimentally determined solubility derives from the concentration of all forms of ampicillin irrespective of the ionization state. For this reason, a parameter is needed to connect the molality of the electrically neutral forms, which are the ones needed for the phase equilibrium, with the solubility of ampicillin:

$$m_0(pH) = \varphi_0(pH) S(pH) \tag{9}$$

wherein m_0 is the molality, φ_0 is the fraction of the electrically neutral molecules of ampicillin and *S* is the solubility of ampicillin at given *pH*.

Because the activity of electrically neutral forms is constant at any *pH*, its value can be considered equal to the value at the isoelectric point *pI*. Due to this effect an equation connecting the solubility at any *pH* with the solubility at the isoelectric point *pI* can be achieved:

$$S(pH) = \frac{\gamma_0(pI)\, \varphi_0(pI)\, S(pI)}{\gamma_0(pH)\, \varphi_0(pH)} \tag{10}$$

wherein γ_0 is the activity coefficient for the electrically neutral ampicillin forms.

2.3.2. Henderson-Hasselbach equations

In an aqueous solution the following chemical equilibria occur:

$$[Amp] \leftrightarrow [Amp^{\pm}] \tag{11}$$

$$K_D = \frac{[Amp^{\pm}]}{[Amp]} \tag{12}$$

$$[Amp^{\pm}] \leftrightarrow [Amp^{-}] + H^+ \tag{13}$$

$$K_{A1} = \frac{[Amp^{-}][H^+]}{[Amp^{\pm}]} \tag{14}$$

$$[Amp^{+}] \leftrightarrow [Amp^{\pm}] + H^+ \tag{15}$$

$$K_{A2} = \frac{[Amp^{\pm}][H^+]}{[Amp^{+}]} \tag{16}$$

wherein K_D is the equilibrium constant of neutral molecules, K_{A1} the equilibrium constant of the carboxylic acid protonation and K_{A2} the equilibrium constant of the amine protonation.

The value of K_D is so high that for all intents and purposes the non-ionized molecules are considered inexistent in the solution. Following this assumption, the fraction of the ionized species of each reaction can be calculated using the Henderson-Hasselbach equations.

For the carboxylic acid protonation reaction:

$$pH = p_{K_{A1}} + \log\left(\frac{[Amp^-]}{[Amp^\pm]}\right) \Rightarrow [Amp^-] = [\mathrm{Amp}^\pm]\cdot 10^{pH-p_{K_{A1}}} \tag{17}$$

$$\alpha_{[Amp^-]}(pH) = \frac{[Amp^-]}{[Amp^-] + [Amp^\pm]} = \frac{10^{pH-p_{K_{A1}}}}{1 + 10^{pH-p_{K_{A1}}}} \tag{18}$$

For the amine protonation reaction:

$$pH = p_{K_{A2}} + \log\left(\frac{[Amp^\pm]}{[Amp^+]}\right) \Rightarrow [Amp^+] = \frac{[Amp^\pm]}{10^{pH-p_{K_{A2}}}} \tag{19}$$

$$\alpha_{[\mathrm{Amp}^+]}(pH) = \frac{[Amp^+]}{[Amp^+] + [Amp^\pm]} = \frac{1}{1+10^{pH-p_{K_{A2}}}} \tag{20}$$

wherein $\alpha_{[\mathrm{Amp}^-]}(pH)$ and $\alpha_{[\mathrm{Amp}+]}(pH)$ are the fractions of the ionized species for each reaction at the respective *pH*. Now the fraction φ of each species in the solution can be calculated.

$$\varphi_{[\mathrm{AMP}]} = \left[1 - \alpha_{[\mathrm{Amp}^-]}(pH)\right]\left[1 - \alpha_{[\mathrm{Amp}^+]}(\mathrm{pH})\right] \tag{21}$$

$$\varphi_{[\mathrm{AMP}^\pm]} = \alpha_{[\mathrm{Amp}^-]}(\mathrm{pH}) \cdot \alpha_{[\mathrm{Amp}^+]}(pH) \tag{22}$$

$$\varphi_{[\mathrm{AMP}^-]} = \alpha_{[\mathrm{Amp}^-]}(\mathrm{pH})\left[1 - \alpha_{[\mathrm{Amp}^+]}(pH)\right] \tag{23}$$

$$\varphi_{[\mathrm{AMP}^+]} = \left[1 - \alpha_{[\mathrm{Amp}^-]}(pH)\right]\alpha_{[\mathrm{Amp}^+]}(pH) \tag{24}$$

From the above expression $\varphi_{[\mathrm{AMP}]}$ and $\varphi_{[\mathrm{AMP}^\pm]}$ correspond to the fraction of electrically neutral ampicillin, so either of those can be used as an input in Eq. (10). Simply for numerical reasons Franko et al[40] chose to use $\varphi_{[\mathrm{AMP}^\pm]}$. Eq. (10) takes into account for liquid phase non-ideality with the γ_0 activity coefficient for the electrically neutral ampicillin forms. In order to calculate γ_0 the extended Pitzer model developed by Filho et al. was used.[41] This method is appropriate for ampicillin, where the electrically neutral form is the zwitterion.

2.3.3. Extended Pitzer model

In presenting the extended Pitzer model one starts with the expression of the activity coefficient. For a solute i in an electrolyte aqueous solution, the natural logarithm of the activity coefficient is given by the sum of a term due to long range interactions (LR) and one due to short range interactions (SR):

$$\ln \gamma_i = \ln \gamma_i^{LR} + \ln \gamma_i^{SR} \tag{25}$$

In this particular case the γ_0 of the zwitterion is needed. The expression of the long-range term is multiplied by the net charge, but the zwitterion has no net charge, for this reason the long-range term on the above equation is null. The short-range interactions are calculated by:

$$\ln \gamma_i^{SR} = 2\sum_{j \neq s} \lambda_{ij}(I) m_j + 3\sum_{j \neq s}\sum_{k \neq s} \Lambda_{ijk} m_j m_k - z_i^2 M_s \sum_{j \neq s}\sum_{k \neq s} \lambda_{ij}^{(1)} \frac{1}{a^2 I^2} \cdot \left[1 - \left(1 + a\sqrt{I} + \frac{a^2 I}{2}\right)\exp\left(-a\sqrt{I}\right)\right] m_j m_k \quad (26)$$

wherein M_S is the molar mass of solvent in kg mol^{-1}, a is a universal parameter equal to 2.0 kg$^{1/2}$mol$^{-1/2}$, Λ_{ijk} is the three-body interaction coefficient and λ_{ij} is the two-body interaction coefficient.
The λ_{ij} depends upon the ionic strength:

$$\lambda_{ij}(I) = \lambda_{ij}^{(0)} + \lambda_{ij}^{(1)} \frac{2}{a^2 I^2}\left[1 - \left(1 + a\sqrt{I}\right)\exp\left(-a\sqrt{I}\right)\right] \quad (27)$$

The ionic strength is defined as:

$$I = \frac{1}{2}\sum_i m_i z_i^2 \quad (28)$$

At this point some significant simplifications are made. Firstly, the three body interactions are neglected ($\Lambda_{ijk} = 0$, for any i, j, k). Secondly the dependence of λ_{ij} to the ionic strength I is neglected. Finally, a correlation between λ_{ij} and temperature T is introduced, using the minimum of adjustable parameters for which a theoretical justification can be provided.
According the aforementioned simplifications the simplified equations are:

$$\ln \gamma_i = \ln \gamma_i^{SR} = 2\sum_{j \neq s} \lambda_{ij}(T) m_j \quad (29)$$

$$\lambda_{ij}(T) = A_{ij} + \frac{B_{ij}}{T} \quad (30)$$

It is apparent that four different λ_{ij} exist: $\lambda_{[Amp]}$, $\lambda_{[Amp^+]}$, $\lambda_{[Amp^-]}$, $\lambda_{[Amp^\pm]}$. The empirical observation of the antibiotic solubility curves as a function of pH reveals a symmetry around the isoelectric point. This allows for the assumption that the interactions among the neutral and charged molecules are indistinguishable, i.e., an electrically neutral molecule interacts the same way with a positive or negative charged molecule. Therefore, it is assumed that:

$$\lambda_{[Amp]} = \lambda_{[Amp^+]} = \lambda_{[Amp^-]} = \lambda_{[Amp^\pm]} = \lambda \quad (31)$$

Thereby, Eq. (10) can be rewritten using the extended Pitzer model.

$$\ln \frac{S(pH)}{S(pI)} = \ln \frac{\varphi_{[AMP^\pm]}(pI)}{\varphi_{[AMP^\pm]}(pH)} + 2\lambda[S(pI) - S(pH)] \quad (32)$$

By replacing Eq. (21)-(24) into Eq. (32) the final expression of ampicillin solubility as a function of pH is reached:

$$\log\frac{S(pH)}{S(pI)} = pI - pH + \log\left[\frac{1+10^{pH-p_{K_{A1}}}}{1+10^{pI-p_{K_{A1}}}}\right] + \log\left[\frac{1+10^{pH-p_{K_{A2}}}}{1+10^{pI-p_{K_{A2}}}}\right] + \frac{2}{\ln 10}\lambda[S(pI) - S(pH)] \quad (33)$$

Finally, the physical meaning of the λ_{ij} should be discussed. With the use of statistical thermodynamics methods like the Mc-Millan-Mayer and DLVO theories, a physical meaning of the parameters A_{ij} and B_{ij} can be reached. Assuming that every form of ampicillin has the same van der Waals diameter σ and that the magnitude of van der Waals interaction parameter between the zwitterionic and the other forms is the same, the following expression can be reached:

$$\ln\frac{S(\text{pH})}{S(\text{pI})} = \ln\frac{\varphi_{[\text{AMP}^{\pm}]}(\text{pI})}{\varphi_{[\text{AMP}^{\pm}]}(\text{pH})} + \frac{4\pi\sigma^3 N_A\rho}{3}\left(1 - \frac{\varepsilon}{k_B T}\right)[S(\text{pI})\text{-}S(\text{pH})] \quad (34)$$

Comparing Eq. (32) and (34) the following expressions can be deduced:

$$A_{ij} = \frac{2\pi\sigma^3 N_A\rho}{3} \quad (35)$$

$$B_{ij} = -A_{ij}\frac{\varepsilon}{k_B} \quad (36)$$

The values of A_{ij} and B_{ij} have to be regressed from experimental data in order to calculate λ_{ij}. In the literature[1] ampicillin solubility data were regressed using the authors own experiments as well as experimental data from other publications.[28,42] The solubility model parameters are presented in Table 2.

Table 2: Parameters for the extended Pitzer and solubility models at 298.15 K.

Symbols	Value	Units	Reference
A_{ij}	11.05	$(\text{kg/mol})^{\frac{1}{2}}$	(1)
B_{ij}	$-3.71\cdot10^{3}$	$(\text{kg/mol})^{\frac{1}{2}}$	(1)
σ	$5.42\cdot10^{-10}$	m	(1)
ε/k_B	336.18	K	(1)
λ_{ij}	-1.42	kg/mol	(1)
$p_{K_{A1}}$	2.14	-	(28)
$p_{K_{A2}}$	7.31	-	(28)
pI	$[p_{K_{A1}}+p_{K_{A2}}]/2=4.725$	-	-
$S(pI)$	0.018	mol/kg	This work

The parameters presented on Table 2 are used in Eq. 33 to calculate the solubility of ampicillin with respect to *pH*. Eq. 33 is an implicit function with respect to the solubility of ampicillin. For this reason, in the case of dynamic simulations it is solved numerically utilizing the fzero MATLAB function, Eq. 33 was solved in the pH range of 5-8 and the solubility curve produced from the solubility model is

presented in Fig. 5. The $S(pI)$ was not explicitly mentioned in the Encarnacion-Gomez article but the solution of Eq. 33 was reported in figure form. $S(pI)$ was selected so that Fig. 5 replicated accurately the reported solubility graph.

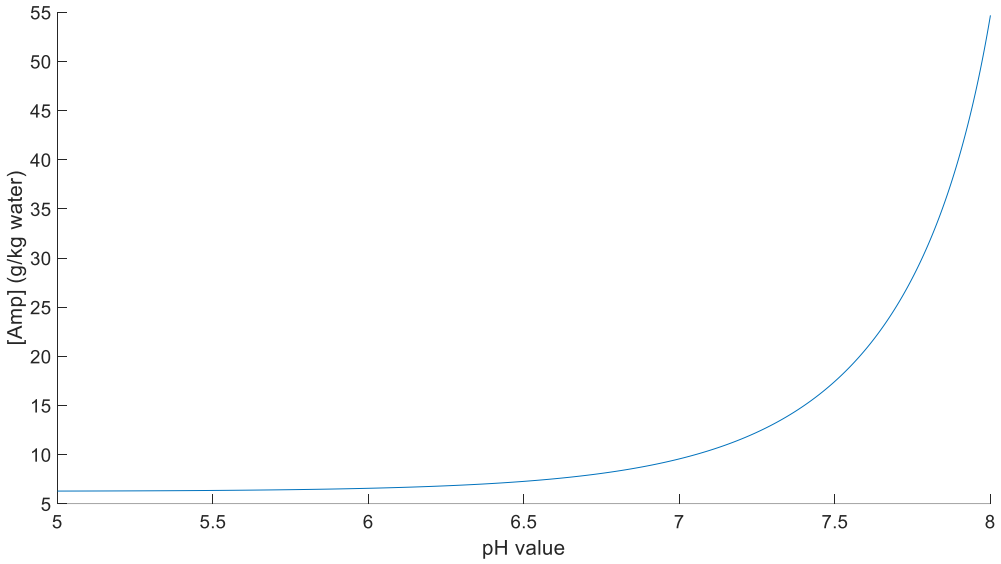

Figure 5: Solution of Eq. 33 using the parameters of Table 2 for pH 5-8.

The calculated solubility curve presented in Fig. 5 was compared to the reported solubility curve and it was established that they match sufficiently. It should be noted that the authors[1] regressed the solubility model with experimental data with pH 5-7.5 and then they proceeded to use the solubility model for values of higher pH.

In the case of dynamic optimization the analytical derivatives for the ODEs, constraints and objective function are required in order to enhance result accuracy and limit run times. A numerical solution of Eq. 33 could not be implemented and an approximation of the solubility was necessary. In Fig. 5 it is apparent that the solubility curve reminds of an exponential function. For this reason, it was decided that the approximation should incorporate an exponential function. The approximation function used was:

$$[Amp^*](pH) = a_s\, e^{b_s\, pH} + c_s\, e^{d_s\, pH} \tag{37}$$

wherein $[Amp^*]$ the solubility of ampicillin, a_s, b_s, c_s and d_s the approximation parameters regressed using the MATLAB curve fitting toolbox.

In Fig. 5 when pH 7.5-8.0 the solubility increases rapidly, increasing the error in the approximation if the whole pH range is used. For this reason, to increase the approximation accuracy two different approximations where performed. An approximation for pH 5.0-7.5 and one for pH 7.5-8.0.
The approximation parameters for each case are presented in Table 3:

Table 3: Solubility curve approximation parameters.		
Symbols	**pH 5.0-7.5**	**pH 7.5-8.0**
a_s	5.741	0.007054
b_s	0.01684	1.013
c_s	$6.25\ 10^{-8}$	$9.08\ 10^{-15}$
d_s	2.531	4.469

The relative error between the solubility model and the solubility calculated from the approximation was defined as:

$$Approx_{\text{Error}}\ (\%) = 100\ \frac{\left|S_{\text{model}} - S_{\text{approx}}\right|}{S_{\text{model}}} \tag{38}$$

wherein $Approx_{\text{Error}}$ is the relative error in the approximation, S_{model} is the solubility calculated from Eq. 33 and S_{approx} the solubility calculated from Eq. 37. The $Approx_{\text{Error}}(pH)$ curve is presented in Fig. 6 where it is shown that the maximum approximation error is below 1.5%.

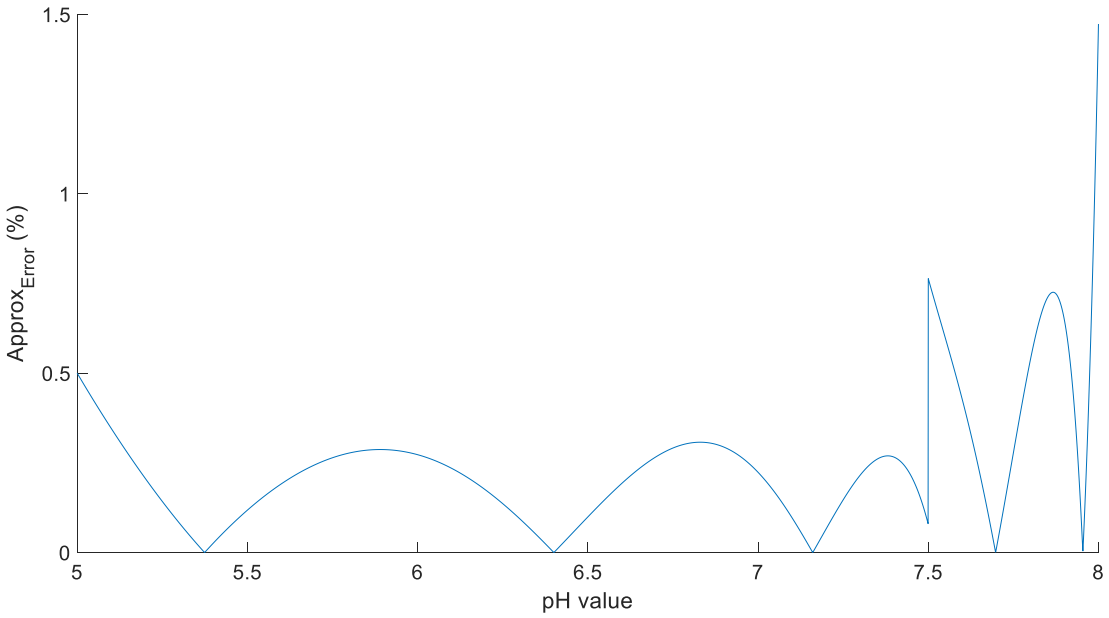

Figure 6: Solubility approxiamation relative error (%) for pH 5-8.

2.4. Population and mass balance equations

The population balance equation serves as the basis for characterising the CSD in suspension crystallization systems. If agglomeration and breakage are neglected the population balance for a batch or semi-batch crystallizer with no net inflow or outflow of crystals can be written as:

$$\frac{\partial n(t,L)}{\partial t} = -\frac{\partial\left(G(t)n(t,L)\right)}{\partial L} \tag{39}$$

wherein $n(t, L)$ is the population density based on the total operating volume of the crystallizer, G is the crystal growth rate and L is the total length of crystals based on the total operating volume of the crystallizer.

Boundary condition $n(t, 0)$ for Eq. 39 is the nuclei population density, while the initial condition $n(0, L)$ is the population balance n_0 at $t = 0$.

$$n(t,\ 0) = \frac{J(t)}{G(t)} \tag{40}$$

$$n(0,\ L) = n_0 \tag{41}$$

In the case for seeded crystallization n_0 is the population density of the initial crystallizer seeding, while for the case of unseeded crystallization the initial condition is zero.

The bulk solute concentration $[Amp](t)$ is calculated from the mass balance with the assumption that in general the volume occupied by the crystals is much smaller than the volume of the mother liquor.

$$\frac{\mathrm{d}[Amp]}{\mathrm{d}t} = -\ \frac{\mathrm{d}m_\mathrm{T}}{\mathrm{d}t} \tag{42}$$

wherein m_T is the crystal suspension density.

In this work the crystallizer is considered isothermal at a steady temperature of 298.15 K. Crystallization is induced only due to the solubility gradient provided by the pH variance.

To determine the CSD and $[Amp](t)$ of the system Eq.1- 6, 33 and 39- 42 (the crystallization kinetics, solubility equation, population and mass balances) should be solved simultaneously. Eq. 39 is a non-linear first-order partial differential equation and the nucleation and growth kinetics are included in Eq. 39 as well as in the boundary conditions. In order to reduce computational difficulties, the method of moments is utilized so as to transform the population balance into a system of ordinary differential equations.[43] In accordance with the method of moments the population balance is multiplied with L^i and subsequently integrated in order to yield equations consisting of moments (m_i) of $n(t, L)$.

$$\frac{\mathrm{d}m_\mathrm{i}}{\mathrm{d}t} + \int_0^\infty L^\mathrm{i}\ \frac{\partial}{\partial L}\ (G\,n)\ \mathrm{d}L \tag{43}$$

$$\frac{\mathrm{d}m_0}{\mathrm{d}t} = J \tag{44}$$

$$\frac{\mathrm{d}m_1}{\mathrm{d}t} = G\,m_0 \tag{45}$$

$$\frac{\mathrm{d}m_2}{\mathrm{d}t} = 2\ G\,m_1 \tag{46}$$

$$\frac{\mathrm{d}m_3}{\mathrm{d}t} = 3\ G\,m_2 \tag{47}$$

wherein m_0, m_1, m_2, m_3 the zeroth, first, second and third moment of the population balance respectively and i is the number of each moment.

Finally, the mass balance can be expressed in terms of the moments:

$$\frac{\mathrm{d}[Amp]}{\mathrm{d}t} = -\rho_c k_V \frac{\mathrm{d}m_3}{\mathrm{d}t} = -3\rho_c k_V G m_2 \tag{48}$$

wherein ρ_c is the crystal density and k_v the crystal volume shape factor.

Using the method of moments, the problem is expressed via Eq. 43- 48, which can be solved with relative ease with an ODE solver in MATLAB like ode113. In order to solve the equations, the initial condition for the population balance should be expressed in accordance with the moments.

Every moment of the population balance holds a physical significance; m_0 represents the total number of crystals per unit volume, m_1 the total crystal length per unit volume, m_2 the total crystal surface area per unit volume and m_3 the total crystal volume per unit volume.[44,45] For unseeded experiments the initial conditions for the moments is zero while for seeded experiments the initial values for the moments should be calculated.[46]

$$M_C = k_V \rho_c L^3 \tag{49}$$

$$N_T = \frac{m_c}{Mc} \tag{50}$$

$$A_T = N_T k_a L^2 \tag{51}$$

$$V_T = N_T k_V L^3 \tag{52}$$

$$m_0(0) = \frac{N_T}{V_s} \tag{53}$$

$$m_1(0) = \frac{L\ N_T}{V_s} \tag{54}$$

$$m_2(0) = \frac{A_T}{k_a V_s} \tag{55}$$

$$m_3(0) = \frac{V_T}{k_V V_s} \tag{56}$$

wherein M_c the average mass of a single crystal, N_T the total number of crystals, A_T the total surface area of the crystals, V_T the total volume of the crystals, k_a the area shape factor of the crystals, k_V the volume shape factor of the crystals, L the length of the crystals, m_c the mass of seed crystals, V_s the volume of the mother solute. It should be noted that ρ the density of the mother liquor has been assumed to be 1kg/ L, since the crystallization is conducted in 25℃.

Through the division of the first moment with the zeroth moment, the mean crystal size of the crystals can be computed. Providing an indication on whether or not the crystallization is able to achieve the production of large crystals.

$$MCS(t) = \frac{m_1(t)}{m_0(t)} \tag{57}$$

wherein $MCS(t)$ is the mean crystal size for time t.

At the start of a seeded run seed crystals are present in the crystallizer. The properties for the seed crystals are presented in Table 4.

Table 4: Properties of ampicillin seed crystals.[1]

Symbol	Value	Units
$\bar{L}_{seed}$	74.00	μm
k_a	0.09	-
k_V	0.03	-
ρ_c	1500.00	kg m^{-3}

At this point it is important to mention a drawback of the method of moments. By transforming the problem, the CSD cannot be recovered and only the moments of the population balance are computed.

2.5. Dynamic optimization

2.5.1. Optimization method

The objective of dynamic optimization is to ascertain, in open loop control, a set of decision variable time profiles (pH, pressure, temperature, …) for a dynamic system that optimizes the objective function subject to specified constraints. The numerical methods used to find a deterministic solution of dynamic optimization problems can be grouped into two categories: indirect and direct methods. In this work a direct method for dynamic optimization (simultaneous strategy) has been performed. Orthogonal polynomials on finite elements were used to approximate the control and state trajectories allowing the continuous problem to be described in an NLP form. Implementation has been accomplished using the DynOpt package for MATLAB.[39] The DynOpt package provides a simple interface to dynamic optimization, while presenting the user with sufficient tools to perform optimization studies on any model. The DynOpt package has been used successfully in the literature to optimize different dynamic models.[39,47–49] Using the DynOpt package total discretization of both control and state variables is performed using Lagrange polynomials, the coefficients of those polynomials then become decision variables to a much larger NLP problem. In essence, the differential equations are converted into algebraic equations using the collocation on finite elements method. The final NLP problem consists of the converted ODEs, continuity equation for the state variables and any other equality and inequality constraints that may be required. The problem is then solved using an NLP solver achieving control profile dynamic optimization. In this work the fmincon NLP MATLAB optimization solver was utilized.

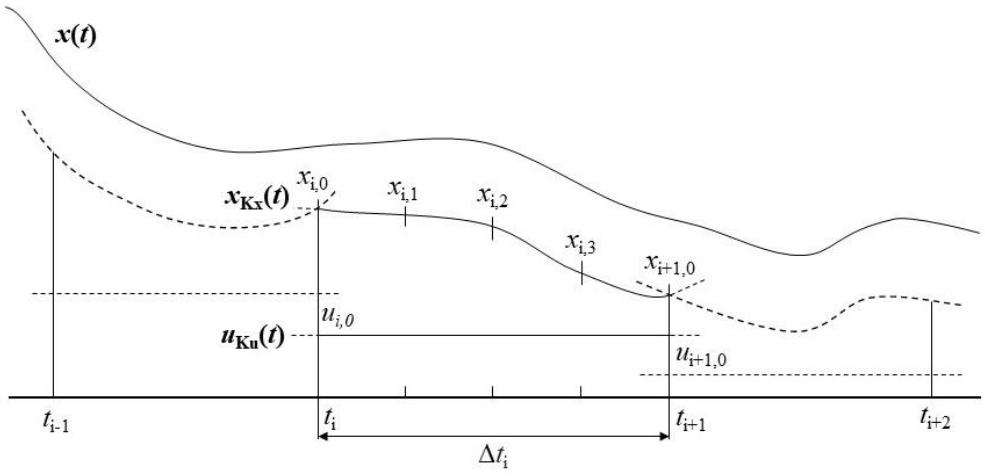

Figure 7: Graphical representation of the orthogonal collocation on finite elements method.

A graphical representation of the model is provided in Fig. 7. The time interval t is discretized into different t_i segments with each being of a length Δt_i, $u(t)$ is the control variable and $x(t)$ is the state variable matrix. In the graph the real value of $x(t)$ with regards to the changing control variable is presented as a solid line at the top. In the DynOpt code $x(t)$ is approximated over each element i, $t_i \leq t \leq t_{i+1}$ by a Lagrange polynomial. The approximation $x_{Kx}(t)$ is a (K_x+1) degree polynomial, wherein K_x is the number of collocation points. The same principle can be applied to u(t) where it is approximated by $u_{Ku}(t)$, a K_u degree polynomial, where in K_u is the number of collocation points. In Fig. 7 three collocation points $x_{i,1\text{-}3}$ are depicted for the state variable and two points $x_{i,0}$ and $x_{i+1,0}$ at the bounds of the time interval are specified. This accounts to five points in total between of which a fourth order

polynomial can be approximated. The locations of the collocation points are the shifted roots of Legendre polynomials. For u_{Ku} only the collocation points are used, as a result these profiles are constrained or bounded only at the collocation points. Meaning that if $K_u = 1$ the control variable is constant in each time interval making for a piece-wise constant (PWC) profile. If $K_u = 2$ the control variable is approximated with a line meaning a piece-wise linear (PWL) profile and so on. In this particular case the control variable corresponds to the $pH(t)$, while the state variables consist of the four moments of the population balance and $[Amp](t)$

This approximation of the state variables depending on the model and the amount of discretization may not be totally accurate, for this reason after the optimized profile for the control has been specified, it is advantageous to solve the model using that profile with an ODE solver and verify the accuracy of the DynOpt approximation.

2.5.2. Quality attributes of the crystalline product

The performance of batch crystallization as a unit operation can be assessed using different product qualities and characteristics. In general, the main goal of the process is to maximize the yield, while the crystals retain a tight CSD with a high MCS. Due to the implementation of the method of moments in order to solve the population balance, only the final moments of the population are known, thus the final CSD cannot be recovered. Methods to approximate and reconstruct the CSD exist and are discussed in the literature but they are beyond the scope of this work. Despite this problem the moments of the population allow for the calculation of parameters like the standard deviation STD and the coefficient of variation CV. These parameters directly express quality attributes and can be implemented in the optimization problems.[50]

One of the most important parameters is the final variance of the crystal size distribution given by:

$$\sigma^2 = \frac{m_2(t_f)}{m_0(t_f)} - \left(\frac{m_1(t_f)}{m_2(t_f)}\right)^2 \tag{58}$$

The standard deviation can then be calculated from:

$$STD = \sqrt{\frac{m_2(t_f)}{m_0(t_f)} - \left(\frac{m_1(t_f)}{m_2(t_f)}\right)^2} \tag{59}$$

The coefficient of variation (CV) can also be calculated from the moments of the distribution.

$$CV = \sqrt{\frac{m_2(t_f)\, m_0(t_f)}{m_1^2(t_f)} - 1} \tag{60}$$

Finally, the final MCS of the product is calculated from Eq. 57 at $t = t_f$.

In a utopic batch crystallization process the final product would exhibit a narrow CSD translating into low values of *CV*, σ^2 and *STD* while maintaining a high MCS. It should be noted that the *CV* is a

standardized measure of the dispersion of the distribution and it thus dimensionless. Moreover, the quality attributes detailed above can also be expressed using different combinations of the moments. In this work the lower moments (0^{th}, 1^{st} and 2^{nd}) where used to calculate quality attributes.

2.5.3. Objective function and constraints

There is a great deal of subtlety associated with selecting an objective function for batch crystallizers.[50] It may be difficult to correlate the cost of downstream processing to the CSD. As a result, usually it is not practical to use process economics to formulate an objective. In this work optimization of a seeded batch crystallization problem will be conducted. The initial condition for the moments of the CSD is given by the properties of the seeds. In order for the problem to be well posed and industrially relevant, it must be possible to apply production rate constraints to the process. For a seeded batch crystallizer this corresponds to specifying the final batch time (t_f) and a final value for the concentration of ampicillin that remains in the solution $[Amp](t_f)$. Finally, it is necessary to choose an objective function (f), which in this work will only incorporate properties of the crystal size distribution deems as essential quality attributes.

The following objective function was chosen:

$$\min_{pH(t),t_f} f(x, t_f) = W_\sigma \, \sigma^2 \; - \; W_{\mathrm{MCS}} \, MCS \tag{61}$$

wherein $f(x, t_f)$ the objective function calculated at final batch time t_f. The objective function aims to minimize the variance of the distribution while maximizing the *MCS*. W_σ and W_{MCS} are the respective weights for the two components of the objective function. In order for the two components to be the same order of magnitude σ^2 was scaled to the 10^{10} and MCS to 10^6. This objective function was deemed appropriate because it combines two of the essential quality attributes and it also proved to require less computational time to converge compared to other possible objective functions.

DynOpt[39] allows the user to apply constraints at the start, end and at the whole duration of the process. The constraints applied to the system were:

$$pH(t_0) > 7 \text{ constraint at } t_0 \tag{62}$$

$$[Amp](t_f) < target_{[Amp]} \text{ constraint at } t_f \tag{63}$$

$$SS(t) > 1 \text{ constraint } \forall t \tag{64}$$

The first constraint aims to maintain the physical meaning of the problem, ampicillin is produced at pH around 7-7.5, this constraint enforces that the system should start at a high pH value. The second constraint ensures that at the end of the batch time the desired amount of ampicillin, specified with $target_{[\mathrm{Amp}]}$, will have crystallized. The third constraint maintains the physical meaning of the model. In order to crystallize any product, the supersaturation *SS* should be greater than unity, this should be maintained for the duration of the process, or else the reverse effect will occur. Alarmingly if during the batch operation the supersaturation falls below unity, the model produces imaginary numbers which have no physical meaning. This constraint safeguards against such instance.

2.5.4. Optimization problem structure

In order to improve the accuracy of DynOpt the analytical derivatives of the ODEs, constraints and objective function were inputted into the problem model. Time has discretized into N intervals (N=10, 20, 30). Three collocation points were used to approximate the state variables, while one collocation point was used for pH meaning that the optimized pH profile is PWC. The tolerances used to converge the algorithm were 10^7, 10^7 and 10^4 for the objective function, state variables and constraints respectively. The initialization pH profile can impact the final optimized pH profile. For this work every optimization was conducted while initializing at a constant pH of 7. In some cases, the solver converged to an infeasible point, those cases were recomputed with an initialization profile of pH 6, so that a realistic profile could be generated. These profiles are adequately marked with (*) on all relevant figures.

During the optimization studies it was observed that the scale of the problem created difficulties for the NLP problem. The zeroth moment which is the number of crystals has a magnitude relevant to 10^9 while the third moment which is correlated to the total volume has a magnitude of 10^{-3}. This large difference in scales contained in a single MATLAB variable should be generally avoided because they can cause issues within the optimization code. For this reason, in order to improve the optimization, scaling was applied to the ODEs. In this kind of optimization problems, the scale of the first order derivatives of the problem is more important that the scale of the ODEs themselves. Despite this fact in this case by only improving the scale of the ODEs, a substantial improvement in the optimization code was observed, meaning that a more sophisticated scaling approach was not required. Thus, the scaled variables are defined by:

$$\overline{m_{\mathrm{i}}} = \frac{m_{\mathrm{i}}}{p_{\mathrm{i}}} \tag{65}$$

wherein $\overline{m_i}$ is the scaled i-th moment, m_{i} the i-th moment and p_{i} the scale parameter for the i-th moment of the distribution.
The scaling parameters used for each moment were:

$$p_0 = 10^9 \qquad p_1 = 10^5 \qquad p_2 = 1 \qquad p_3 = 10^{-4}$$

With the application of this scaling strategy the optimization code demanded less computational time and was able to satisfy the applied constraints.

3. Results and discussion

3.1. Model replication

Before proceeding with the dynamic optimization of the process, the reproduction of the published model results should be performed. This step is important in order to ensure that the model used in this work is trustworthy and able to predict the same behavior as the published model.[1] Moreover, the dynamic simulations performed serve as an investigation into the design space of the process. In the published model six different experiments A-F under different conditions were conducted. During the course of the experiments, parameters including pH, ampicillin concentration and the chord-length distribution of the crystals were tracked in real time using the results to fit the seven parameters used in the model. The model is able to estimate the ampicillin concentration profile as well as the MCS.

In this work the same procedure was followed. Using the authors' initial conditions for each experiment, the model was solved with respect to time and $[Amp](t)$ as well as the $MCS(t_f)$ were obtained. Afterwards the results were compared with the authors published results in order to ascertain that the model used in this work is able to reproduce the published results.

Due to the way the initial conditions and the results were presented in the article, further steps were necessary to successfully replicate the model. In the article a table is presented detailing the experimental conditions for each experiment:

Table 5: Experimental conditions of crystallization runs.[1]

Run	Seeding Conc. (wt %)	$[Amp]_0$ (g kg^{-1})	Initial supersaturation SS_0	pH rate hr^{-1}	pH_0	pH_f
A	0.0	18.09	0.54	1.0	7.84	6.45
B	0.0	17.93	0.47	3.1	7.89	6.41
C	0.0	15.94	0.98	6.0	7.47	5.97
D	1.8	11.30	1.07	1.5	7.09	6.25
E	3.0	11.36	1.18	1.4	7.01	6.34
F	15	14.00	1.64	0.6	7.06	6.51

wherein seed (wt %) is the percentage of seed crystals with respect to the initial mass of the mother liquor, $[Amp]_0$ the initial ampicillin concentration, S_0 the initial saturation of the solution, pH rate the rate of the pH decrease, pH_0 and pH_f the initial and final pH of the solution respectively.

Assuming that the pH rate remains constant, a linearly decreasing pH profile based on Table 5 was produced. Starting from an initial value of pH_0, the pH is decreased linearly with a constant pH rate until the final pH value pH_f. The time at which the pH stops decreasing will be referred as t_{decr}. After time t_{decr} the pH value remains constant until the end of the experiment.

In the Encarnacion-Gomez article[1] the results for the mother solute concentration with respect to time are provided in figure form, for this reason information such as the final experiment time t_f had to be calculated by digitizing the given figures. In order to compare this work's calculated concentration profile with the published one, every figure presented in the article was digitised and then the data were fitted with a smoothing line approximation using the Curve Fitting MATLAB toolbox. After this procedure the relative error between the two results was calculated.

$$Error_{[\mathrm{Amp}]}(t) = 100\ \frac{\left|\ [Amp]_{\mathrm{digit}}(t)\ -\ [Amp]_{\mathrm{calc}}(t)\right|}{[Amp]_{\mathrm{digit}}\ (t)} \tag{66}$$

wherein $Error_{[\mathrm{Amp}]}(t)$ is the relative error (%) between $[Amp]_{digit}(t)$ and $[Amp]_{calc}(t)$, $[Amp]_{digit}(t)$ is the digitized ampicillin concentration reported in the Encarnacion-Gomez article[1] and $[Amp]_{calc}(t)$ is the calculated concentration of the mother liquor. $Error_{[\mathrm{Amp}]}(t)$ was calculated with respect to time and it's the minimum and maximum values were computed. Finally, the estimated MCS at t_f was calculated and the relative error was calculated.

$$Error_{MCS} = 100\ \frac{\left|MCS_{reported} - MCS_{calc}\right|}{MCS_{reported}} \tag{67}$$

wherein $Error_{MCS}$ is the relative error (%) in the calculation of the *MCS*, $MCS_{reported}$ is the estimated *MCS* reported in the Encarnacion-Gomez article[1] and MCS_{calc} is the MCS calculated in this work.

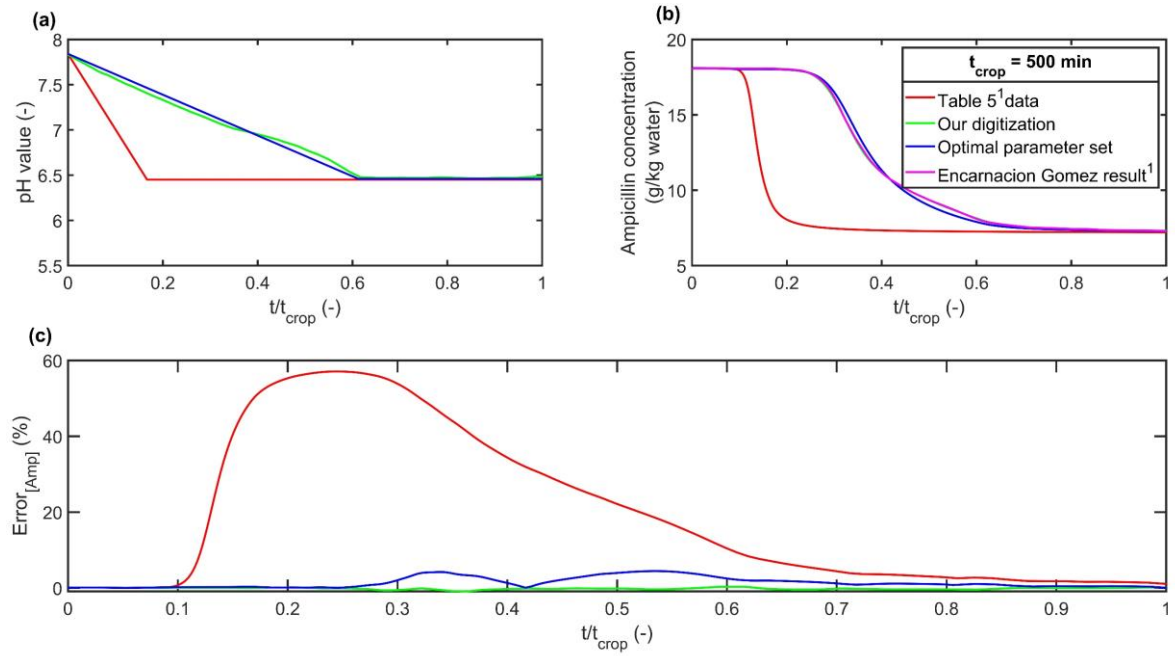

Figure 8: Dynamic simulation results for experiment A (unseeded). (a) Different pH profiles simulated, (b) [Amp](t), (c) $Error_{[Amp]}(t)$ (%) between our simulations and published results.

Table 6: Mean crystal size (*MCS*) at t_f.

Run	t_f (min)	$MCS_{reported}$[1] (μm)	MCS_{calc} (μm)	$Error_{MCS}$ (%)
A	1000.00	86.74	69.60	19.76
B	250.00	82.86	83.06	0.24
C	73.15	66.24	86.78	31.01
D	254.00	63.77	63.95	0.29
E	350.00	-	60.37	-
F	1500.00	68.28	64.79	5.11

The published estimated MCS as well as this work's estimates for each experiment are presented in Table 6. A thing that should be noted is that the authors have omitted to publish their result for experiment E. In Table 6 the first column corresponds with the experiment name conducted in the Encarnacion-Gomez article, in the second column the final run time t_f for each experiment is reported, were as in the third, fourth and fifth columns the $MCS_{reported}$, MCS_{calc} and $Error_{MCS}$ (%) are presented respectively.

Between Table 5 and the published figures inconsistencies were observed. The main issue of concern is the *pH* decrease rate. From the published solubility curves, it was established that *pH* decreased faster or slower than reported, moreover it is not apparent if the rate was indeed constant for the duration of the experiments. In addition, in experiment (E) a spike in the concentration is observed at the start of

experiment, while in experiment (C) the solubility remains constant for a limited time at the start of experiment and then decreases.

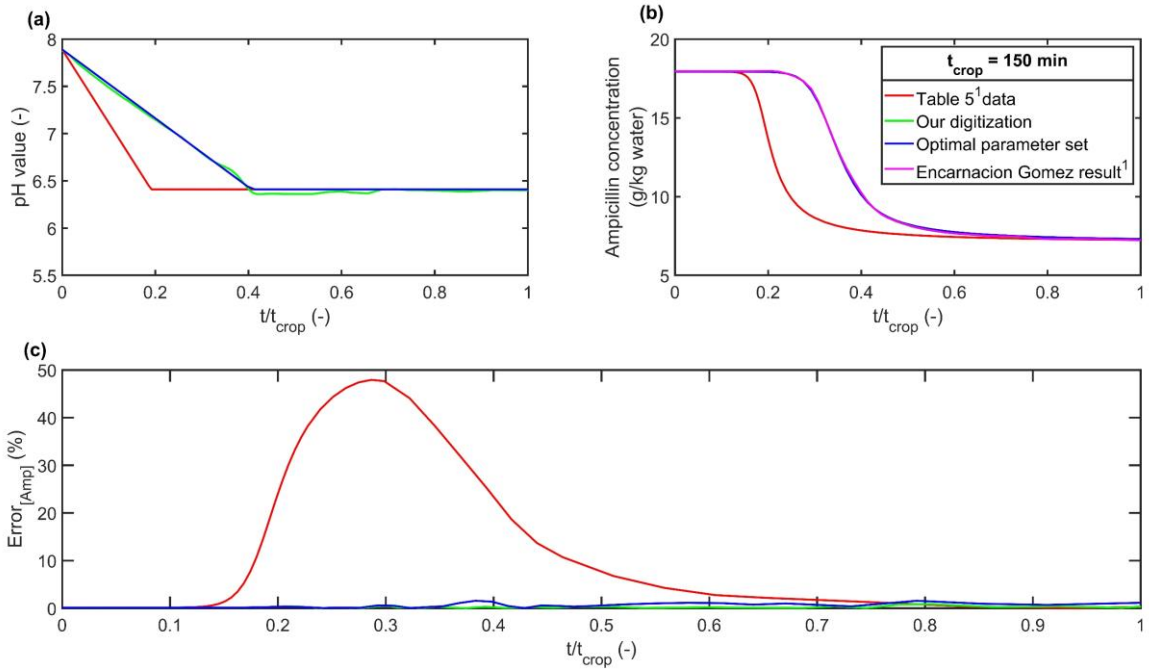

Figure 9: Dynamic simulation results for experiment B (unseeded). (a) Different pH profiles simulated, (b) [Amp](t), (c) $Error_{[Amp]}(t)$ (%) between our simulations and published results.

In order to replicate each experiment, the following procedure was followed. The published solubility curve was digitized using a smoothing line curve fit with MATLAB. From the solubility curve utilizing the solubility model the pH profile was reproduced, and it was then then used to solve the crystallization model. This profile was labeled 'Our digitization' and it presents an approximation of the real *pH* profile that was used. Although profile 'Our digitization' did decrease for all experiments in a linear like way it was not explicitly linear supporting the conclusion that during the experimental run the pH decrease rate was not constant. The crystallization model was solved for the profiles from 'Table 5' and for 'Our digitization'. The results between them were different enough to require the testing of pH profiles with different values for pH_0, pH_f and t_{decr}. The values tested for these three parameters were between the values of the two profiles. The ultimate goal from this procedure was to test various different profiles and find an optimal parameter set that produces a linearly decreasing profile with a desupersaturation curve closest to the one reported while the computed final *MCS* is also similar to the reported value. All tested profiles started from an initial pH_0 value and followed a linear decrease up to the final pH_f value. For each experiment the profile that replicated better the published results was labelled as "Optimal parameter set". For each profile tested the $Error_{[AMP]}(t)$ was calculated and the maximum and minimum values of the $Error_{[Amp]}(t)$ where recorded. Moreover the $Error_{[MCS]}(t_f)$ was recorded. The optimal parameter set was chosen according with the following equation:

$$\text{Optimal parameter set} = \min_{i}\left(\sum \max\left(\left|Error_{[AMP]}(t)\right|\right) + \left|Error_{[MCS]}(t_f)\right|\right)(i) \qquad (68)$$

wherein i is the number of each profile tested. In other words, the optimal profile exhibited the lowest summation of errors.

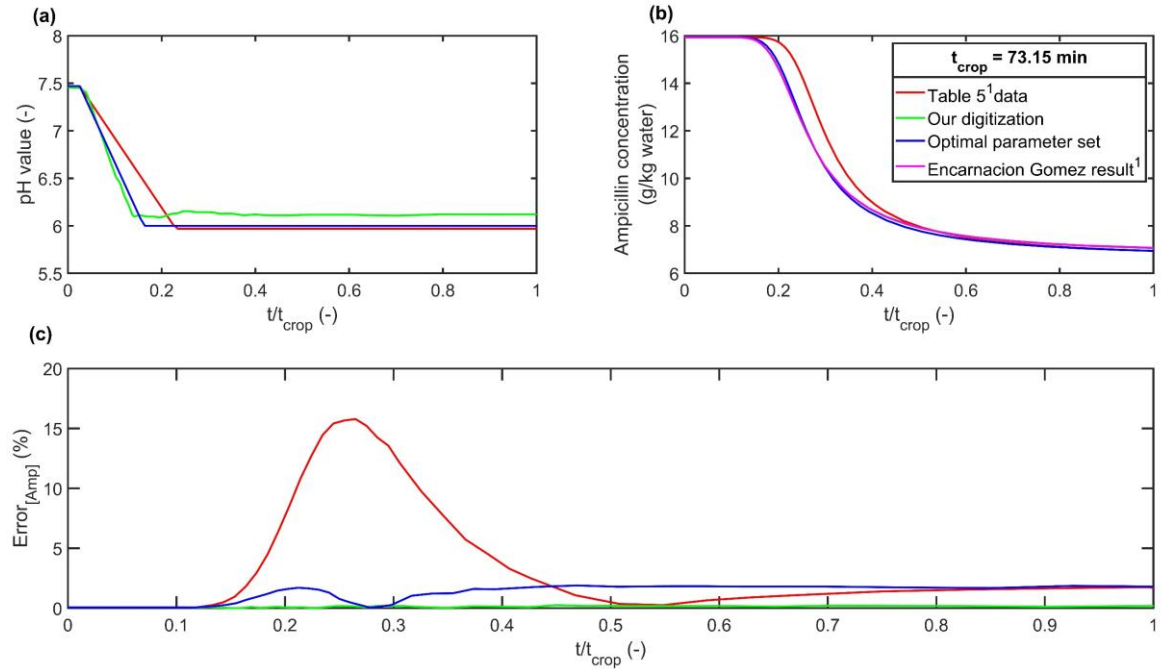

Figure 10: Dynamic simulation results for experiment C (unseeded). (a) Different pH profiles simulated, (b) [Amp](t), (c) $Error_{[Amp]}(t)$ (%) between our simulations and published results.

The results of the dynamic optimization for each profile are presented in Table 7 and in Fig. 8-13 with every figure simulating a different experiment A-F.

Table 7: Dynamic Simulation Results for each experiments vs published data.[1]

Exp.	Profile	pH_0	pH_f	t_{decr} (min)	Max. $Error_{[Amp]}$ (%) (eq. 58)	MCS (μm)	$Error_{MCS}$ (%) (eq. 59)	$\sum \lvert \text{Error} \rvert$ (%)
	Table 5	7.84	6.45	83.40	+ 57.08	80.70	+ 6.96	64.04
A	Our digitization	7.83	6.49	306.00	− 0.92	66.87	+ 22.91	23.83
	Optimal par set	7.84	6.46	306.00	+ 4.46	69.60	+ 19.76	24.22
	Table 5	7.89	6.41	28.65	− 47.92	84.74	− 2.27	50.19
B	Our digitization	7.88	6.40	62.00	− 1.24	83.30	− 0.53	1.77
	Optimal par set	7.89	6.41	61.00	+ 1.77	83.06	− 0.24	2.02
	Table 5	7.47	5.97	15.00	− 15.78	86.68	− 30.86	46.64
C	Our digitization	7.45	6.11	10.00	− 0.25	86.89	− 31.18	31.43
	Optimal par set	7.47	6.00	10.00	+ 1.89	86.78	− 31.01	32.90
	Table 5	7.09	6.25	33.60	+ 10.91	65.16	− 2.18	13.09
D	Our digitization	7.10	6.34	64.00	− 3.92	64.15	+ 3.16	7.09
	Optimal par set	7.09	6.31	64.00	+ 0.66	63.95	− 0.28	0.93
	Table 5	7.01	6.34	28.71	+ 12.00	-	-	12.00
E	Our digitization	7.00	6.40	55.50	+ 2.28	-	-	2.28
	Optimal par set	7.01	6.40	55.50	+ 4.09	-	-	4.09
	Table 5	7.06	6.51	55.00	− 18.98	62.11	+ 9.04	28.02
F	Our digitization	6.84	6.56	37.00	− 1.97	64.48	+ 5.56	7.53
	Optimal par set	6.84	6.51	37.00	− 2.19	64.79	+ 5.11	7.29

In Table 7 the first two columns entail the experiment and profile information for each simulated case, the third to fifth columns present the parameters for pH_0, pH_f and t_{decr} respectively. In the sixth column the maximum value of $Error_{[AMP]}(t)$ is reported, while in the seventh and eighth columns the calculated *MCS* and the $Error_{[MCS]}(t_f)$ are reported. Finally the last column reports the summation of max$Error_{[AMP]}(t)$ and $Error_{[MCS]}(t_f)$.

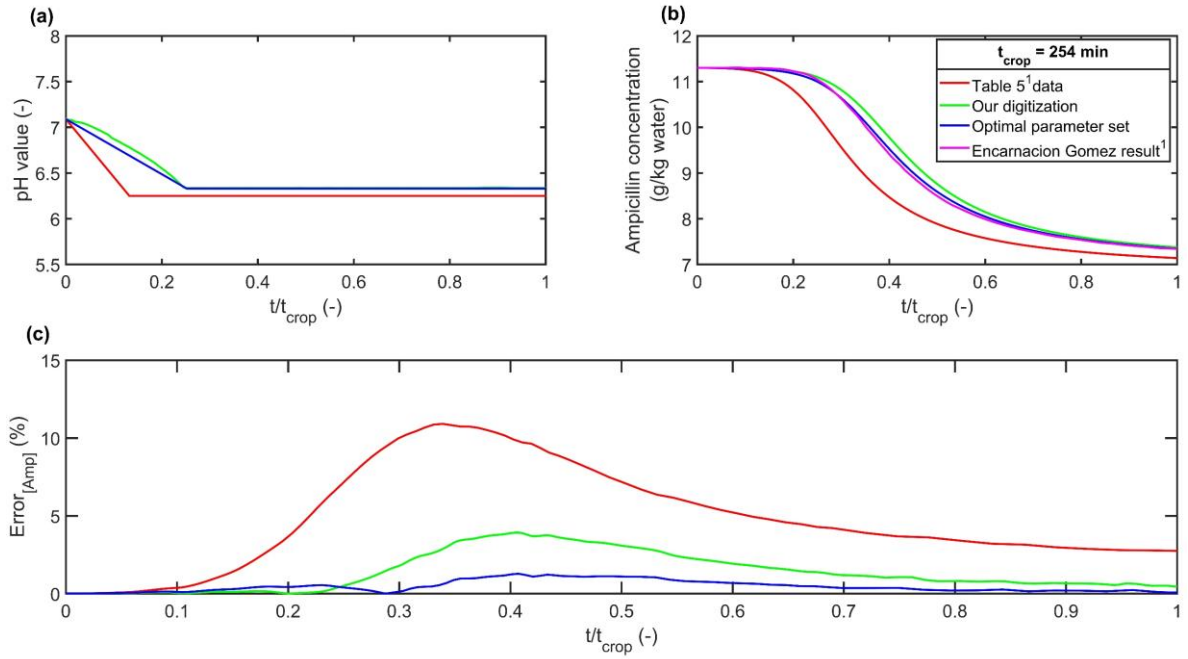

Figure 11: Dynamic simulation results for experiment D (seeded). (a) Different pH profiles simulated, (b) [Amp](t), (c) $Error_{[Amp]}(t)$ (%) between our simulations and published results.

In Fig. 8-13 the dynamic results for each experiment are reported. In particular the $pH(t)$, $[Amp](t)$ and $Error_{[AMP]}(t)$ for each profile are presented. Every experiment was simulated up to the final time t_f digitized from the Encarnacion-Gomez article. For each experiment after time $t_{crop} < t_f$ no variation on the reported variables was observed. For this reason, the variables where plotted up to time t_{crop}, which is mentioned in the legend for each figure. Moreover, in order to achieve a uniform time x-axis, t/t_{crop} was used instead of t. It is noted that the final time t_f remains of significance because the final MCS is computed at time t_f.

Analysing Table 7 it is observed that for experiments D and F the optimal parameter set has a smaller summation of errors than the other profiles. While for experiments A, B, C and E the optimal set has a higher summation of errors than 'Our digitization' but the values are similar. Both 'Our digitization' and 'Optimal parameter set' exhibit much lower error values than 'Table 5'. A conclusion can be reached that indeed the parameters used in the experiments deviated from the reported values of Table 5. The t_{decr} value of the 'Optimal parameter set' is for every experiment identical to the t_{decr} of 'Our digitization'. The pH_0 value for experiments (A-E) is almost the same for every profile, meaning that the initial pH value was reported correctly. The pH_0 value for experiment (F) showed a substantial deviation between profiles 'Table 5' and 'Our digitization' with the optimal profile matching the value of 'Our digitization'. The pH_f value presented small deviation between the profiles. For experiments A, B, E and F the difference between 'Table 5' and 'Our digitization' for every profile was below 0.06 pH

units. On the other hand, for experiment (D) the difference was 0.09 pH units and the optimal parameter set profile had a pH_f value in between the value for profiles 'Table 5' and 'Our digitization'.

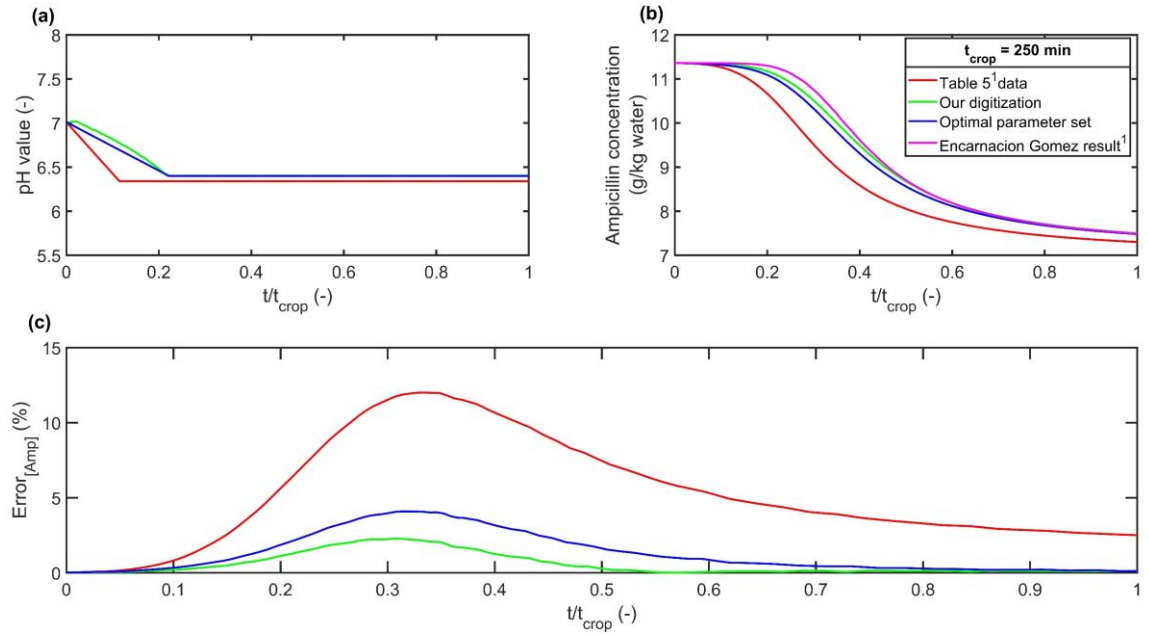

Figure 12: Dynamic simulation results for experiment E (seeded). (a) Different pH profiles simulated, (b) [Amp](t), (c) $Error_{[Amp]}(t)$ (%) between our simulations and published results.

The largest difference of 0.14 pH units was observed was in experiment C with the optimal parameter set profile matching the value of 'Table 5'. 'Table 5' had a proportionally higher max$Error_{[AMP]}(t)$ which adds merit to the observation that the optimal parameter set tends to match the conditions of 'Our digitization'.

The calculation of the *MCS* is more difficult to replicate. The *MCS* is estimated from the division between the first and the zeroth moments of the population balance. A slight change in starting or ending conditions is able to drastically change the result as shown in Table 7. For the optimal parameter set for experiments (B, D and F) the $Error_{[MCS]}(t_f)$ is below 5 % meaning that the estimation matches closely the published results. Experiment C presents the highest deviation of 31% and experiment A also has a high $Error_{[MCS]}(t_f)$, but in this case, each profile has a distinctly different MCS calculated, while for experiment C the values are almost identical. This allows for the consideration that maybe there is a typographical error in the reported value. If the MCS is (86.24 μm) and not (66.24 μm) then the MCS relative error for the optimal profile is actually (0.63%). Moreover, experiment C is an unseeded experiment like experiments A and B. For experiments A and B, the reported MCS values are in the 80 μm range so the assumption that a typographical error exists has some merit. The results presented in Fig. 8-13 confirm the conclusions derived from Table 7. The calculated concentration curves for the optimal profile match closely the published curves. Moreover, every profile exhibits a dynamic behaviour that matches closely the published. All in all, it is concluded that the published results have been replicated within an acceptable degree.

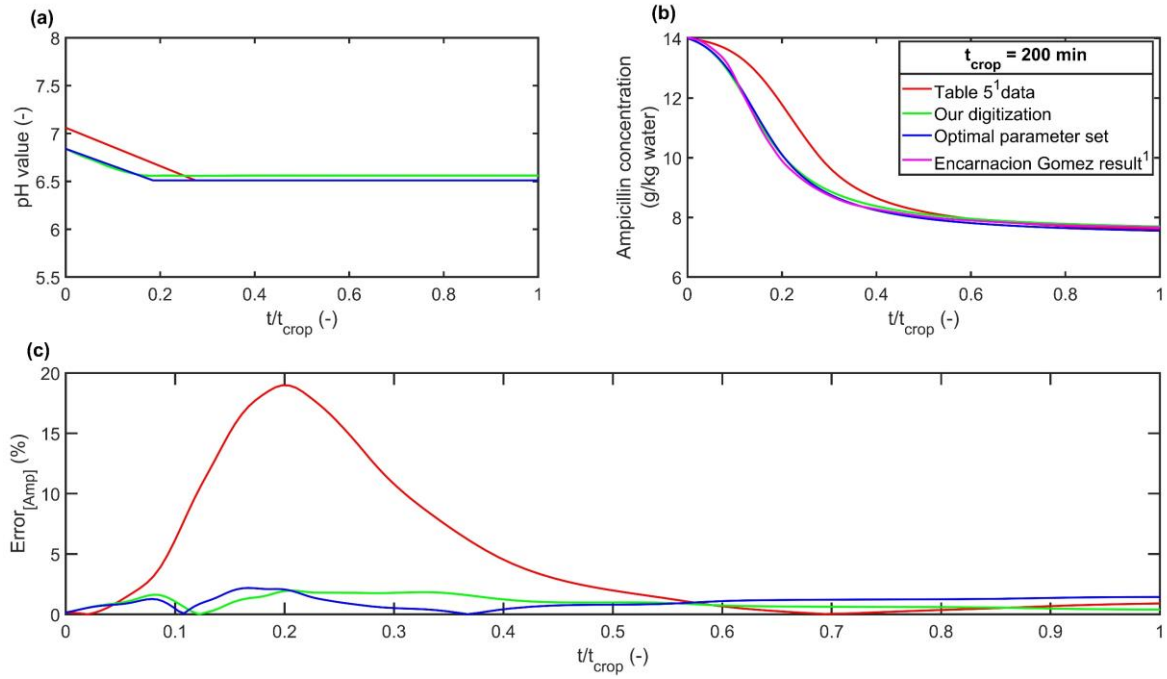

Figure 13: Dynamic simulation results for experiment F (seeded). (a) Different pH profiles simulated, (b) [Amp](t), (c) $Error_{[Amp]}(t)$ (%) between our simulations and published results.

3.2. Dynamic optimization

PWC profiles between discrete time points were computed in order to investigate the performance of the algorithm under different objective function weight parameters and how the performance is affected by varying the degree of discretization. To achieve these three discretization levels (N=[10 20 30]) have been considered and four different combinations for the weights of the objective function have been tested:

Table 8: Different combinations of examined objective function weights.

W_σ	W_{MCS}
1.0	0.0
1.0	0.5
1.0	1.0
1.0	1.5

In order to maintain the physical meaning of the system to be optimized a realistic case should be used. As an initial optimization study of this particular system it was deemed appropriate start with a system with a low amount of initial seeding. Experiment D was the experiment with the lowest summation of errors in Table 7 and it had the lowest seeding. Thus, the starting conditions of experiment D were utilized in the optimization studies. In accordance with experiment D, $[Amp]_0$ was 11.30 g/kg, *wt* % was 1.8% and t_f was 250 min. In experiment D the range of the pH used was between 7.09 and 6.25 but the crystallization kinetics were obtained over a pH range of 6.00 to 7.84. In Fig. 5 it can be observed that pH 5.5 and pH 6 have similar solubility values. For this reason, a pH range of 5.5-7.84 was used in the optimization code.

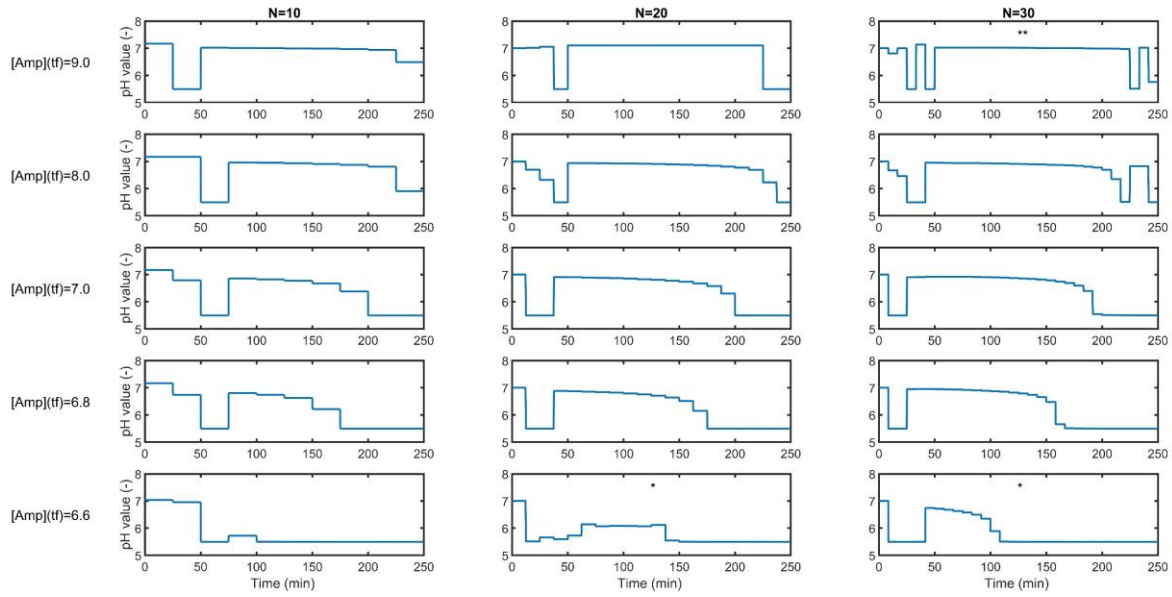

Figure 14: Piecewise constant pH(t) solutions with fmincon & fixed endpoint $K_X = 3$, $W_\sigma = 1$, $W_{MCS} = 0$. Intialised at constant pH= 7 (*, initialized at constant pH= 6), (**, $K_X = 6$).

For experiment D the best pH profile which achieves yield maximization is a constant profile at *pH* = 5.5 this profile produces crystals with (*STD* = 64.83 μm, *CV* = 0.90, *MCS* = 72.03 μm and [*Amp*](t_f)=6.52 g/kg) this result serves as a baseline where maximum yield is achieved but at the expense of the CSD quality attributes. The strategy that was adopted in this work is to apply different [*Amp*](t_f) constraints between 9 and 6.6 g/kg. Namely in Fig. 14- 17 [*Amp*](t_f) constraints of 9, 8, 7, 6.8 and 6.6 g/kg are presented.

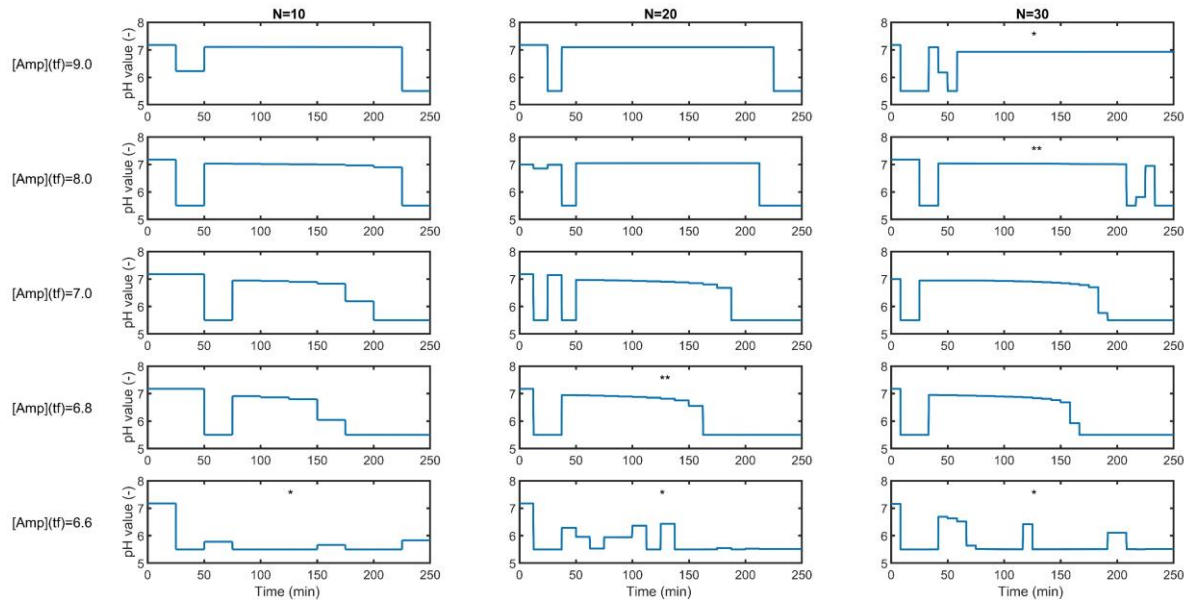

Figure 15: Piecewise constant pH(t) solutions with fmincon & fixed endpoint K_X = 3, W_σ= 1, W_{MCS}= 0.5. Intialised at constant pH= 7 (*, initialized at constant pH= 6), (**, K_X= 6).

Since three collocation points were used to approximate the state variables, DynOpt approximates by calculating a fourth-order Langrange polynomial in each discretized time interval.

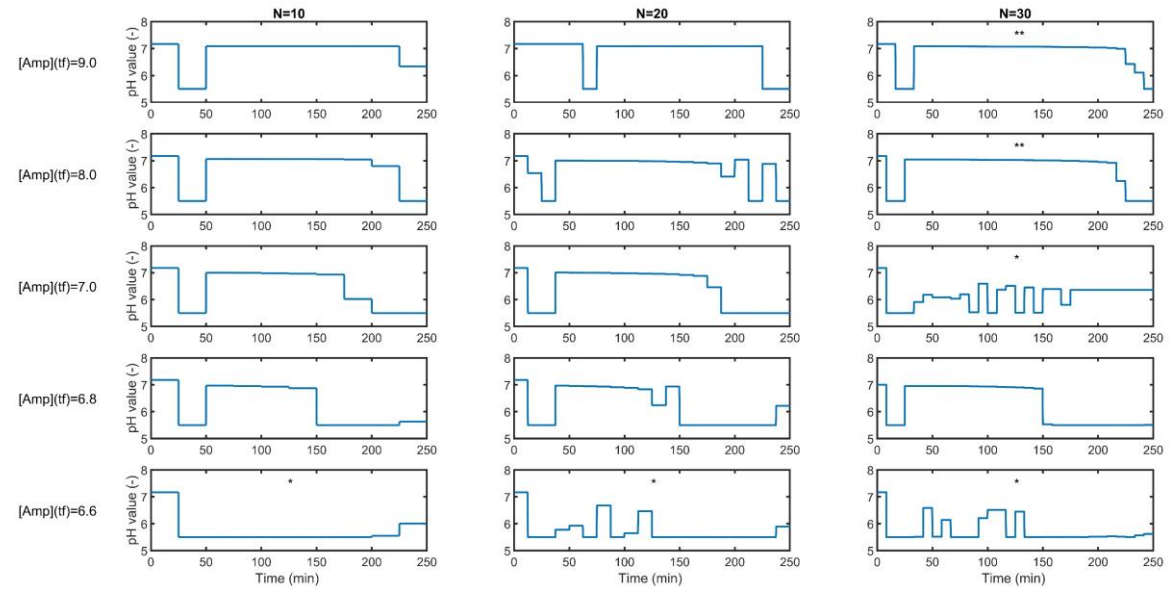

Figure 16: Piecewise constant pH(t) solutions with fmincon & fixed endpoint K_X = 3, W_σ= 1, W_{MCS}= 1.0. Intialised at constant pH= 7 (*, initialized at constant pH= 6), (**, K_X= 6).

Whilst increasing the number of collocation points increases the accuracy of the model it also increases computational time. In order to make sure that the approximation of the state variables is sufficient, the optimized pH profile was used to perform a final dynamic simulation of the process. The subsequent result was compared to the DynOpt approximation.

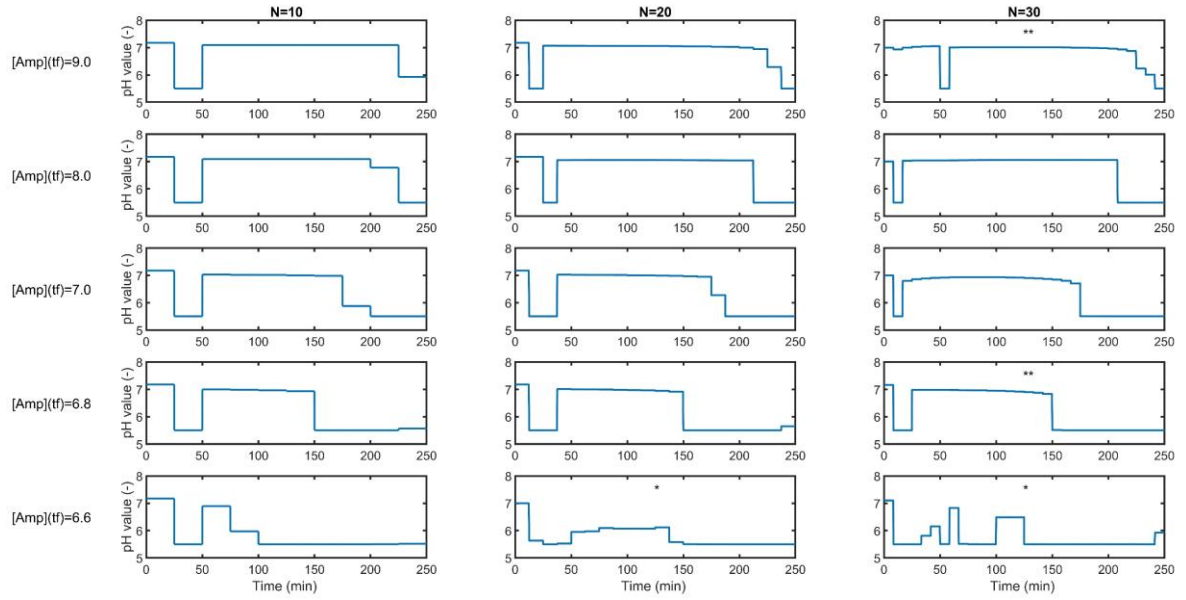

Figure 17: Piecewise constant pH(t) solutions with fmincon & fixed endpoint $K_X = 3$, $W_\sigma = 1$, $W_{MCS} = 1.5$. Intialised at constant pH= 7 (*, initialized at constant pH= 6), (**, $K_X = 6$).

In the vast majority of cases the approximation was sufficient but in a small number of optimization solutions deviations were present. As a result, in some cases while the algorithm provided feedback that a feasible solution had been reached, the dynamic simulation showed that the solution had not satisfied the constraints. In other words, the DynOpt approximation satisfied the constraints but only because the approximation deviated from the real state trajectories. This discrepancy is inherent to the approximation method via Lagrange polynomials. If the pH change induced by the optimization code is severe then sometimes the approximated polynomial fails to represent accurately the model, hence the discrepancy. Unfortunately, if such a discrepancy occurs at any time segment the optimization code may converge because the inaccurate approximation achieved objective function minimization while satisfying the constraints. This particular discrepancy seems to occur only when N=30 and for loose yield constraints like 9.0, 8.5 and 8 g/kg.

In order to ensure that the calculated quality attributes and [*Amp*](*tf*) correspond to realistic values for the state variables, every optimized pH profile was used to simulate the model with ode23t and it is these results that are presented. In the cases where the approximation was deemed insufficient the optimization was recomputed using $K_X = 6$ collocation points for the state variables. Optimized pH profiles that used six collocation points are marked by (**) on the figures. On other cases where the $target_{[Amp]}$ constraint was too strict namely at 6.60 g/kg the algorithm straggled to converge. On those cases the system was initialized at a constant $pH = 6$ in order to acquire a realistic result. Those solutions with a different initialization are marked by (*) on the figures. In general solutions that were obtained with pH= 6 as an initialization profile tended to differ from the other solutions. The pH values were

noticeably lower, mandating for rapid pH manipulation due to the existence of 'spikes' in the profile. This leads to the conclusion that the initialization strategy influences the final solution.

3.2.1. Effect of [*Amp*](t_f) constraint

Computed optimal control profiles on an identically discretized *pH*(t) domain for the chosen [*Amp*](t_f) constraints can be seen in each column in Fig. 14-17. From top to bottom [*Amp*](t_f) constraint at 9, 8, 7, 6.8 and 6.6 g/kg were used respectively with an initialization *pH* of 7. Performance of each solution obtained with fmincon is tabulated in Appendix. A.

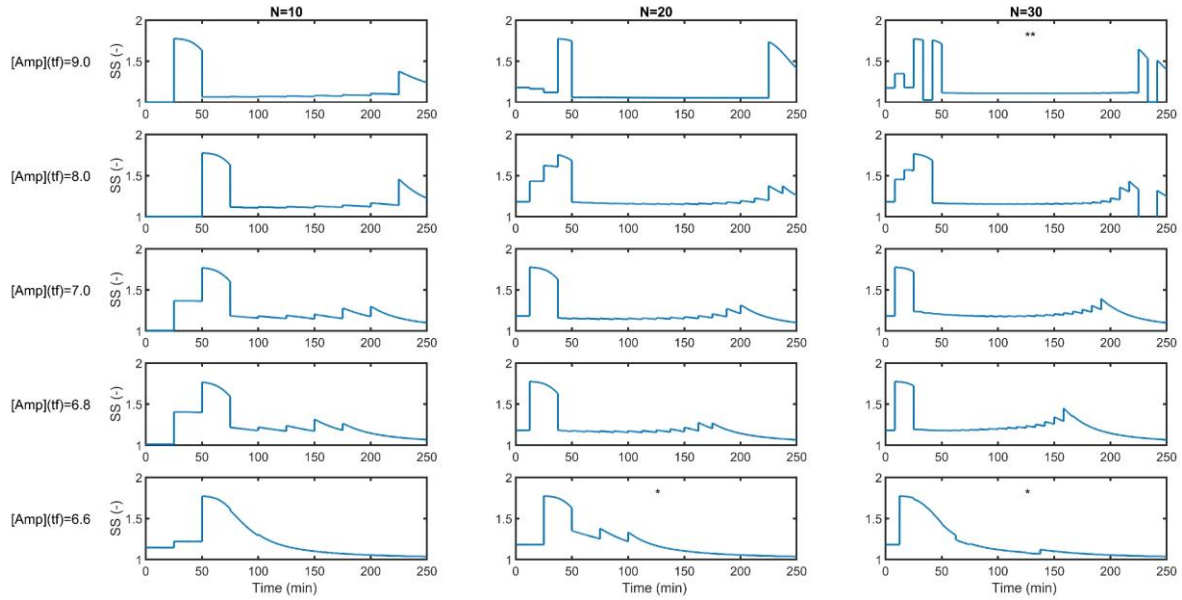

Figure 18: SS(t) corresponding to pH(t) solutions with fmincon & fixed endpoint K_X = 3, W_σ= 1, W_{MCS}= 0.0. Intialised at constant pH= 7 (*, initialized at constant pH= 6), (**, K_X= 6).

The optimization strives for *MCS* maximization and for *STD* and *CV* minimization while fulfilling the [*Amp*](t_f) constraint. In almost every case the [*Amp*](t_f) in the obtained solutions matched the $target_{[Amp]}$, meaning that a definite tradeoff between [*Amp*](t_f) and the quality attributes exists and that in order to enhance the quality attributes, yield reduction is necessary. In Fig. 14 it is apparent that the *pH* profiles follow a trend. Before time 50 min a significant drop of *pH* occurs resulting in the abrupt increase of supersaturation. This increase induces rapid nucleation and a vast amount of new crystals are generated as shown in Fig. 19-20 with the sudden drop in *MCS* observed at that time. After this initial drop a sudden increase in *pH* is observed. In the solutions with stricter [*Amp*](t_f) constraints the increase is less profound. Afterwards over the course of the process the *pH* remains high but is slightly decreasing, resulting in minute spikes in the supersaturation inducing crystal growth. Finally, a final drop in *pH* is observed resulting into further crystal nucleation and crystal growth allowing for the satisfaction of the [*Amp*](t_f) constraint while producing crystals with enhanced quality attributes.

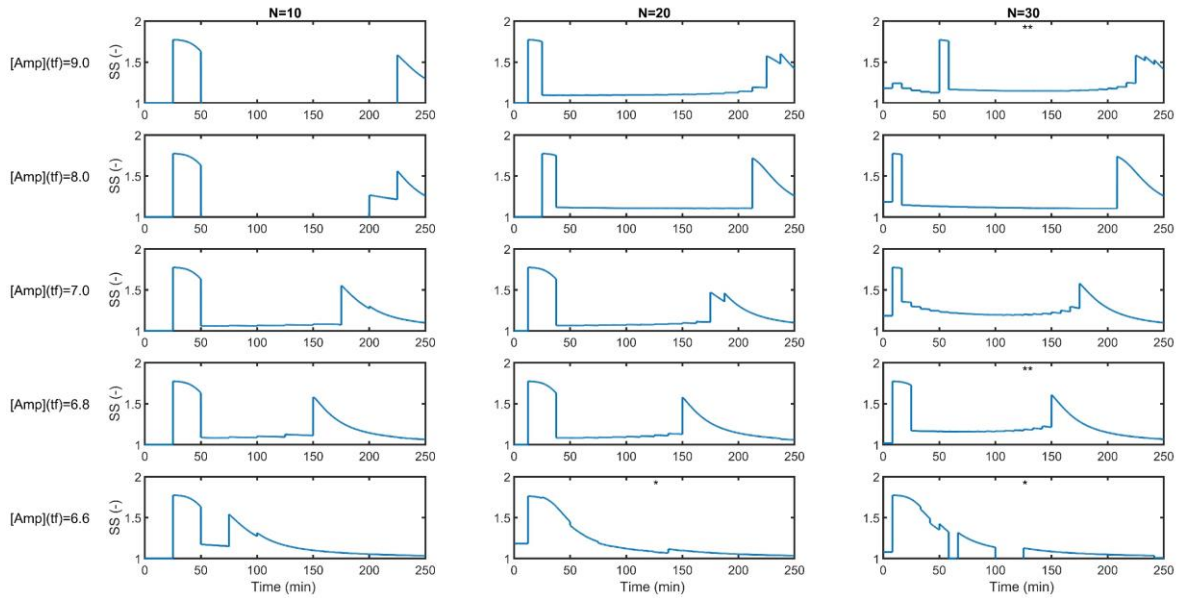

Figure 19: SS(t) corresponding to pH(t) solutions with fmincon & fixed endpoint $K_X = 3$, $W_\sigma = 1$, $W_{MCS} = 1.5$. Intialised at constant pH= 7 (*, initialized at constant pH=6), (**, K_X=6).

In Fig. 14 it can be observed that when a stricter constraint is applied, the last pH decrease occurs sooner. When the [*Amp*](t_f) constraint is 6.60 g/kg, after the initial pH drop, which results into a peak in supersaturation as shown in Fig. 17, the supersaturation decreases in an exponential fashion with the pH maintaining low values for the duration of the experiment, with only slight increases to the pH observed.

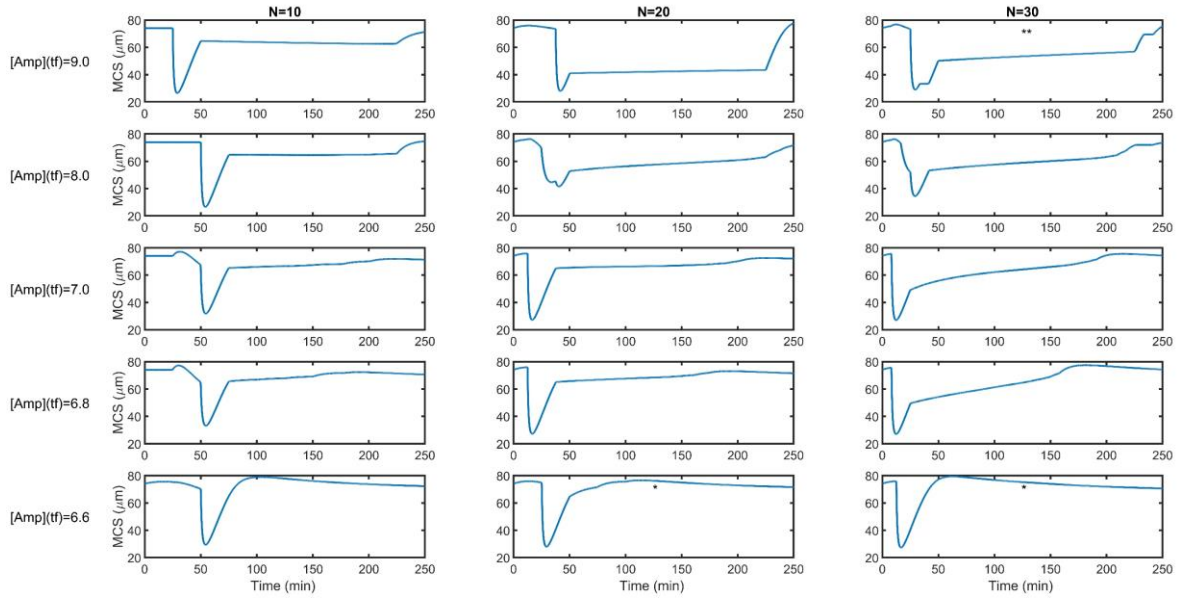

Figure 20: MCS(t) corresponding to pH(t) solutions with fmincon & fixed endpoint $K_X = 3$, $W_\sigma = 1$, $W_{MCS} = 0$. Intialised at constant pH= 7 (*, initialized at constant pH=6), (**, K_X=6).

Meaning that in order to increase yield more abrupt pH profiles with a constantly decreasing supersaturation is required. As expected, making the constraint tighter decreases MCS and increases CV and STD.

3.2.2. Effect of increasing time domain discretization N

To assess the effect of increasing the discretization level of the control profile, the computed results for N=10, 20, 30 (representing the number of equispaced time segments in which the crystallizer pH is piecewise constant) is shown in each row of Fig. 14-17 for a specific [*Amp*](t_f) constraint. The lowest discretization was N=10 which was sufficient enough that in general the differences between the different discretization levels were not substantially profound. Having said that, increasing the discretization allows the system to reduce the *pH* more significantly in a shorter period of time, which is more desirable in this case due to acting to decrease nucleation and favor crystal growth. In essence the nature of the profile remains the same but further refinement upon the case is achieved by increasing N. In some cases, this refinement can affect slight differences to the profile like the existence of two high *pH* drops at the start or a step wise pH decrease at the start or at the end.

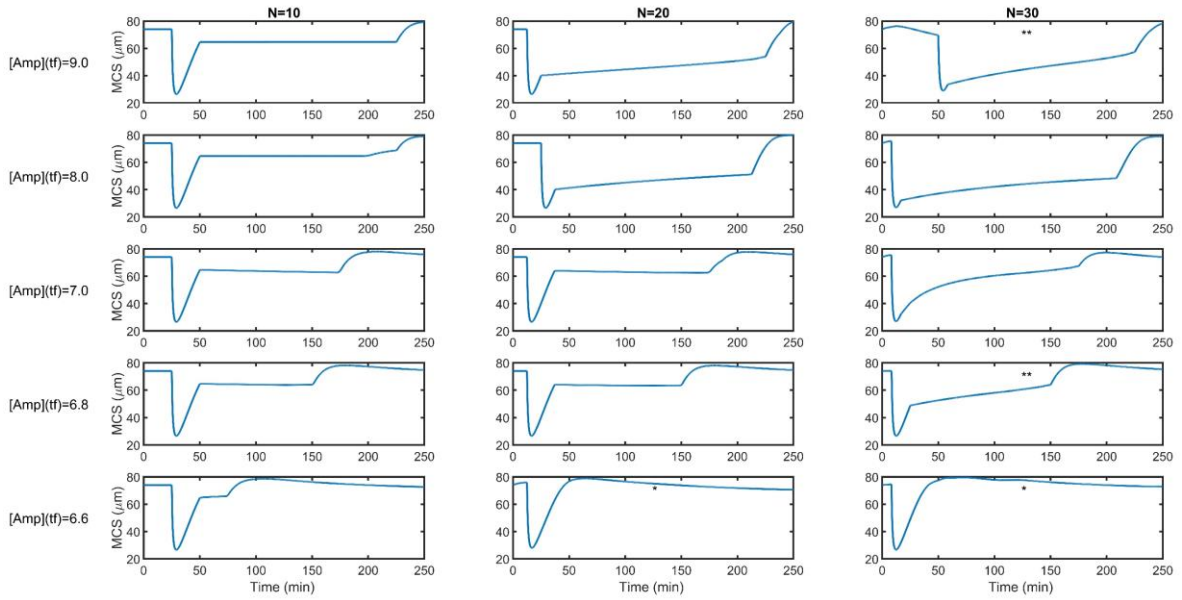

Figure 21: MCS(t) corresponding to pH(t) solutions with fmincon & fixed endpoint $K_X = 3$, $W_\sigma = 1$, $W_{MCS} = 1.5$. Intialised at constant pH= 7 (*, initialized at constant pH=6), (**, K_X=6).

By studying the data presented in Appendix A. it can be not be concluded whether the quality attributes improve by increasing the discretization level. Increasing the discretization level increases the decision variables for fmincon which can lead in some cases the system to local minima for the objective function. Discretization at N=30 presented difficulties for the optimization algorithm. The computational time needed was high and the system was prone to not converge when stricter constraints were applied.

3.2.3. Effect of the objective function weights

The effect of different objective function weights can be observed in Fig 14-17. The computed objective function weights are detailed on Table 8. The effect the weights have to the optimized pH profile is somewhat expected. When W_{σ}= 1 and W_{MCS}= 0 (Fig. 14) the sole focus of the optimization is on variance minimization thus the solutions exhibit lower *CV* and *STD* but also lower *MCS* values. Increasing the value for W_{MCS} up to 1.5 increases the MCS while increases in *CV* and *STD* are observed.

The effect that a high W_{MCS} has on *CV* and *STD* is less profound than the effect that W_{MCS}=0 has on the *MCS*. Meaning that weights of both *MCS* and variance should be present in order to improve all the quality attributes. Comparing Fig. 14 with Fig. 17 between W_{MCS}=0 and W_{MCS}=1.5 it seems that by maintaining high and constant *pH* values after the initial *pH* drop at t=50-150 min produces solutions with increased MCS. In contrast in cases with W_{MCS}=0 it is observed that after the initial drop and the subsequent increase of pH the value does not stay relatively constant but decreases in a stepwise manner at t=50-150 managing further *CV* and *STD* minimization but also decreasing *MCS*. This effect can be observed in Fig. 19 and 20 where the *MCS* as well as the *SS* diagrams are provided.

3.2.4. Pareto fronts

Pareto front is a set of nondominated solutions, being chosen as optimal, if no objective can be improved without sacrificing at least one other objective. On the other hand, a solution x* is referred to as dominated by another solution x if, and only if, x is equally good or better than x* with respect to all objectives.[51]

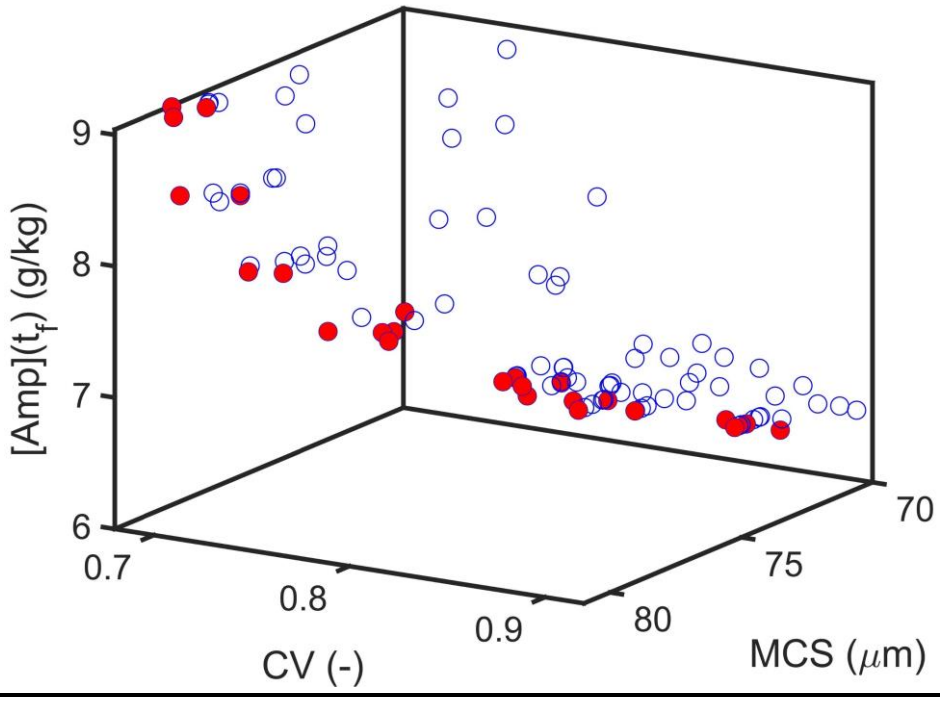

Figure 22: 3D Pareto front of the multiobjective problem showcasing the tradeoff bewteen [Amp](t_f) CV and MCS. (non-dominated solutions are presented as red points).

This procedure was used to assess the performance of the solution profiles with regards to the quality attributes as well as the ([*Amp*](t_f). In Fig 22 the 3-D pareto front of ([*Amp*](t_f), *CV* and *MCS*) is presented, with the non-dominated optimal solutions plotted as red points. In Fig. 23 and 25 projections of the 3D Pareto front are detailed in order to discuss the tradeoff between any two parameters. In Fig. 23 the tradeoff between the [*Amp*](t_f) and *CV* is presented while Fig. 25 handles the tradeoff between [*Amp*](t_f) and MCS. Because CV is a dimensionless expression of STD, only CV was used in the Pareto fronts. In Fig. 23 and 25 the red points represent the non-dominated optimal solutions of the 3D Pareto front and this fact justifies why on these graphs some non-dominated points seem to not find themselves on the front. Meanwhile, the dashed line connects only the non-dominated solutions inherent to each 2D pareto front. In both plots several key non-dominated solutions have been numbered and their corresponding solutions are presented in Fig. 24 and 26.

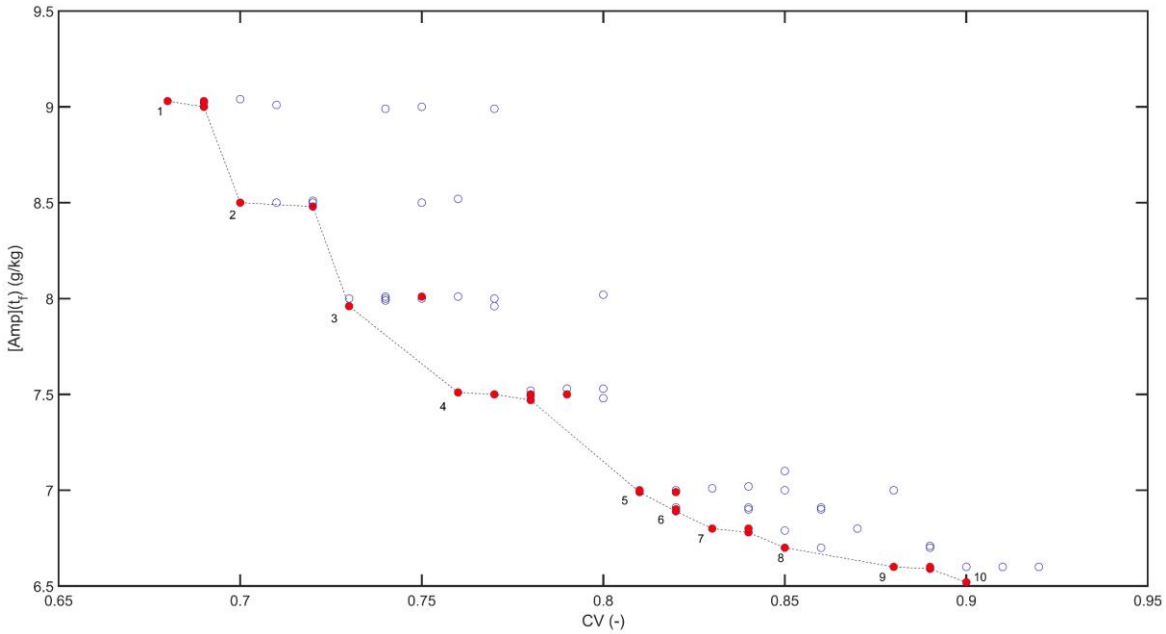

Figure 23: 2D projection of the 3D pareto front for the multiobjective problem showcasing the tradeoff bewteen [Amp](t_f) and CV. The non-dominated solutions of the 3D front are presented as red points while those inherent to the 2D projection are connected with the dashed line.

In Fig. 23 it is observed that the non-dominated points form a front which explicitly highlights the tradeoff between the two variables. A tradeoff exists between [*Amp*](t_f) and *CV*, a decrease in *CV* mandates an increase in [*Amp*](t_f). It is possible to enhance *CV* from 0.9 to 0.8 without severe effects to the produced crystalline product. The inverse effect is identified when *CV* is lower than 0.8, the amount of final crystalline product loss is too severe to justify the improvement in *CV*. In Fig. 22 the pH profiles for the labeled non-dominated solutions of Fig. 21 are presented. It is observed that all the solutions (except the baseline at constant pH= 5.5) follow the pattern described in section 3.2.1. An initial *pH* drop is recorded at the start with a subsequent increase afterwards. Then a phase where the *pH* remains constant or decreases at a small rate is recorded up until a final *pH* drop. When more product is desired thus a lower [*Amp*](t_f) results in the duration reduction of the intermediate phase with *pH* decreasing at a faster rate. Allowing for the conclusion that this intermediate phase is indeed responsible for the *CV* of the final crystalline product.

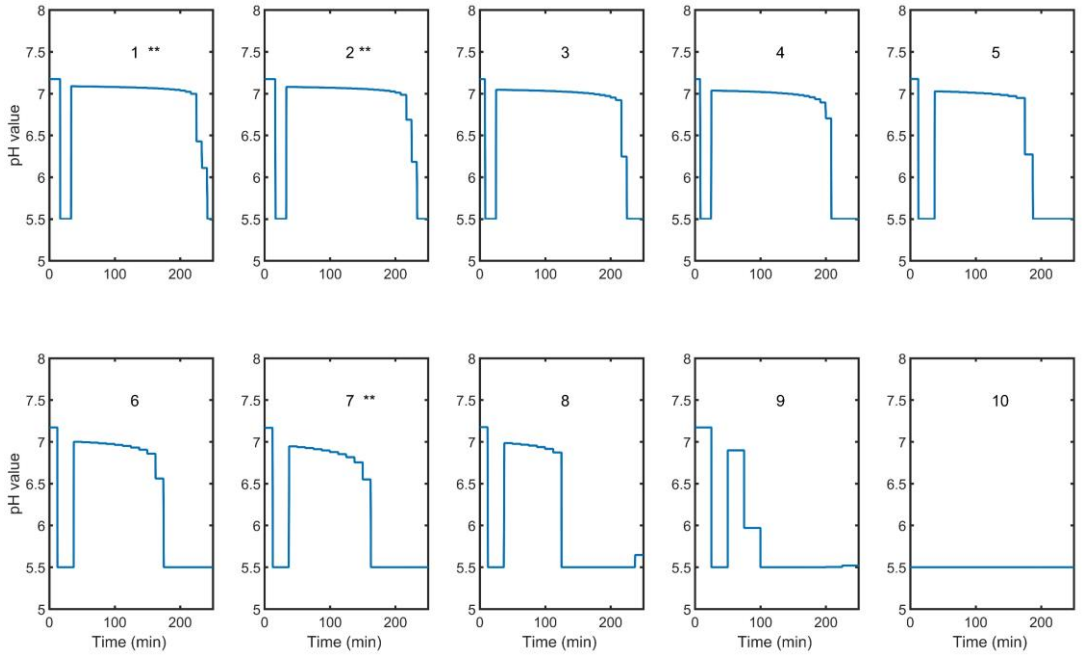

Figure 24: pH profiles for the numbered Pareto front solutions in Fig. 23 (** K_x=6).

From Fig. 25 relevant conclusions can be made. In order to increase MCS by 4 µm (from 72 to 76 µm) only a small increase in [*Amp*](*t*f) is necessary. While a further increase in MCS translates into a severe increase of [*Amp*](*t*f).

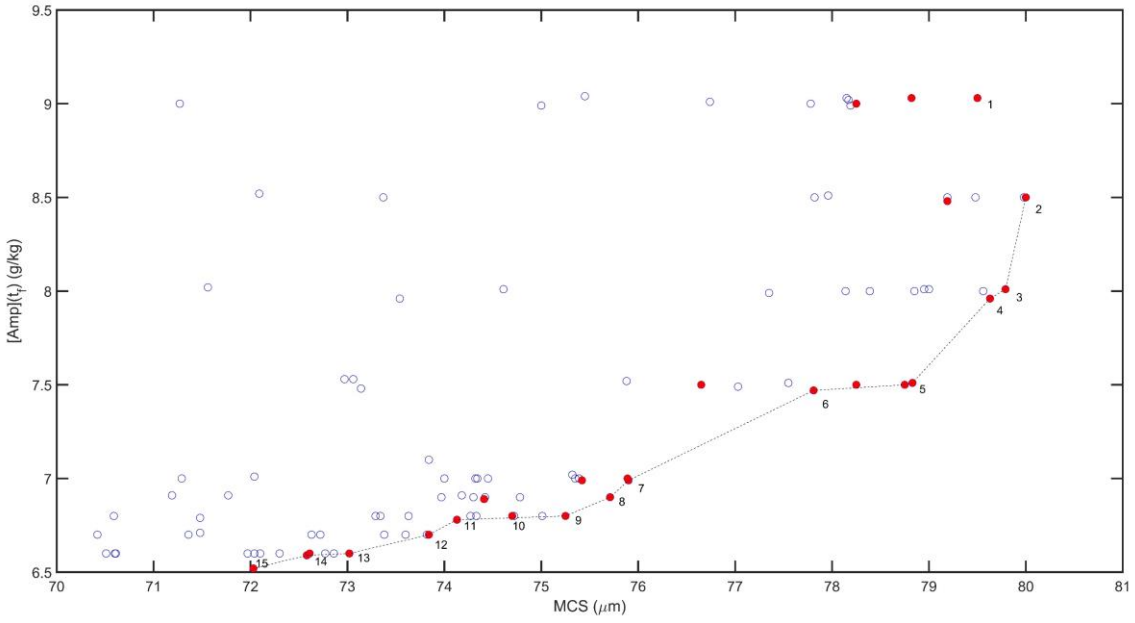

Figure 25: 2D projection of the 3D pareto front for the multiobjective problem showcasing the tradeoff bewteen [Amp](t_f) and MCS. The non-dominated solutions of the 3D front are presented as red points while those inherent to the 2D projection are connected with the dashed line.

Taking into account Fig. 26 it is apparent that the pH profiles for the non-dominated solutions follow the general trend described. When maximum yield is preferable with no qualms about the quality of the product the best pH profile is a constant pH equal to 5.5, wherein 5.5 is the smallest value possible due to crystallization and solubility model restrictions. In this case as well the duration and pH value of the intermediate phase are inherently linked to the final MCS of the product.

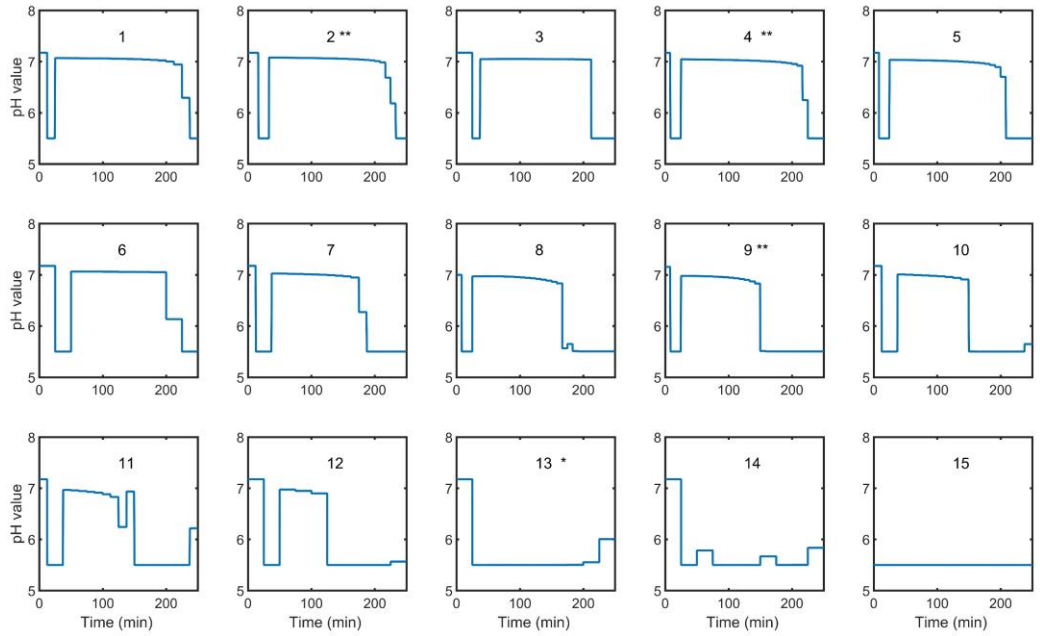

Figure 26: pH profiles for the numbered Pareto front points in Fig. 25 (*, init. at pH= 6) (**, K_x=6).

Finally, is worth mentioning that solutions which derived from W_σ= 1 and W_{MCS}= 0 were not found in the pareto front, strengthening the conclusion that the objective to maximize the MCS is an integral part of the objective function which leads to better solutions.

3.2.5. Pareto fronts for experiments E and F an investigation of different initial crystallization seeding.

In order to ascertain the effect that different initial crystallizer seeding has on the optimal solution two different case scenarios were optimized. In particular experiments E and F detailed in Table 5 were utilized. Experiment E has for all intents and purposes the same conditions as experiment D with the difference that instead of a wt= 1.8% for experiment D, experiment E has a wt=3.0% meaning that experiment E constrains twice the amount of crystals than experiment D at the start of operation. Moreover, experiment E has a final batch time t_f = 350 min, which is 100 more minutes than experiment D. This difference makes the ability to make direct comparisons between the optimal profiles somewhat difficult.

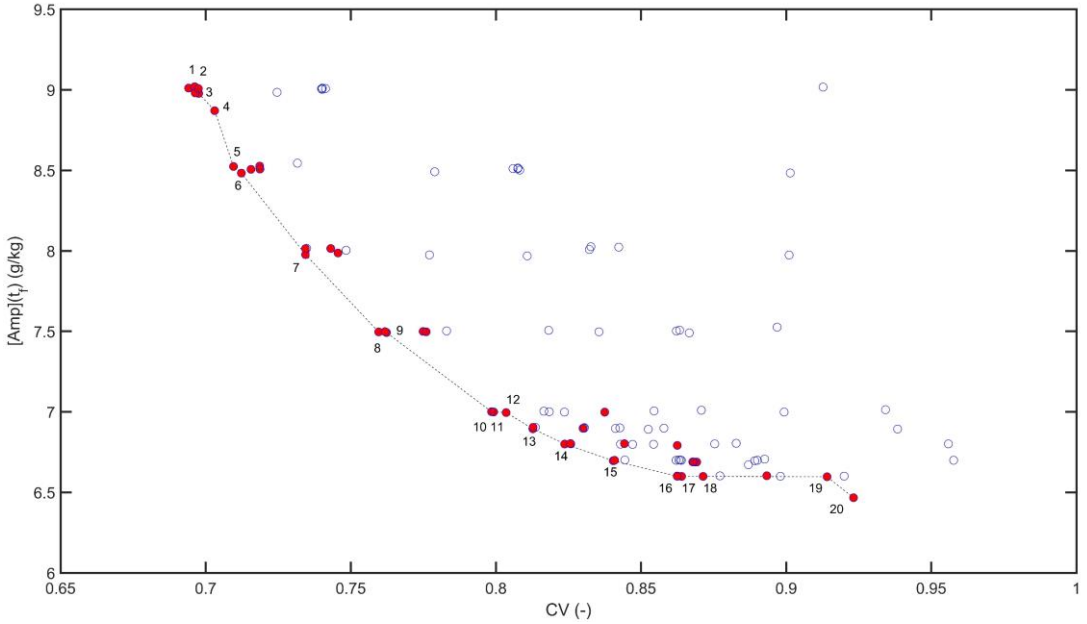

Figure 27: Exp E. 2D projection of the 3D pareto front for the multiobjective problem showcasing the tradeoff bewteen [Amp](t_f) and CV. The non-dominated solutions of the 3D front are presented as red points while those inherent to the 2D projection are connected with the dashed line.

On the other hand experiment F has a wt=15% the highest amount of seeding from the three. Moreover experiment F has a higher [*Amp*](t_0) concentration while pH_0 remains at around 7.

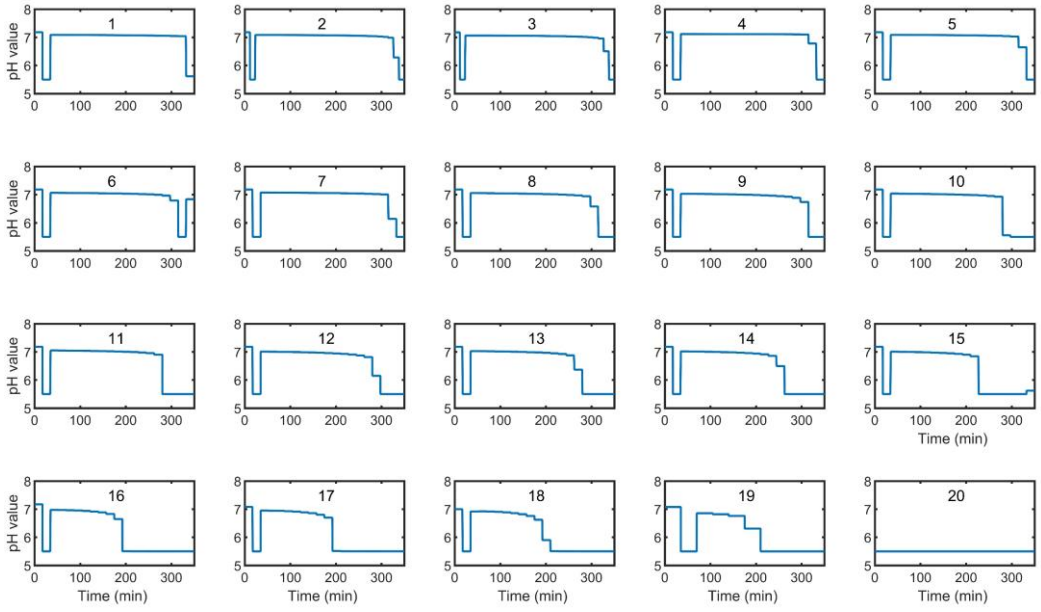

Figure 28: Exp E. pH profiles for the numbered Pareto front solutions in Fig. 27 (** K_x=6).

Meaning that initially the solution starts at an already high amount of supersaturation coupled with an increased amount of seed crystals. Experiment F also had the highest final batch time at t_f = 1500 min. For experiments E and F the same optimization strategy was utilized. Optimal scenarios were obtained

for the same objective function weights, discretization levels and the optimization problem setup was exactly the same.

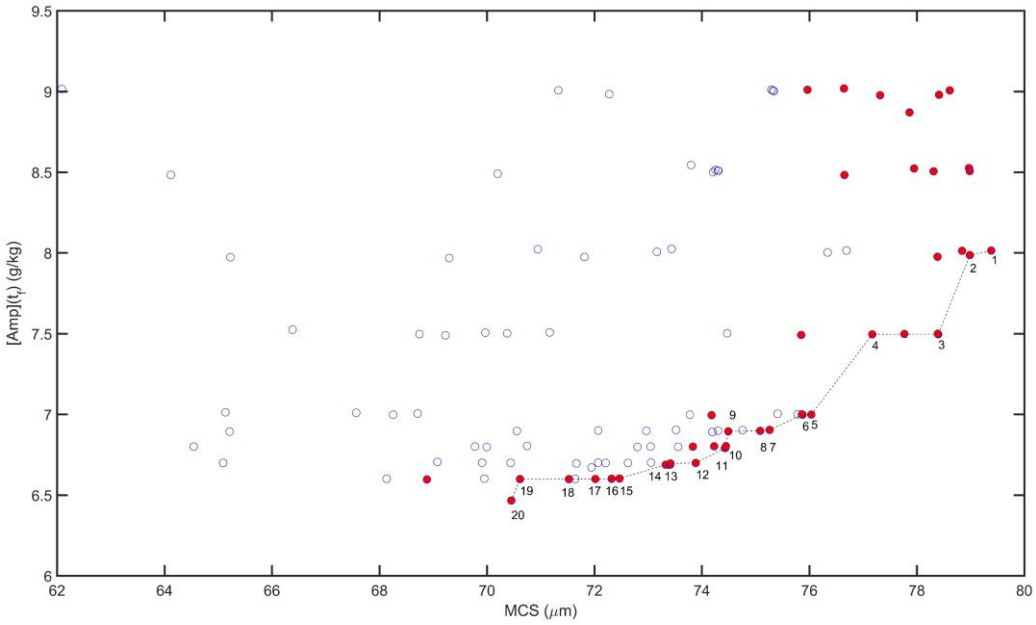

Figure 29: Exp E. 2D projection of the 3D pareto front for the multiobjective problem showcasing the tradeoff bewteen [Amp](t_f) and MCS. The non-dominated solutions of the 3D front are presented as red points while those inherent to the 2D projection are connected with the dashed line.

The only difference was for experiment F, due to the higher initial [*Amp*](t_0) different $target_{con}(t_f)$ values were used to stay in accordance with the other experiments.

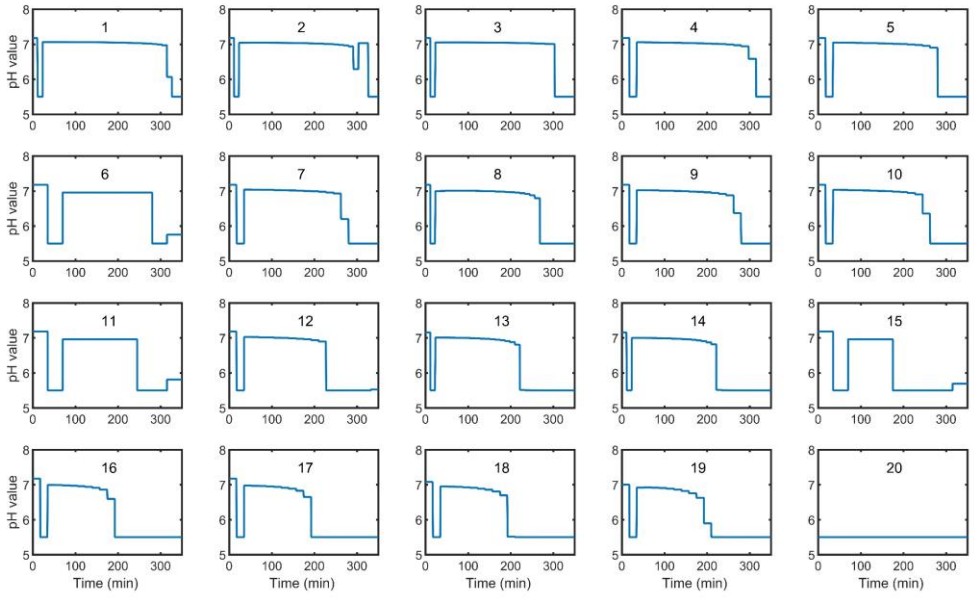

Figure 30: Exp E. pH profiles for the numbered Pareto front solutions in Fig. 29 (** K_x=6).

After obtaining the optimization results for both experiments their separate 3D Pareto fronts were created and as per experiment D the 2D Pareto projections were plotted. The 2D-projections of the Pareto fronts as well as the optimal pH profiles in each case are presented in Fig. 26-34.

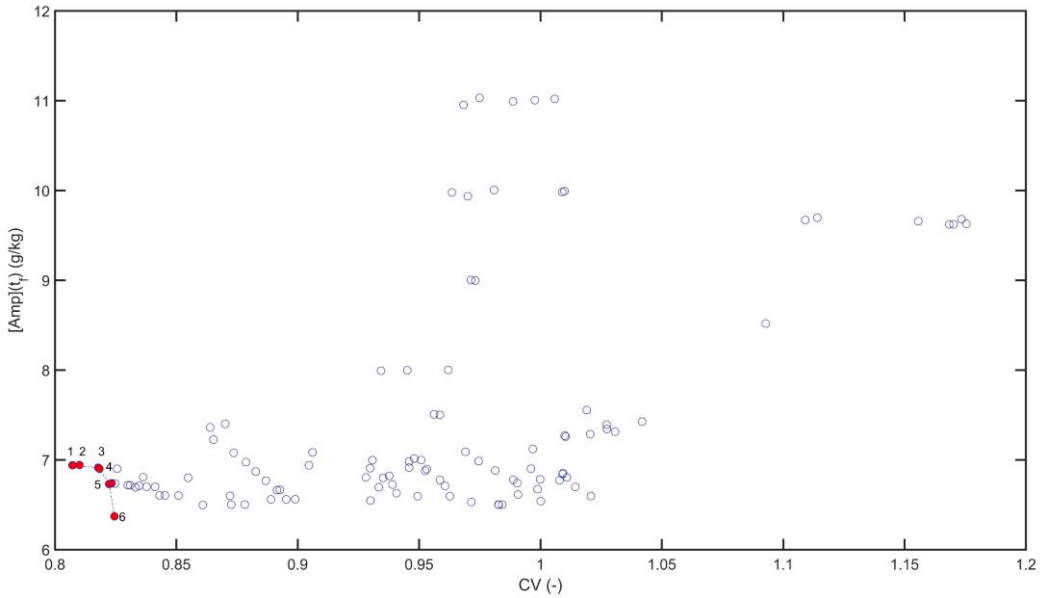

Figure 31: Exp F. 2D projection of the 3D pareto front for the multiobjective problem showcasing the tradeoff bewteen [Amp](t_f) and CV. The non-dominated solutions of the 3D front are presented as red points while those inherent to the 2D projection are connected with the dashed line.

Comparing and contrasting the results between experiments D and E the following conclusions can be reached. The Pareto fronts for those two experiments are directly comparable both 2D projections have the same shape. A definite tradeoff between [*Amp*](t_f) and CV as well as [*Amp*](t_f) and MCS exists. In order to increase the final amount of product both quality characteristics have to be 'sacrificed'. In Fig. 27 it is again noted that a 0.1 reduction in CV corresponds with a limited reduction of yield while further reduction constitutes of high yield reduction. The same conclusion can be reached in Fig. 29 where a 6 μm reduction in MCS can be achieved with limited yield reduction. In Fig. 28 and 30 it is noted that the optimal pH profiles maintain the pattern highlighted. An initial drop pH exists, with a subsequent increase in pH, then is the intermediate phase followed by the final pH drop. Again when high yield is required the intermediate phase shrinks and the final pH drop occurs sooner. All in all between experiments D and E the increase in initial crystallizer seeding does not seem to create a significant enough difference in the Pareto fronts and the optimal pH solutions.

On the other hand a definite difference between experiment D and experiment F can be highlighted. Both Pareto front projections highlight completely different Pareto fronts. In Fig. 31 it is clear that no tradeoff exists between [*Amp*](t_f) and CV if [*Amp*](t_f)>7. And for the points in the Pareto front only an approximate 0.02 CV reduction can be achieved by losing 7% of the recoverable product. For all intents and purposes it seems that in this case the baseline pH is directly comparable with regards to performance with the optimized profiles. Furthermore, in Fig. 32 it can be seen that the optimal profiles exhibit a different solution than experiment D. No initial reduction in pH can be observed, a phase were pH is almost constant and only slightly decreasing is observed until the final pH drop. The absence of

the initial pH profile could be attributed to the fact that the system is already highly supersaturated at the start and contains a high already amount of seed crystals.

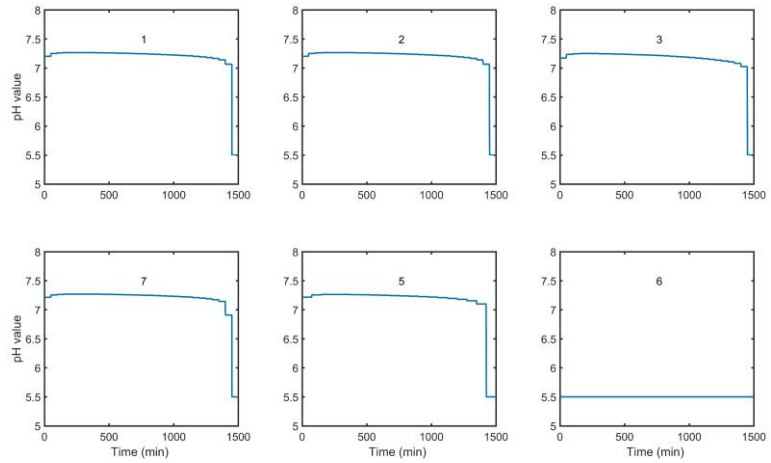

Figure 32: Exp F. pH profiles for the numbered Pareto front solutions in Fig. 31

For this reason no initial creation of crystals is needed and the system can only focus in crystal growth from the start with only a brief pH reduction at the end needed to satisfy the yield constraint.

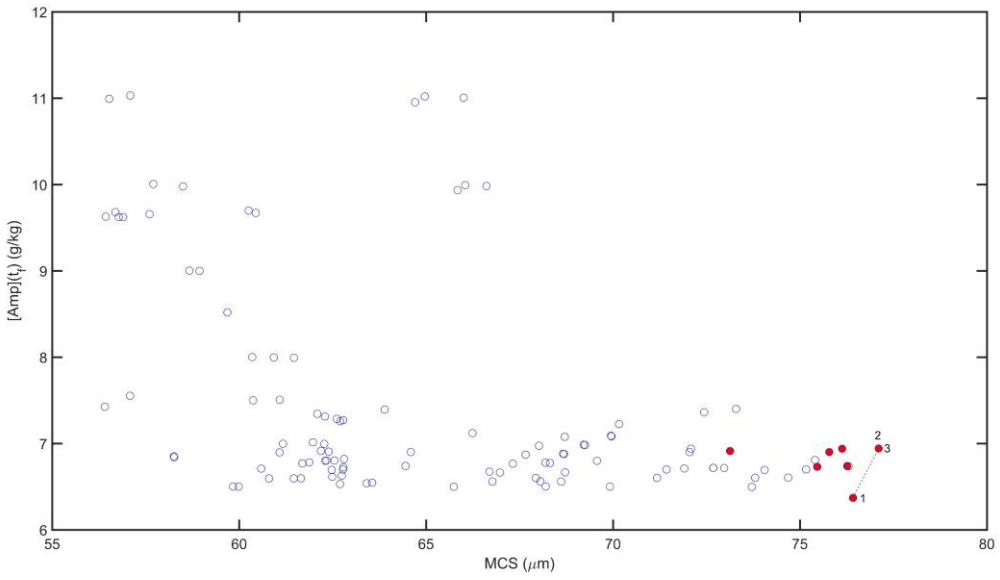

Figure 33: Exp F. 2D projection of the 3D pareto front for the multiobjective problem showcasing the tradeoff bewteen [Amp](t_f) and MCS. The non-dominated solutions of the 3D front are presented as red points while those inherent to the 2D projection are connected with the dashed line.

Even more extreme differences are observed in Fig. 33 out of nearly 130 optimization runs only 3 solutions find themselves into the 2D Pareto front. Once more there is no tradeoff between MCS and [*Amp*](t_f) and only an increase of approximately 0.7 μm can be achieved for MCS, demanding a 7.5% reduction in the recoverable final product. It is clear that the baseline scenario is the best operating point in such a scenario. The amount of seeding is so severe that a rapid increase in supersaturation does not

result in uncontrolled nucleation but in crystal growth, meaning that the baseline is the best option. On the other hand such a system does not allow for the control of the quality attributes, the process should be operated at a specific point meaning that high amounts of seeding limit the flexibility of the process. Of course it should be noted that this loss in flexibility conclusion comes with the assumption that the final batch time is constant at t_f = 1500 min.

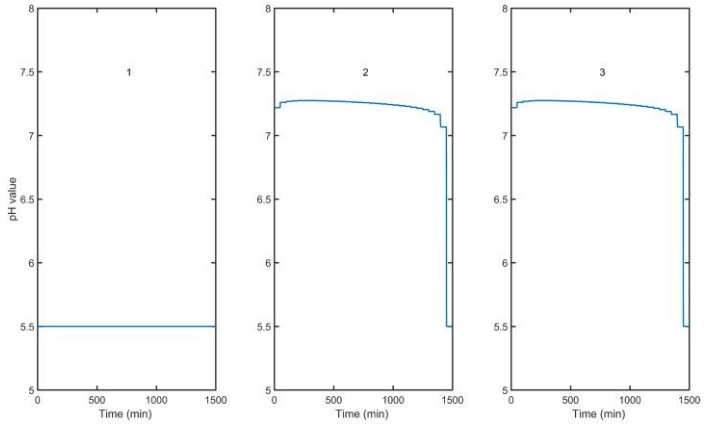

Figure 34: Exp F. pH profiles for the numbered Pareto front solutions in Fig. 33.

4. Conclusions

Ampicillin is a societally important antibiotic essential to the World healthcare system. Crystallization is an essential unit operation in the production of ampicillin influencing many crucial quality attributes which allow for a safe and effective pharmaceutical product. This work features dynamic optimization results for the batch crystallization of ampicillin where pH was used to induce supersaturation and in turn induce nucleation and crystal growth. A recently published crystallization kinetics model was utilized which handled both primary and secondary nucleation as well as initial crystallizer seeding. The model adopted the method of moments allowing the population balance to be expressed with a series of ODEs, consisting of the moments of the population. The solubility model proposed by Franco et al[40] was utilized, allowing for a model specific to ampicillin by using adjustable extended Pitzer parameters.

Initially a series of dynamic simulations were conducted in MATLAB using the ode113 function in order to replicate the reported results and to conduct design space investigation. In order to successfully replicate the model a special procedure was followed which tracked both the mother solute liquor concentration and MCS replication. This procedure allowed to finally conclude that the model was replicated successfully.

Afterwards, optimized pH profiles for the batch crystallization of ampicillin were utilized using the DynOpt package for MATLAB[39]. DynOpt applied the simultaneous method of orthogonal collocation on finite elements using Lagrange polynomials to approximate the state variables. Initially only one case, a seeded scenario with a small amount of seeds, was selected for optimization. Numerical modifications of the model like scaling and an approximation of the solubility model were necessary in order to conduct the optimization studies. A weighted multi-objective objective function was selected aiming to simultaneously enhance MCS and CV, essential quality attributes of the CSD. The effect of the discretization level, different configurations of objective function weights and changes in the yield constraints were discussed. Finally, a 3-D pareto front of the solutions as well as some of its 2-D projections were presenting clearly showing a trade-off between yield and the quality attributes. Optimal pH profiles were highlighted and presented on each case.

From the results it is clear that at the start of the process an initial pH drop is necessary to induce primary and secondary nucleation, afterwards pH is increased to allow for crystal growth. Then an intermediate phase is observed where pH remains stable while observing a slight decrease with time the severity of which depends on the magnitude of the yield constraint. This slight decrease allows for controlled supersaturation increases resulting in enhanced crystal growth. At the end of the intermediate phase a final pH drop is observed forcing more product to crystallize in order to achieve the yield constraint whilst maximizing the quality attributes. Through the study of the Pareto fronts and the optimal pH profiles, it was concluded that the duration and pH values of the intermediate phase where inherently linked to CV and MCS. Finally two different cases were optimized using the exact same methodology. These cases shined light to the impact of higher amounts of seeding. It was concluded that doubling the seeding leads to similar Pareto fronts and optimal pH profiles. On the other hand increasing the seeding 8-times and increasing the starting supersaturation leads to an inflexible system where no trade-off between yield and the quality attributes exists, with the base line being the reasonable operation pH profile.

This work allows for further work to be conducted. This would be to apply the model for unseeded cases and to add batch time optimization to the multi-objective objective function.

5. Nomenclature and Acronyms

5.1. Acronyms

API	Active pharmaceutical ingredient
CSD	Crystal size distribution
FDA	Food and drug administration
MCS	Mean crystal size
NLP	Nonlinear programming
ODE	Ordinary differential equation
PBP	Penicillin-binding proteins
WHO	World Health Organisation
CV	Coefficient of variation
STD	Standard deviation
LR	Long range interactions
SR	Short range interactions
PWC	Piecewise constant
PWL	Piecewise linear

5.2. Variables

Latin Letters	
$[Amp^*]$	Solubility of ampicillin (g kg^{-1})
$[Amp^-]$	Concentration of anionic ampicillin molecules (g kg^{-1})
$[Amp]_0$	Concentration of ampicillin in the mother liquor at t_0 (g kg^{-1})
$[Amp]_{calc}$	Calculated ampicillin mother solute concentration from our model (g/kg)
$[Amp]_{digit}$	Digitized ampicillin mother solute concentration (g/kg)
$[Amp]_t$	Concentration of ampicillin in the mother liquor at time t (g kg^{-1})
$[Amp^+]$	Concentration of cationic ampicillin molecules (g kg^{-1})
$[Amp^\pm]$	Concentration of zwitterionic ampicillin molecules (g kg^{-1})
a	Universal parameter of the Pitzer's model ($kg^{1/2}$ $mol^{-1/2}$)
A_{ij}	Pitzer's model adjustable parameter (kg $mol^{-1/2}$)
$Approx_{Error}$	Solubility approximation error (%)
a_s	Solubility approximation parameter
A_T	Total surface area of crystals (m^2)
b	Secondary nucleation mass exponent (−)
B_0	Primary nucleation constant (−)
B_1	Primary nucleation rate (#crystals (g kg^{-1})$^{-1}$ min^{-1})
B_2	Secondary nucleation rate (#crystals (g kg^{-1})$^{-1}$ min^{-1})
B_{ij}	Pitzer's model adjustable parameter (kg $mol^{-1/2}$)
b_s	Solubility approximation parameter
c_s	Solubility approximation parameter
d_s	Solubility approximation parameter
$Error_{[Amp]}$	Error in the calculation of [Amp] between our model and the published results (%)

$Error_{MCS}$	Error in the calculation of MCS between our model and the published results (%)
f	Optimization objective function (−)
G	Crystal growth rate (m/min)
g	Growth rate exponent (−)
I	Ionic strength (mol kg^{-1})
J	Total nucleation rate (#crystals (g kg^{-1})$^{-1}$ min^{-1})
k_a	Crystal area shape factor (−)
K_{A1}	Equilibrium constant of acid protonation of ampicillin
K_{A2}	Equilibrium constant of amine protonation of ampicillin
k_B	Boltzmann's constant (m^2 kg s^{-2} K^{-1})
k_{B1}	Primary nucleation rate constant (#crystals (g kg^{-1})$^{-1}$ min^{-1})
k_{B2}	Secondary nucleation rate constant (#crystals (g kg^{-1})$^{-1}$ min^{-1})
K_D	Equilibrium constant of neutral ampicillin molecules
k_G	Growth rate constant (m/min)
K_U	Number of control variable collocation points (−)
k_V	Crystal volume shape factor (−)
K_X	Number of state variable collocation points (−)
L	Total length of crystals (m)
$\overline{L_{seed}}$	Average length of seed crystals (m)
M	Mass of crystals inside the crystallizer (g)
m	Mass of mother liquor (kg)
m^*	Molality of component i in the reference state (mol kg^{-1})
m_0	Molality of electrically neutral ampicillin (mol kg^{-1})
m_0	Zeroth moment of the population balance (#/m^3)
m_1	first moment of the population balance (m/m^3)
m_2	Second moment of the population balance (m^2/m^3)
m_3	Third moment of the population balance (m^3/m^3)
M_C	Average mass of a single crystal (g)
m_c	Mass of seed crystals (g)
MCS_{calc}	Calculated MCS using our model (μm)
$MCS_{reported}$	Reported MCS (μm)
m_i	Molality of component i (mol kg^{-1})
M_S	Solvent molecular mass (kg mol^{-1})
m_T	Crystal suspension density
n	Population density (#crystals m^{-1} g kg^{-1})
N	Number of discretized time intervals (−)
n_0	Initial population density (#crystals m^{-1} g kg^{-1})
N_A	Avogadro's number (mol^{-1})
N_T	Total number of crystals (#crystals)
pH	pH value of the mother liquor (−)
pH_0	pH value at t_0 (−)
pH_f	pH value at t_f (−)
pI	Isoelectric point for ampicillin (−)
p_i	Model scaling parameters (−)
R	Gas constant (kg m^2 mol^{-1} K^{-1} s^{-2})

S	Solubility of ampicillin in water at 298.15K (mol/kg)
s	Secondary nucleation supersaturation exponent (−)
S(pI)	Solubility of ampicillin in water at the isoelectric point at 298.15K (mol/kg)
S_{approx}	Approximated solubility of ampicillin (g/kg)
S_{model}	Solubility of ampicillin calculated from Eq. 33 (g/kg)
SS	Ampicillin supersaturation in the mother liquor (−)
t	Time (min)
T	Temperature (K)
t_0	Initial time point (min)
$target_{[Amp]}$	Target mother solute concentration of ampicillin at t_f (g/kg)
t_{crop}	Final time point used to plot the dynamic simulation graphs (min)
t_{decr}	Time point where pH is stops decreasing (min)
t_f	Final crystallizer time (min)
$u(t)$	Control variable in the optimization problem-pH
V_T	Total volume of crystals (m^3)
W_{MCS}	MCS weight parameter in the objective function (−)
W_σ	Variance weight parameter in the objective function (−)
$x(t)$	State variables in the optimization problem- ODEs
z_i	Electric charge of component i

Greek Letters	
α_i	Ionized fraction of component i (−)
γ_0	Activity coefficient of electrically neutral ampicillin molecules
γ_i	Activity coefficient of component i
Δ_{ti}	Time of each discretized time interval (min)
ε	Van der Waals attractive interaction parameter (m^2 kg s^{-2})
λ_{ij}	Pitzer's binary interaction parameter (kg mol^{-1})
Λ_{ijk}	Pitzer's ternary interaction parameter (kg^2 mol^{-2})
μ_i^*	Chemical potential of component i in the reference phase (kg m^2 mol^{-1} s^{-2})
μ_i^L	Chemical potential of component i in the liquid phase (kg m^2 mol^{-1} s^{-2})
μ_i^S	Chemical potential of component i in the solid phase (kg m^2 mol^{-1} s^{-2})
ρ	Number of ampicillin molecules per volume unity (m^{-3})
ρ_c	Density of seed crystals density (kg/m^3)
σ	Van der Waals diameter (m)
σ^2	Variance of the CSD (m)
φ_0	Fraction of electrically neutral ampicillin molecules (−)
φ_i	Fraction of component i

5.3. Molecules and Reagents

6-APA	6-aminopenicillanic acid
PG	α-phenylglycine
PGA	Penicillin G acylase
PGME	D-phenylglycine methyl ester
MeOH	Methanol

6. References

(1) Encarnación-Gómez, L. G.; Bommarius, A. S.; Rousseau, R. W. Crystallization kinetics of ampicillin using online monitoring tools and robust parameter estimation. *Ind. Eng. Chem. Res.* **2016**, *55* (7), 2153–2162.

(2) Klein, E. Y.; Van Boeckel, T. P.; Martinez, E. M.; Pant, S.; Gandra, S.; Levin, S. A.; Goossens, H.; Laxminarayan, R. Global increase and geographic convergence in antibiotic consumption between 2000 and 2015. *Proc. Natl. Acad. Sci. U. S. A.* **2018**, *115* (15), E3463–E3470.

(3) Encarnación-Gómez, L. G.; Bommarius, A. S.; Rousseau, R. W. Reactive crystallization of β-lactam antibiotics: strategies to enhance productivity and purity of ampicillin. *React. Chem. Eng.* **2016**, *1* (3), 321–329.

(4) Kirwan, D. J.; Orella, C. J. Crystallization in the pharmaceutical and bioprocessing industries. *Handb. Ind. Cryst.* **2002**, 249–266.

(5) Chen, J.; Sarma, B.; Evans, J. M. B.; Myerson, A. S. Pharmaceutical crystallization. *Cryst. Growth Des.* **2011**, *11* (4), 887–895.

(6) Godwin, F. *FDA Warning Letter 320-16-21 to SmithKline Beecham Limited 6/30/16*; 2016.

(7) gCRYSTAL. Limited, Process Systems Enterprise.

(8) DynoChem. Scale-up Systems Ltd.

(9) COMSOL multiphysics. Comsol INC.

(10) Nagy, Z. K.; Fevotte, G.; Kramer, H.; Simon, L. L. Recent advances in the monitoring, modelling and control of crystallization systems. *Chem. Eng. Res. Des.* **2013**, *91* (10), 1903–1922.

(11) Liu, W. J.; Ma, C. Y.; Liu, J. J.; Zhang, Y.; Wang, X. Z. Analytical technology aided optimization and scale-up of impinging jet mixer for reactive crystallization process. *AIChE J.* **2015**, *61* (2), 503–517.

(12) Jiang, X.; Lu, D.; Xiao, W.; Ruan, X.; Fang, J.; He, G. Separations: materials, devices and processes membrane assisted cooling crystallization: process model, nucleation, metastable zone, and crystal size distribution. *Am. Inst. Chem. Eng. AIChE J* **2015**, *62*, 829–841.

(13) Clercq, S.; Mouahid, A.; Gérard, P.; Badens, E. Investigation of crystallization mechanisms for polymorphic and habit control from the supercritical antisolvent process. *J. Supercrit. Fluids* **2018**, *141*, 29–38.

(14) Drioli, E.; Di Profio, G.; Curcio, E. Progress in membrane crystallization. *Curr. Opin. Chem. Eng.* **2012**, *1* (2), 178–182.

(15) Ottens, M.; Lebreton, B.; Zomerdijk, M.; Rijkers, M. P. W. M.; Bruinsma, O. S. L.; van der Wielen, L. A. . Impurity effects on the crystallization kinetics of ampicillin. *Ind. Eng. Chem. Res.* **2004**, *43* (24), 7932–7938.

(16) Su, M.; Sun, H.; Zhao, Y.; Lu, A.; Cao, X.; Wang, J. Degradation kinetics and mechanism of a β-lactam antibiotic intermediate, 6-aminopenicillanic acid, in a new integrated production process. *J. Pharm. Sci.* **2016**, *105* (1), 139–146.

(17) Trampuž, M.; Teslić, D.; Likozar, B. Crystallization of fesoterodine fumarate active pharmaceutical ingredient: modelling of thermodynamic equilibrium, nucleation, growth, agglomeration and dissolution kinetics and temperature cycling. *Chem. Eng. Sci.* **2019**, *201*, 97–111.

(18) Xie, X.; Schenkendorf, R. Stochastic back-off-based robust process design for continuous crystallization of ibuprofen. *Comput. Chem. Eng.* **2019**, *124*, 80–92.

(19) Gao, Z.; Rohani, S.; Gong, J.; Wang, J. Recent developments in the crystallization process: toward the pharmaceutical industry. *Engineering* **2017**, *3* (3), 343–353.

(20) Jolliffe, H. G.; Diab, S.; Gerogiorgis, D. I. Nonlinear optimization via explicit nrtl model solubility prediction for antisolvent mixture selection in artemisinin crystallization. *Org. Process Res. Dev.* **2018**, *22* (1), 40–53.

(21) Jolliffe, H. G.; Gerogiorgis, D. I. Process modelling, design and technoeconomic evaluation for continuous paracetamol crystallisation. *Comput. Chem. Eng.* **2018**, *118*, 224–235.

(22) Diab, S.; Gerogiorgis, D. I. Technoeconomic optimization of continuous crystallization for three active pharmaceutical ingredients: cyclosporine, paracetamol, and aliskiren. *Ind. Eng. Chem.*

Res. **2018**, *57* (29), 9489–9499.
(23) Kong, K.-F. F.; Schneper, L.; Mathee, K. Beta-lactam antibiotics: from antibiosis to resistance and bacteriology. *APMIS* **2010**, *118* (1), 1–36.
(24) Doyle, F. P.; Fosker, G. R.; Nayler, J. H. C.; Smith, H. 272. derivatives of 6-aminopenicillanic acid. part i: α-aminobenzylpenicillin and some related compounds. *J. Chem. Soc.* **1962**, *0* (0), 1440–1444.
(25) *WHO List of Critically Important Antimicrobials for Human Medicine (WHO CIA List)*; 2017.
(26) Demain, A. L.; Elander, R. P. *The β-Lactam Antibiotics: Past, Present, and Future*; 1999; Vol. 75.
(27) Florey, K.; Brewer, G. A.; Cohen, E. M.; Guttman, D. E.; Olin, S. M.; Papariello, G. J.; Florey, K.; Fusari, S. A. Analytical profiles of drug substances. **1973**, *2*, 4–61.
(28) Santana, M.; Ribeiro, M. P. A.; Leite, G. A.; Giordano, R. L. C.; Giordano, R. C.; Mattedi, S. Solid-liquid equilibrium of substrates and products of the enzymatic synthesis of ampicillin. *AIChE J.* **2010**, *56* (6), 1578–1583.
(29) Giordano, R. C.; Ribeiro, M. P. A.; Giordano, R. L. C. Kinetics of β-lactam antibiotics synthesis by penicillin g acylase (pga) from the viewpoint of the industrial enzymatic reactor optimization. *Biotechnol. Adv.* **2006**, *24* (1), 27–41.
(30) McDonald, M. A.; Bommarius, A. S.; Rousseau, R. W. Enzymatic reactive crystallization for improving ampicillin synthesis. *Chem. Eng. Sci.* **2017**, *165*, 81–88.
(31) Chandel, A. K.; Rao, L. V.; Narasu, M. L.; Singh, O. V. The realm of penicillin g acylase in β-lactam antibiotics. *Enzyme Microb. Technol.* **2008**, *42* (3), 199–207.
(32) Dicosimo, R.; Mcauliffe, J.; Poulose, A. J.; Bohlmann, G. Industrial use of immobilized enzymes. *Chem. Soc. Rev* **2013**, *42*, 6437.
(33) Ottens, M.; Lebreton, B.; Zomerdijk, M.; Rijkers, M. P. W. M.; Bruinsma, O. S. L.; Van Der Wielen, L. A. M. Crystallization kinetics of ampicillin. *Ind. Eng. Chem. Res.* **2001**, *40* (22), 4821–4827.
(34) Censi, R.; Di Martino, P.; Censi, R.; Di Martino, P. Polymorph impact on the bioavailability and stability of poorly soluble drugs. *Molecules* **2015**, *20* (10), 18759–18776.
(35) Baraldi, C.; Tinti, A.; Ottani, S.; Gamberini, M. C. C. Characterization of polymorphic ampicillin forms. *J. Pharm. Biomed. Anal.* **2014**, *100*, 329–340.
(36) Raza, K.; Kumar, P.; Ratan, S.; Ruchi, M.; Arora, S. Polymorphism: the phenomenon affecting the performance of drugs. *SOJ Pharm. Pharm. Sci.* **2014**, *1* (2).
(37) McDonald, M. A.; Bommarius, A. S.; Rousseau, R. W.; Grover, M. A. Continuous reactive crystallization of β-lactam antibiotics catalyzed by penicillin g acylase. part i: model development. *Comput. Chem. Eng.* **2019**, *123*, 331–343.
(38) Bezerra, I. M.; Moreira, L. C.; Chiavone-Filho, O.; Mattedi, S. Effect of different variables in the solubility of ampicillin and corresponding solid phase. *Fluid Phase Equilib.* **2018**, *459*, 18–29.
(39) Čižniar, M.; Salhi, D.; Fikar, M.; Latifi, M. A. Matlab dynamic optimization code dynopt, user's guide. **2006**, 1–7.
(40) Franco, L. F. M.; Mattedi, S.; Filho, P. D. A. P. A new approach for the thermodynamic modeling of the solubility of amino acids and β-lactam compounds as a function of ph. *Fluid Phase Equilib.* **2013**, *354*, 38–46.
(41) Filho, P. D. A. P.; Maurer, G. An extension of the pitzer equation for the excess gibbs energy of aqueous electrolyte systems to aqueous polyelectrolyte solutions. *Fluid Phase Equilib.* **2008**, *269*, 25–35.
(42) Rudolph, E. S. J.; Zomerdijk, M.; Ottens, M.; van der Wielen, L. A. M. Solubilities and partition coefficients of semi-synthetic antibiotics in water + 1-butanol systems. *Ind. Eng. Chem. Res.* **2001**, *40* (1), 398–406.
(43) Wey, J. S.; Karpinski, P. H. Batch crystallization. *Handb. Ind. Cryst.* **2002**, 231–248.
(44) Jha, S. K.; Karthika, S.; Radhakrishnan, T. K. Modelling and control of crystallization process. *Resour. Technol.* **2017**, *3* (1), 94–100.
(45) Erum, A. (Loughborough U. Population balance model-based optimal control of batch crystallisation processes for systematic crystal size distribution design, Loughborough University, 2010.

(46) Chianese, A. Characterization of crystal size distribution. In *Industrial Crystallization Process Monitoring and Control*; Wiley-VCH Verlag GmbH & Co. KGaA: Weinheim, Germany, 2012; pp 1–6.
(47) Ozana, S.; Pies, M.; Docekal, T. Dynamic optimization case studies in dynopt tool. In *AIP Conference Proceedings*; AIP Publishing LLC, 2016; Vol. 1738, p 480118.
(48) Zhai, C.; Wang, R.; Ren, Z.; Sun, W. Dynamic optimization of fed-batch fermentation with constraint on wastewater discharge . *Chem. Eng. Trans.* **2017**, *61*, 499-504 SE-Research Articles.
(49) Rodman, A. D.; Gerogiorgis, D. I. An investigation of initialisation strategies for dynamic temperature optimisation in beer fermentation. *Comput. Chem. Eng.* **2019**, *124*, 43–61.
(50) Ward, J. D.; Mellichamp, D. A.; Doherty, M. F. Choosing an operating policy for seeded batch crystallization. *AIChE J.* **2006**, *52* (6), 2046–2054.
(51) Reddy, M. J.; Kumar, D. N. Elitist-mutated multi-objective particle swarm optimization for engineering design. In *Encyclopedia of Information Science and Technology, Third Edition*; Mehdi Khosrow-Pour, D. B. A., Ed.; IGI Global: Hershey, PA, USA, 2015; pp 3534–3545.

Appendix A: Batch Crystallization Optimization results

Full details of the optimization solutions in Fig. 14-17 are presented in Table 9.

Table 9: Dynamic optimization results.

Figure	N	Init. pH	K_X	W_{MCS}	$Target_{[Amp]}$ (g/kg)	[Amp](tf) (g/kg)	MCS (μm)	STD (μm)	CV (−)
14	10	7	3	0.0	9.00	9.00	71.27	53.33	0.75
	20	7	3	0.0	9.00	8.50	77.78	53.67	0.69
	30	7	6	0.0	9.00	9.04	75.45	52.45	0.70
	10	7	3	0.0	8.00	8.01	74.61	56.96	0.76
	20	7	3	0.0	8.00	8.02	71.56	56.97	0.80
	30	7	3	0.0	8.00	7.96	73.54	56.79	0.77
	10	7	3	0.0	7.00	7.00	71.29	60.46	0.85
	20	7	3	0.0	7.00	7.01	72.04	59.92	0.83
	30	7	3	0.0	7.00	7.00	74.34	60.93	0.82
	10	7	3	0.0	6.80	6.80	70.59	61.53	0.87
	20	7	3	0.0	6.80	6.79	71.48	60.98	0.85
	30	7	3	0.0	6.80	6.80	74.27	62.38	0.84
	10	7	3	0.0	6.60	6.60	72.30	64.56	0.89
	20	6	3	0.0	6.60	6.60	70.61	64.72	0.92
	30	6	3	0.0	6.60	6.60	70.60	63.21	0.90
15	10	7	3	0.5	9.00	8.99	75.00	57.82	0.77
	20	7	3	0.5	9.00	9.02	78.17	53.60	0.69
	30	6	3	0.5	9.00	9.03	78.15	53.76	0.69
	10	7	3	0.5	8.00	7.99	77.35	57.32	0.74
	20	7	3	0.5	8.00	8.01	78.95	59.06	0.75
	30	6	3	0.5	8.00	8.00	79.56	58.11	0.73
	10	7	3	0.5	7.00	7.00	74.32	60.86	0.82
	20	7	3	0.5	7.00	7.00	74.45	60.45	0.81
	30	7	3	0.5	7.00	6.99	75.42	61.20	0.81
	10	7	3	0.5	6.80	6.80	73.63	61.95	0.84
	20	7	6	0.5	6.80	6.80	73.34	61.18	0.83
	30	7	3	0.5	6.80	6.80	73.29	61.16	0.83
	10	6	3	0.5	6.60	6.59	72.58	64.71	0.89
	20	6	3	0.5	6.60	6.60	71.97	64.53	0.90
	30	6	3	0.5	6.60	6.60	72.04	63.92	0.89
16	10	7	3	1.0	9.00	9.01	76.74	54.16	0.71
	20	7	3	1.0	9.00	9.00	78.25	53.80	0.69
	30	7	6	1.0	9.00	9.03	78.82	53.34	0.68
	10	7	3	1.0	8.00	8.00	78.39	57.99	0.74
	20	7	3	1.0	8.00	8.00	78.14	58.95	0.75
	30	7	6	1.0	8.00	7.96	79.63	58.16	0.73
	10	7	3	1.0	7.00	7.00	75.39	61.35	0.81
	20	7	3	1.0	7.00	7.00	75.35	60.88	0.81
	30	6	3	1.0	7.00	7.02	75.32	63.13	0.84
	10	7	3	1.0	6.80	6.80	74.33	62.10	0.84

	20	7	3	1.0	6.80	6.78	74.13	62.04	0.84
	30	7	3	1.0	6.80	6.80	75.01	62.85	0.84
	10	6	3	1.0	6.60	6.60	73.02	64.66	0.89
	20	6	3	1.0	6.60	6.60	72.77	64.60	0.89
	30	6	3	1.0	6.60	6.60	72.10	64.31	0.89
17	10	7	3	1.5	9.00	8.50	79.19	56.81	0.72
	20	7	3	1.5	9.00	9.03	79.50	55.02	0.69
	30	7	6	1.5	9.00	8.99	78.19	57.48	0.74
	10	7	3	1.5	8.00	8.01	79.00	58.55	0.74
	20	7	3	1.5	8.00	8.01	79.79	59.46	0.75
	30	7	3	1.5	8.00	8.00	78.85	60.66	0.77
	10	7	3	1.5	7.00	6.99	75.90	62.00	0.82
	20	7	3	1.5	7.00	7.00	75.89	61.51	0.81
	30	7	3	1.5	7.00	7.00	74.00	64.86	0.88
	10	7	3	1.5	6.80	6.80	74.72	62.48	0.84
	20	7	3	1.5	6.80	6.80	74.70	62.32	0.83
	30	7	3	1.5	6.80	6.80	75.25	63.14	0.84
	10	6	3	1.5	6.60	6.60	72.61	64.02	0.88
	20	6	3	1.5	6.60	6.60	70.51	64.50	0.91
	30	6	3	1.5	6.60	6.60	72.86	64.58	0.89